RESULTS

The results of this thesis are reported in the following papers:

I. Hillion, J., Canals, M., Torvinen, M., Casadó, V., Scott, R., Terasmaa, A., Hansson, A., Watson, S., Olah, M., Mallol, J., Canela, E.I., Zoli, M., Agnati, L., Ibañez, C., Lluís, C., Franco, R., Ferré, S. and Fuxe, K., 2002, "Coaggregation, cointernalization, and codesensitization of adenosine A_{2A} receptor and dopamine D_2 receptors". *Journal of Biological Chemistry*, 20, 18091-18097.

II. Canals, M., Marcellino, D., Fanelli, F., Ciruela, F., Benedetti, P., Goldberg, S., Neve, K., Fuxe, K., Agnati, L., Woods, A., Ferré, S., Lluís, C., Bouvier, M. and Franco, R., 2003, "Adenosine A_{2A}-dopamine D_2 receptor-receptor heteromerization. Qualitative and quantitative assessment by fluorescence and bioluminescence energy transfer". *Journal of Biological Chemistry*, 47, 46741-46749.

III. Canals, M., Burgueño, J., Marcellino, D., Cabello, N., Canela, E.I., Mallol, J., Agnati, L., Ferré, S., Bouvier, M., Fuxe, K., Ciruela, F., Lluís, C. and Franco, R., 2004, "Homodimerization of adenosine A_{2A} receptors: qualitative and quantitative assessment by fluorescence and bioluminescence energy transfer". *Journal of Neurochemistry*, 88, 726-734.

IV. Canals, M., Angulo, E., Casadó, V., Canela, E.I., Mallol, J., Viñals, F., Staines, W., Tinner, B., Hillion, J., Agnati, L., Fuxe, K., Ferré, S., Lluís, C. and Franco, R., 2004, "Molecular mechanisms involved in the adenosine A_1 and A_{2A} receptor-induced neuronal differentiation in neuroblastoma cells and striatal primary cultures". *Submitted manuscript*.

I-. Hillion, J., Canals, M., Torvinen, M., Casadó, V., Scott, R., Terasmaa, A., Hansson, A., Watson, S., Olah, M., Mallol, J., Canela, E.I., Zoli, M., Agnati, L., Ibañez, C., Lluís, C., Franco, R., Ferré, S. and Fuxe, K., 2002, "Coaggregation, cointernalization, and codesensitization of adenosine A_{2A} receptor and dopamine D_2 receptors". *Journal of Biological Chemistry*, 20, 18091-18097.

THE JOURNAL OF BIOLOGICAL CHEMISTRY Vol. 277, No. 20, Issue of May 17, pp. 18091–18097, 2002
Printed in U.S.A.

Coaggregation, Cointernalization, and Codesensitization of Adenosine A_{2A} Receptors and Dopamine D_2 Receptors*

Received for publication, August 13, 2001, and in revised form, January 22, 2002
Published, JBC Papers in Press, February 28, 2002, DOI 10.1074/jbc.M107731200

Joëlle Hillion‡§¶, Meritxell Canals‡§, Maria Torvinen‡, Vicent Casadó‖, Rizaldy Scott‡, Anton Terasmaa‡, Anita Hansson‡, Stanley Watson, Mark E. Olah‡‡, Josefa Mallol‖, Enric I. Canela‖, Michele Zoli§§, Luigi F. Agnati§§, Carlos F. Ibáñez‡, Carme Lluis‖, Rafael Franco‖, Sergi Ferré‡ ¶¶, and Kjell Fuxe‡**

*From the ‡Department of Neuroscience, Karolinska Institute, 17177 Stockholm, Sweden, the ‖Department of Biochemistry and Molecular Biology, University of Barcelona, 08028 Barcelona, Spain, the **Mental Health Institute, University of Michigan, Ann Arbor, Michigan 48109, the ‡‡Department of Medicine, Duke University Medical Center, Durham, North Carolina 27710, the §§Department of Biomedical Sciences, University of Modena, 41100 Modena, Italy, and the ¶¶National Institute on Drug Abuse, Baltimore, Maryland 21224*

Antagonistic and reciprocal interactions are known to exist between adenosine and dopamine receptors in the striatum. In the present study, double immunofluorescence experiments with confocal laser microscopy showed a high degree of colocalization of adenosine A_{2A} receptors ($A_{2A}R$) and dopamine D_2 receptors (D_2R) in cell membranes of SH-SY5Y human neuroblastoma cells stably transfected with human D_2R and in cultured striatal cells. $A_{2A}R/D_2R$ heteromeric complexes were demonstrated in coimmunoprecipitation experiments in membrane preparations from D_2R-transfected SH-SY5Y cells and from mouse fibroblast Ltk^- cells stably transfected with human D_2R (long form) and transiently cotransfected with the $A_{2A}R$ double-tagged with hemagglutinin. Long term exposure to $A_{2A}R$ and D_2R agonists in D_2R-cotransfected SH-SY5Y cells resulted in coaggregation, cointernalization and codesensitization of $A_{2A}R$ and D_2R. These results give a molecular basis for adenosine-dopamine antagonism at the membrane level and have implications for treatment of Parkinson's disease and schizophrenia, in which D_2R are involved.

Adenosine and dopamine signaling exert opposite effects in the basal ganglia, a brain region involved in sensory-motor integration. Thus, adenosine agonists induce motor depression and adenosine antagonists, such as caffeine, produce motor activation (1). These opposite effects result from specific antagonistic interactions between subtypes of adenosine and dopamine receptors in the striatum, the main input structure of the basal ganglia. In fact, striatal dopamine receptors and, to some extent, adenosine receptors are segregated in the two main populations of γ-aminobutyric acid (GABA) efferent neurons. Striopallidal neurons express dopamine receptors predominantly of the D_2 subtype (D_2R)[1] and the highest density of adenosine A_{2A} receptors ($A_{2A}R$) in the brain (2, 3). In the rat, the strionigro-strioentopeduncular neurons contain dopamine receptors predominantly of the D_1 subtype (D_1R) and express exclusively adenosine receptors of the A_1 subtype (A_1R) (2–4). Experimental evidence supports the existence of antagonistic $A_{2A}R/D_2R$ and A_1R/D_1R interactions, respectively, in the GABA striopallidal and strionigro-strioentopeduncular neurons (1, 5). Taken together, these data suggested proximity between receptors, which could allow them to form heteromeric complexes (directly or indirectly by means of adaptor proteins). In fact, A_1R and D_1R were found to form heteromeric complexes (6). Although antagonistic $A_{2A}R/D_2R$ interactions have been reported to play an important role in basal ganglia function, it is still not known whether the formation of heteromeric $A_{2A}R/D_2R$ complexes is also involved. In the present work, the existence of selective intramembrane interactions between $A_{2A}R$ and D_2R in neuronal cells is demonstrated, including formation of heteromeric $A_{2A}R/D_2R$ complexes and their potential involvement in cross-desensitization mechanisms via agonist-induced coaggregation and cointernalization of $A_{2A}R$ and D_2R. These results have clinical implications for Parkinson's disease and other basal ganglia disorders where dopamine D_2R are the target for therapy (1, 5).

EXPERIMENTAL PROCEDURES

Cell Cultures—Maintenance of SH-SY5Y cells (parental and D_2R-transfected cells) as well as the pharmacological characterization and maintenance of D_2R- and D_1R-transfected mouse fibroblast Ltk^- cells are described in detail elsewhere (7–9). For primary cultures, striata were removed from 16-day-old Sprague-Dawley rat embryos (B&K Universal) in Ca^{2+}/Mg^{2+}-free PBS supplemented with 20 units/ml penicillin and 20 μg/ml streptomycin (Invitrogen). The tissue fragments were pooled and mechanically dissociated in SFM Neurobasal serum-free medium (Invitrogen), supplemented with B27 (Invitrogen), glutamine (2 mM; Invitrogen), penicillin/streptomycin (20 units/ml/20 μg/ml; Invitrogen), and β-mercaptoethanol (25 μM) (Invitrogen). Cells were collected by centrifugation at 100 × *g* for 5 min and resuspended in fresh medium. The resulting single-cell suspension was seeded on 24-well plates coated with gelatin (Sigma) and poly-L-lysine (Sigma), and cells were grown at 37 °C in saturation humidity with 5% CO_2.

Immunolabeling Experiments—Neuroblastoma cells were grown on glass coverslips coated with poly-L-lysine (Sigma) and exposed to vari-

* This work was supported by Swedish Medical Research Council Grant 14X-00715, European Commission Grant QLG3-CT-2001-01056, Spanish Commission of Science and Technology National Plan of Biotechnology Grant BIO99-0601-C02-02), an Italian Ministero della Università e della Ricerca Scientifica e Tecnologica ex60% grant, and a grant from the Knut and Alice Wallenberg Foundation. The costs of publication of this article were defrayed in part by the payment of page charges. This article must therefore be hereby marked "*advertisement*" in accordance with 18 U.S.C. Section 1734 solely to indicate this fact.

§ These authors contributed equally to this manuscript.

¶ To whom correspondence should be addressed. Present address: Stroke Branch, NINDS, National Institutes of Health, Bethesda, MD 20892-4128. Tel.: 301-594-2597; Fax: 301-402-2769; E-mail: hillionj@ninds.nih.gov.

[1] The abbreviations used are: D_2R, dopamine D_2 receptor; $A_{2A}R$, adenosine A_{2A} receptor; HA, hemagglutinin; ANOVA, analysis of variance; PBS, phosphate-buffered saline; FITC, fluorescein isothiocyanate; IR, immunoreactive; GI, Gini's index; DOPA, 3,4-dihydroxyphenylalanine.

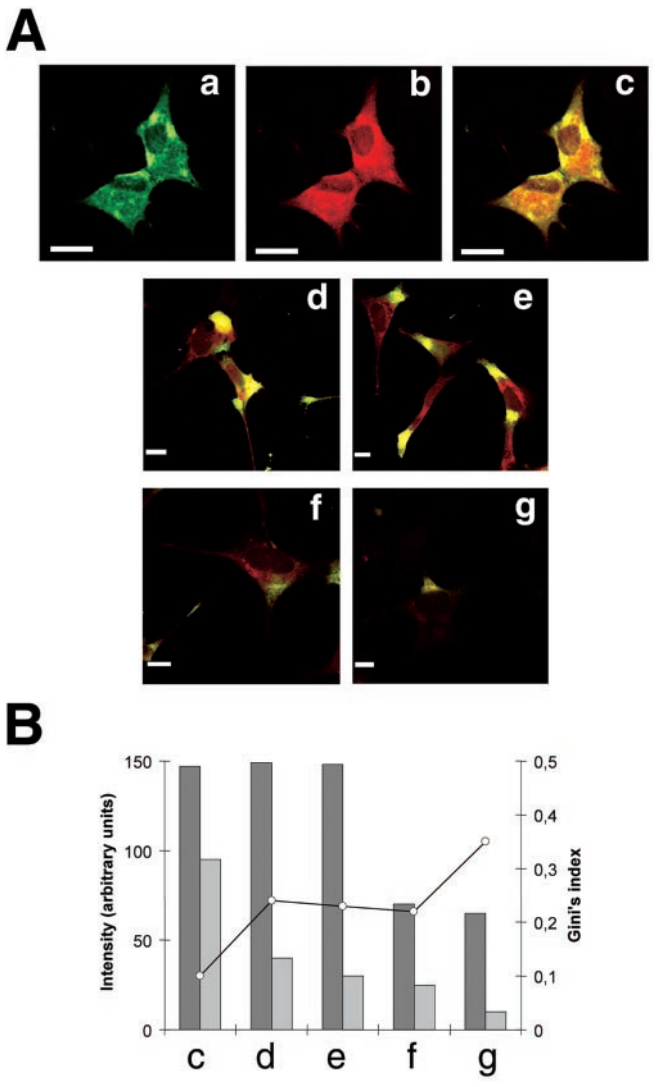

FIG. 1. *A*, double immunofluorescence staining and confocal images of SH-SY5Y neuroblastoma cells stably transfected with the cDNA encoding for human D_2R (long form). Cells were processed for immunostaining using fluorescein (*green*)-conjugated rabbit anti-$A_{2A}R$ antibodies and rhodamine (*red*)-conjugated rabbit anti-D_2R antibodies and analyzed by confocal microscopy. Superimposition of images (*panels c–h*) reveals the colocalization of $A_{2A}R$ and D_2R in *yellow*. *Panels a–c* show $A_{2A}R$ immunoreactivity (*a*), D_2R immunoreactivity (*b*), and $A_{2A}R/D_2R$ colocalization (*c*) in nontreated cells (no agonist preincubation). *Panels d–g* show the effects of 3 h of treatment at 37 °C with CGS-21680 (100 nM) alone (*d*), quinpirole (10 μM) alone (*e*), CGS-21680 (100 nM) and quinpirole (10 μM) (*f*), or CGS-21680 (200 nM) and quinpirole (50 μM) (*g*). Cells were processed for immunostaining after agonist preincubation. Representative images from four independent experiments/treatment are shown; *scale bars*, 10 μm. *B*, semiquantitation of images from *panels c–g* in *A*. The area (*light gray*) where diffuse IR (no or few coaggregates) and the area (*dark gray*) where several coaggregates could be detected were interactively selected. The median intensity values (*left y* axis) for these two types of areas, obtained in the four experimental conditions mentioned above (*c–g*), are given. The Gini's indexes (*right y* axis) for the four experimental conditions (*c–g*) are given. It should be noticed that the Gini's index is low (rather even distribution of the IR intensity among pixels) for nontreated cells (*c*), whereas the Gini's index is high (rather uneven distribution of the IR intensity among pixels) for co-treatment with CGS-21680 (200 nM) plus quinpirole (50 μM) (*g*).

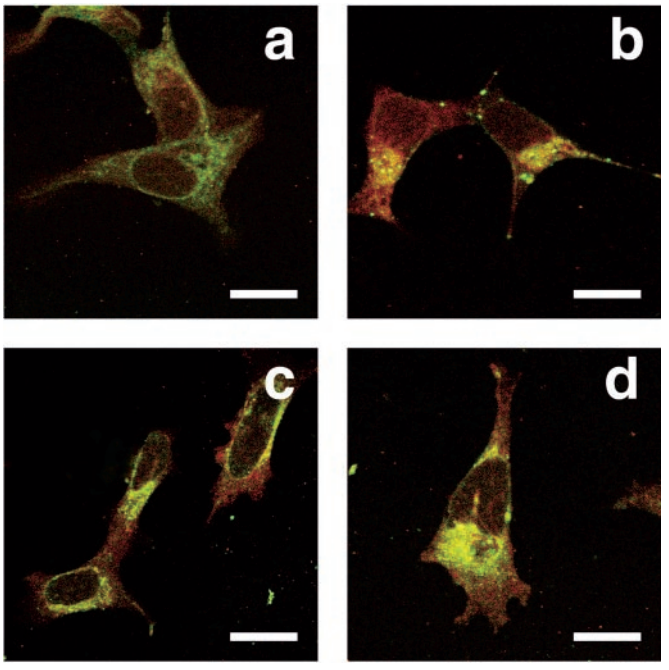

FIG. 2. **Agonist-induced internalization of $A_{2A}R$ and D_2R in SH-SY5Y neuroblastoma cells stably transfected with the cDNA encoding for human D_2R (long form).** Cells were processed for immunostaining using fluorescein (*green*)-conjugated rabbit anti-$A_{2A}R$ antibodies and rhodamine (*red*)-conjugated rabbit anti-D_2R antibodies and analyzed by confocal microscopy. Superimposition of images reveals the colocalization of $A_{2A}R$ and D_2R (*yellow*). Cells were first incubated with anti-$A_{2A}R$ and anti-D_2R antibodies for 2 h at 4 °C in the presence (*b–d*) or absence (*a*) of the agonists. The cells were then placed at 37 °C for 3 h allowing ligand-induced internalization of previously labeled receptors. *Panel a* shows the weak diffuse immunoreactivity of nonpretreated control cells (compare with Fig. 1, *panels c*). *Panels b–d* show the effects of 3 h of treatment at 37 °C with CGS-21680 (200 nM) alone (*b*), quinpirole (50 μM) alone (*c*), or CGS-21680 (200 nM) and quinpirole (50 μM) (*d*). Representative images from four independent experiments/treatment are shown; *scale bars*, 10 μm.

ous amounts of CGS21680 (RBI) and/or quinpirole (RBI) in serum-free medium for 3 h at 37 °C. They were then rinsed with PBS, fixed in 4% paraformaldehyde and 0.06 M sucrose for 15 min, and washed with PBS containing 20 mM glycine. Cells were subsequently treated with PBS, containing 20 mM glycine, and 1% bovine serum albumin for 30 min at room temperature. Double immunostaining was performed with fluorescein-conjugated anti-$A_{2A}R$ antibodies (VC21-FITC, 40 μg/ml) (10) and rhodamine-conjugated anti-D_2R antibodies (D2-246-316, 30 μg/ml) (11) for 1 h at 37 °C. Antipeptide antisera against $A_{2A}R$ were raised in New Zealand White rabbits and characterized as described elsewhere (12). The specific peptide corresponds to the second extracellular loop of the receptor. Anti-$A_{2A}R$ antibodies (VC21) were purified by affinity chromatography using the specific peptide coupled to activated thiol-Sepharose 4B. The coverslips were rinsed for 40 min in the same buffer and mounted with medium suitable for immunofluorescence (ICN). Internalization assays were made as reported elsewhere (12) with some modifications. Cells were incubated in serum-free medium (4 °C, 2 h) with VC21-FITC and rhodamine-conjugated D2-246-316 in the absence (control) or presence of 200 nM CGS 21680 and/or 50 μM quinpirole. Cells were washed with the same medium (without ligands in the control experiments), and internalization of labeled receptors was induced by incubation at 37 °C for 3 h. Cells were fixed and processed as described above. Striatal cultures were exposed to various amounts of CGS21680 and/or quinpirole in the same medium for 6 h at 37 °C. They were then rinsed with PBS, fixed with 4% paraformaldehyde containing 2% picric acid for 1 h, and washed with PBS supplemented with 20 mM glycine. Double or single immunostaining was performed with fluorescein-conjugated anti-$A_{2A}R$ antibodies and rhodamine-conjugated anti-D_2R (D2-246-316) antibodies or fluorescein-conjugated anti-A_1R antibodies (PC21-FITC) (13) for 1 h at 37 °C. Microscopic observations were made in Leica TCS 4D (Leica Lasertechnik) confocal scanning laser equipment adapted to an inverted Leitz DMIRBE microscope. Image analysis was performed with a KS 400 image analyzer (Zeiss). After acquisition of the superimposed images (yellow color) of the $A_{2A}R/D_2R$ IR, the area of the cell nucleus was interactively discarded. Densitometric evaluation was performed on this new image. The median values of the histograms representing the intensity of A_2R/D_2R IR in areas with coaggregates (interactively encircled) and in areas with no or few aggregates (interactively encircled) were taken as representative val-

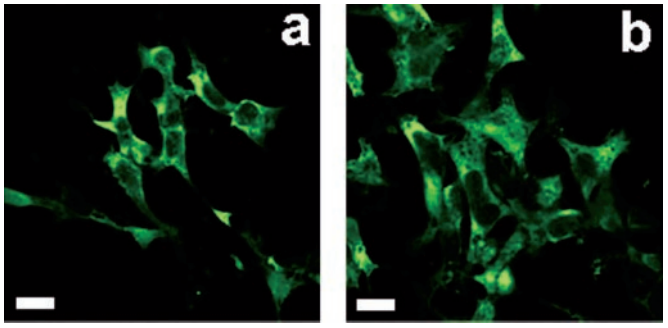

FIG. 3. **Immunostaining of parental SH-SY5Y neuroblastoma cells.** Untransfected SH-SY5Y cells were processed for immunostaining using fluorescein (*green*)-conjugated rabbit anti-A_{2A}R antibodies after exposure to medium in the absence (*a*) or presence (*b*) of 100 μM quinpirole (3 h, 37 °C). Representative images from three independent experiments are shown; *scale bar*, 10 μm.

ues in their respective areas. A quantitative evaluation of the degree of unevenness of the $A_{2A}R/D_2R$ receptor codistribution was obtained by calculating the Gini's index (14, 15), which here measures the distribution of the IR intensity, pixel by pixel, in the sampled area. The Gini's index ranges from 0 (even distribution, *i.e.* the IR intensity is equally distributed among pixels) to 1 (maximal concentration, *i.e.* the IR intensity is concentrated in one single pixel) (14).

Coimmunoprecipitation Experiments—SH-SY5Y neuroblastoma cell membranes were obtained by disrupting the cells with a Polytron homogenizer (Kinematica, PTA 20TS rotor, setting 4; Brinkmann) for three 5-s periods in 50 mM Tris-HCl, pH 7.4. Membranes were separated by centrifugation at 105,000 × *g* for 45 min at 4 °C. They were then solubilized in ice-cold lysis buffer (PBS, pH 7.4, Nonidet P-40, 0.5% sodium deoxycholate, 0.1% SDS) for 1 h on ice and then centrifuged at 80,000 × *g* for 90 min. The supernatant was immunoprecipitated as previously described (6) using anti-A_{2A}R antibodies (VC21) or an irrelevant IgG covalently coupled to protein A-Sepharose. Immunoprecipitates were resolved by SDS-PAGE, and Western blots were performed with anti-A_{2A}R, anti-A_1R (PC11), or anti-D_2R antibodies (for details, see Ref. 6).

D_2R- and D_1R transfected mouse fibroblast Ltk^- cells were transiently transfected with A_{2A}R cDNA double-tagged with hemagglutinin (HA-A_{2A}R-HA) (16) by calcium phosphate precipitation (8, 9). Immunoprecipitation of HA-A_{2A}R-HA was performed with anti-HA antibodies (Babco) covalently coupled to protein G-Sepharose. Immunoprecipitation and immunoblotting were done following standard protocols (6). Immunoblots were developed with ECL Western blot detection system.

cAMP Accumulation Experiments—Neuroblastoma or striatal cells were incubated with [^{3}H]adenine (24 Ci/mmol; Amersham Biosciences; 1 μCi/well) for 2 h at 37 °C in serum-free medium. They were subsequently washed with PBS and incubated for 10 min at 37 °C in PBS containing 100 μM phosphodiesterase inhibitor RO-20-1724 (Calbiochem). Various concentrations of forskolin, CGS 21680, and/or quinpirole were then added and the cells placed at 37 °C for an additional 10 min. The incubation solution was then discarded and replaced by ice-cold 0.3 M perchloric acid containing [^{14}C]cAMP (51.3 mCi/mmol; PerkinElmer Life Sciences) as an internal standard. After sonication and centrifugation (8,000 × *g* for 5 min), [^{3}H]cAMP present in the supernatant was identified by sequential chromatography (17). Formation of cAMP was expressed as the percentage of conversion of total [^{3}H]ATP into [^{3}H]cAMP. For statistical analysis, one-way ANOVA (followed by *post hoc* Scheffe's multiple comparison test) and Mann-Whitney's *U* test were used.

RESULTS

Colocalization of $A_{2A}R$ and D_2R in Nontreated SH-SY5Y Neuroblastoma Cells: Immunolabeling Experiments—$A_{2A}R/D_2R$ interactions were first studied in a previously characterized human neuroblastoma cell line (SH-SY5Y) stably transfected with human D_2R (long form) (about 1100 fmol/mg of protein) (7). This cell line constitutively expresses functional A_{2A}R (about 200 fmol/mg of protein), the activation of which decreases the affinity of the transfected D_2R for dopamine and counteracts D_2R-mediated intracellular [$Ca^{2+}{}_i$] response (7). Double immunofluorescence experiments including image

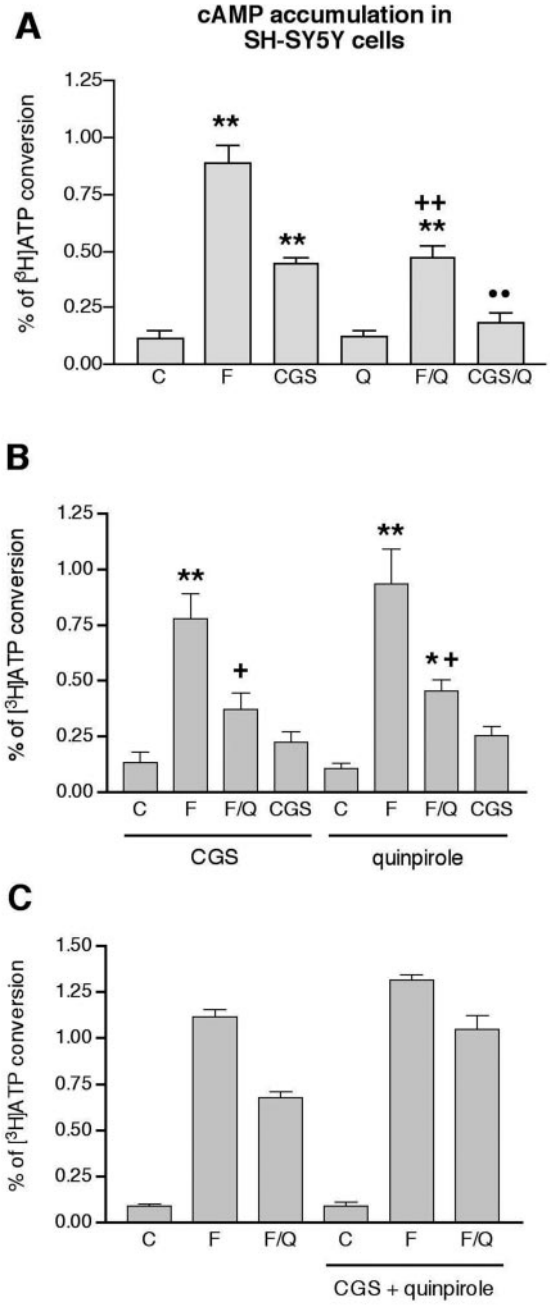

FIG. 4. **cAMP accumulation experiments in SH-SY5Y neuroblastoma cells stably transfected with D_2R (long form).** Results represent means ± S.E. and are expressed as percentage of conversion of total [^{3}H]ATP to [^{3}H]cAMP (n = 6–8). *A*, effects of 10 μM forskolin (*F*), 1 μM CGS 21680 (*CGS*), and 1 μM quinpirole (*Q*), alone or in combination, without agonist preincubation. Quinpirole significantly decreased forskolin- and CGS-induced cAMP accumulation. **, $p < 0.01$ compared with control (*C*); ++, $p < 0.01$ compared with forskolin; ••, $p < 0.01$ compared with CGS; one-way ANOVA and *post hoc* Scheffe's multiple comparison test. *B*, effects of 10 μM forskolin (*F*), 1 μM CGS 21680 (*CGS*), and 1 μM quinpirole (*Q*), alone or in combination, after preincubation for 3 h with either 200 nM CGS 21680 or 50 μM quinpirole. Preincubating the cells with either agonist counteracted CGS 21680-induced cAMP accumulation. ** and *, $p < 0.01$ and $p < 0.05$, respectively, compared with control (*C*); +, $p < 0.05$ compared with forskolin; one-way ANOVA and *post hoc* Scheffe's multiple comparison test. *C*, effects of 10 μM forskolin in the absence (*F*) and presence of 1 μM quinpirole (*F*/*Q*) with and without preincubation for 3 h with 200 nM CGS 21680 and 50 μM quinpirole. The counteractive effect of quinpirole on forskolin-induced cAMP accumulation was significantly lower after simultaneous preincubation with A_{2A}R and D_2R agonists (17.1%/11.4%, in median/interquartile range; n = 7) than without preincubation (40.7%/5.8%, in median/interquartile range; n = 7) ($p < 0.01$; Mann-Whitney *U* test).

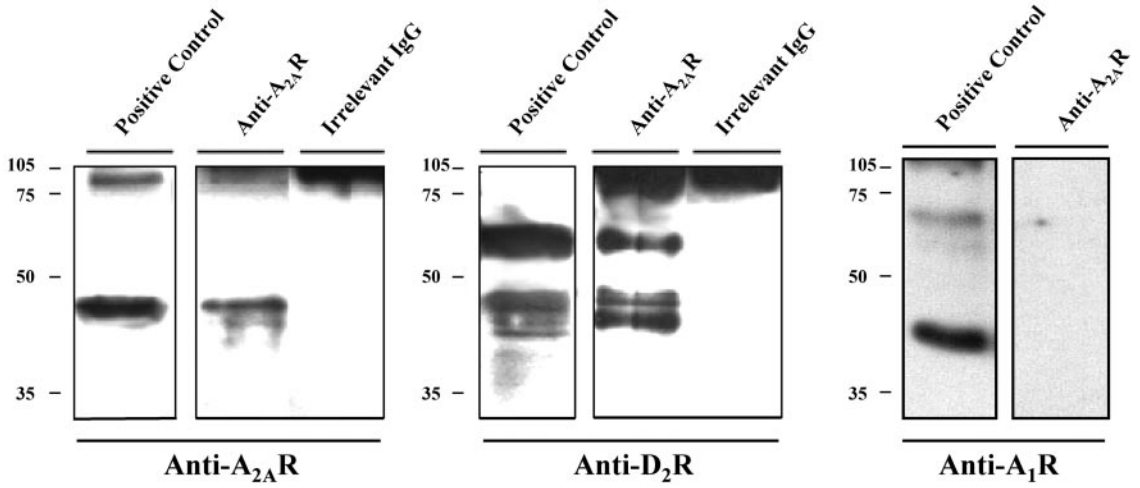

FIG. 5. **Coimmunoprecipitation of $A_{2A}R$ and D_2R from membrane preparations of SH-SY5Y neuroblastoma cells stably transfected with D_2R (long form).** Immunoprecipitation with anti-$A_{2A}R$ antibodies was followed by Western blotting with antibodies against $A_{2A}R$ (*left*), against D_2R (*middle*), or against A_1R (*right*). For positive control an aliquot of cell membrane extracts was used.

analysis were performed in nonpermeabilized cells, using fluorescein-conjugated anti-$A_{2A}R$ antibodies (*green color*) and rhodamine-conjugated anti-D_2R antibodies (*red color*). As seen in Fig. 1*A* (*panels a* and *b*), there is a clear spatial predominance of D_2R *versus* $A_{2A}R$ immunoreactivity, which is in agreement with the higher D_2R density found in previous binding experiments (7). Confocal analysis revealed substantial colocalization of both receptors at the membrane level (*yellow color* in Fig. 1*A*, *panel c*), which indicates that in the absence of exogenous agonists the lateral distance between the two receptor proteins is less than 0.1 μm. A semi-quantitative analysis of the distribution of the *yellow* was done by evaluating the intensity of the color (which directly reflects the amount of coexisting receptors) and calculating the Gini's index or GI (a measure of unevenness, which evaluates the proportion of coaggregates in the sampled area). These calculations were completed on the whole cell body membrane, as well as on the areas of the cell body membrane containing coaggregates and on the parts with few or no coaggregates (Fig. 1*B*). In nontreated cells (Fig. 1*A*, *panel c*), high amounts of coexisting receptors were found both in the cell body membrane with coaggregates and in the cell body membrane displaying a more diffuse distribution of $A_{2A}R/D_2R$ IR. The GI value of these cells was 0.10, indicating a rather even distribution of the colocated $A_{2A}R/D_2R$ IR and few coaggregates of the two receptors (Fig. 1*B*).

Coaggregation of $A_{2A}R$ and D_2R in CGS 21680- or Quinpirole-treated SH-SY5Y Cells: Immunolabeling Experiments—Substantial modifications of $A_{2A}R$ and D_2R distribution were obtained when the cells were treated with the $A_{2A}R$ agonist CGS 21680 or the D_2R agonist quinpirole. Hence, 3 h of treatment with either CGS 21680 (100 nM, Fig. 1*A*, *panel d*) or quinpirole (10 μM, Fig. 1*A*, *panel e*) induced an aggregation of both $A_{2A}R$ and D_2R. Similar effects were also observed with shorter incubation times at higher agonist concentrations (data not shown). Thus, 3 h of incubation at these concentrations give a maximal effect. The computer-assisted analysis of the confocal images showed an increase in unevenness of the yellow distribution (GI for the entire cell body membrane was 0.23 for CGS 21680- and 0.20 for quinpirole-treated cells). Furthermore, the yellow intensity value was still high for the cell body membrane with $A_{2A}R/D_2R$ coaggregates but very low for the cell body membrane with diffusely distributed $A_{2A}R/D_2R$ IR (Fig. 1*B*). Altogether, this analysis indicates the presence on the cell body membrane of an increased proportion of $A_{2A}R/D_2R$ coaggregates.

Cointernalization of $A_{2A}R$ and D_2R in CGS 21680- or Quinpirole-treated SH-SY5Y Cells: Immunolabeling Experiments—Cotreatment with CGS 21680 (100 nM) and quinpirole (10 μM) markedly decreased the yellow intensity values of the cell body membrane associated with coaggregates and diffusely distributed $A_{2A}R/D_2R$ IR as compared with untreated cells (Fig. 1, *A (panel f)* and *B*). This indicates that cotreatment with CGS 21680 (100 nM) and quinpirole (10 μM) induces coaggregation followed by cointernalization of $A_{2A}R$ and D_2R. A stronger reduction in D_2R IR (*red*) was, however, obtained with higher concentrations of quinpirole (50 μM) and CGS 21680 (200 nM) (Fig. 1*A*, *panel g*). At these concentrations of the agonists, the Gini's index was high (0.30) reflecting an uneven distribution of $A_{2A}R/D_2R$ IR. In addition, the values for the yellow intensity in the cell body membrane with $A_{2A}R/D_2R$ coaggregates and the cell body membrane with diffusely distributed $A_{2A}R/D_2R$ IR were, respectively, low and very low (Fig. 1*B*). This suggests that a cotreatment of the cells with high doses of the agonists potentiates both coaggregation and cointernalization of $A_{2A}R$ and D_2R. Ligand-induced cointernalization was confirmed in experiments where cells were first labeled with anti-$A_{2A}R$ and anti-D_2R antibodies for 2 h at 4 °C in the absence (Fig. 2, *panel a*) or in the presence of CGS21680 (200 nM) and/or quinpirole (50 μM) (Fig. 2, *panels b–d*). Subsequently, the ligand-induced internalization of labeled receptors was allowed to occur by incubating the cells for 3 h at 37 °C. Confocal analysis revealed colocalized $A_{2A}R/D_2R$ aggregates inside the cell after pretreatment with either CGS 21680 (200 nM) or quinpirole (50 μM) (Fig. 2, *panels b* and *c*), which became more pronounced after pretreatment with both compounds (Fig. 2, *panel d*).

Absence of Quinpirole-induced Aggregation of $A_{2A}R$ in Parental SH-SY5Y Cells: Immunolabeling Experiments—The involvement of D_2R in quinpirole-mediated effects was assessed using parental neuroblastoma SH-SY5Y cells, which express very low levels of D_2R (7). Hence, quinpirole at 100 μM for 3 h did not induce any modification of $A_{2A}R$ immunolabeling pattern (Fig. 3).

Codesensitization of $A_{2A}R$ and D_2R in CGS 21680- and Quinpirole-treated SH-SY5Y Cells: cAMP Accumulation Experiments—Under basal conditions 1 μM CGS 21680 significantly increased cAMP accumulation in SH-SY5Y neuroblastoma cells (Fig. 4*A*). Quinpirole (1 μM) did not modify cAMP levels but significantly counteracted both forskolin (10 μM)-induced and CGS 21680-induced increases in cAMP accumulation (Fig. 4*A*). These results confirm the existence of functional and in-

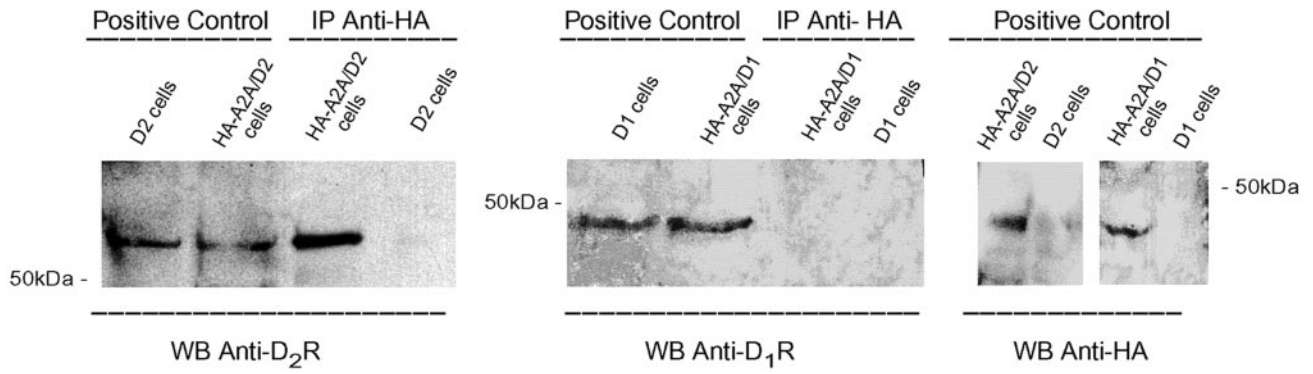

FIG. 6. **Coimmunoprecipitation of HA-A_{2A}R-HA and D_2R from membrane preparations of mouse Ltk$^-$ fibroblasts.** Ltk$^-$ fibroblasts stably transfected with either human dopamine D_2R (long form) or human dopamine D_1R were transiently transfected with either double-tagged HA-A_{2A}R-HA (HA-A_{2A}R-HA/D_2R and HA-A_{2A}R-HA/D_1R cells) or an irrelevant plasmid (D_2R and D_1R cells). An aliquot of cell membrane extracts was used as a positive control. *WB*, Western blot; *IP*, immunoprecipitation.

teracting A_{2A}R and D_2R in D_2R-transfected neuroblastoma cells (7). After 3 h of incubation with either 200 nM CGS 21680 or 50 μM quinpirole (and subsequent withdrawal of the agonists, see "Experimental Procedures"), CGS 21680 was no longer able to significantly increase cAMP levels (Fig. 4*B*). This demonstrates the existence of both homologous and D_2R-mediated heterologous desensitization of A_{2A}R. Instead, the inhibitory effect of quinpirole on forskolin-induced elevation of cAMP levels was about the same (40–50% inhibition) under basal conditions and after a 3-h incubation with the A_{2A}R or the D_2R agonist (Fig. 4, *A* and *B*). Thus, as already described, A_{2A}R clearly desensitized after A_{2A}R agonist incubation (18, 19) and D_2R (long form) showed resistance to D_2R agonist-induced desensitization (20). However, after 3 h of incubation with both quinpirole (50 μM) and CGS 21680 (200 nM), quinpirole (1 μM) inhibited forskolin-induced cAMP accumulation by only 17.1%/11.4% (median/interquartile range) (Fig. 4*C*). This effect, when compared with the effect of quinpirole on untreated cells, was significantly different (Mann-Whitney *U* test: $p < 0.01$). Hence, quinpirole was found to inhibit forskolin-induced cAMP accumulation by 40.7%/5.8% (median/interquartile range) (Fig. 4*C*). Therefore, costimulation of A_{2A}R and D_2R accelerates D_2R desensitization, likely by causing increased D_2R internalization (see above).

Coimmunoprecipitation of A_{2A}R and D_2R in Membrane Preparations from SH-SY5Y Neuroblastoma Cells and Ltk$^-$ Fibroblast Cells—The possible existence of A_{2A}R/D_2R heteromeric complexes was then analyzed by coimmunoprecipitation performed on membrane preparation of D_2R-transfected SH-SY5Y neuroblastoma cells. Immunoprecipitation with anti-A_{2A}R antibodies followed by Western blotting with anti-D_2R antibodies revealed three bands of 43, 47, and 63 kDa (Fig. 5), corresponding to different glycosylated states of the D_2R (21). The same three bands were also obtained in control lysate preparations (Fig. 5). On the other hand, immunoprecipitation with anti-A_{2A}R antibodies followed by Western blotting with anti-A_1R did not reveal any band corresponding to A_1R, indicating the absence of A_{2A}R-A_1R co-immunoprecipitation (Fig. 5). A Western blotting performed with control lysate preparations showed a band of ~40 kDa, which corresponds to the A_1R (Fig. 5). A_{2A}R/D_2R interactions were also examined in mouse fibroblast Ltk$^-$ cells stably transfected with the human D_2R (long form) or human D_1R (8, 9). These two cell lines express a similar density of transfected dopamine receptors (2.8 pmol/mg protein of D_2R in the D_2R-Ltk$^-$ cell line and 4.2 pmol/mg protein of the D1R in the D1R-Ltk$^-$ cell line (Refs. 8 and 9)). Both cell lines were transiently transfected with either dog A_{2A}R cDNA double-tagged with hemagglutinin (HA-A_{2A}R-HA) or an irrelevant plasmid. Antibodies against the hemagglutinin tag (anti-HA) were able to precipitate a band of ~65 kDa detected in Western blot with the anti-D_2R antibodies but only from cells that express both D_2R and HA-A_{2A}R-HA (Fig. 6). This band corresponds to the highly glycosylated state of D_2R (21). As a positive control, we showed that this band could also be obtained from lysates of D_2R-transfected Ltk$^-$ cells, thus being independent of the presence of HA-A_{2A}R-HA. Antibodies against anti-HA failed to coimmunoprecipitate D_1R in cells expressing D_1R/HA-A_{2A}R antibodies, assessing for the specificity of the A_{2A}R/D_2R coimmunoprecipitation (Fig. 6). These results demonstrate for the first time that A_{2A}R and D_2R assemble into heteromeric complexes in two different cell lines that coexpress both receptors and that these complexes exist in the absence of exogenous agonists.

Colocalization and Coaggregation of A_{2A}R and D_2R in Cultured Striatal Neurons: Immunolabeling Experiments—A_{2A}R/D_2R interactions were also studied in neuronal primary cultures of rat striatum. Cells were grown for 2 weeks and immunostained for A_{2A}R and D_2R (see above). Immunolabeling of A_1R on nonpermeabilized cells was also performed. Most neurons exhibited A_{2A}R and D_2R IR in the soma and in the dendrites, however, with predominance of D_2R to A_{2A}R IR in the dendrites (Fig. 7*A*). As for neuroblastoma cells, confocal analysis revealed a high degree of A_{2A}R/D_2R colocalization in the absence of exposure to exogenous agonists (Fig. 7*A*). Treatment (6 h) with either the A_{2A}R agonist CGS 21680 (100 nM) or the D_2R agonist quinpirole (10 μM) induced aggregation of both A_{2A}R and D_2R (Fig. 7*A*) and reduction in IR intensity. However, no synergism was observed when cells were cotreated with CGS 21680 (100 nM) and quinpirole (10 μM) for the same time (Fig. 7*A*). To assess the specificity of A_{2A}R/D_2R interactions, cells were incubated with 10 μM quinpirole for 6 h and immunostained with anti-A_1R antibodies. No change in the pattern of distribution of A_1R present in the soma and dendrites was observed (Fig. 7*B*). In addition and instead of A_{2A}R/D_2R, no aggregates were seen, which confirms the specificity of A_{2A}R/D_2R interactions. Cointernalization experiments analogous to those described in Fig. 2 could not be performed in cultured striatal cells, which did not tolerate the temperature conditions of the experimental internalization protocol (cells changed morphology and fell off the coverslip).

Interaction between A_{2A}R and D_2R in Cultured Striatal Neurons: cAMP Accumulation Experiments—Both basal and forskolin-induced cAMP accumulation were about 10 times higher than in neuroblastoma cells (Fig. 8*A*). This could explain why, unlike what was observed in neuroblastoma cells, CGS 21680 (1 μM) did not induce any significant increase in cAMP accumulation compared with basal values (Fig. 8*A*). As for neuroblastoma cells, quinpirole (1 μM) did not modify cAMP levels

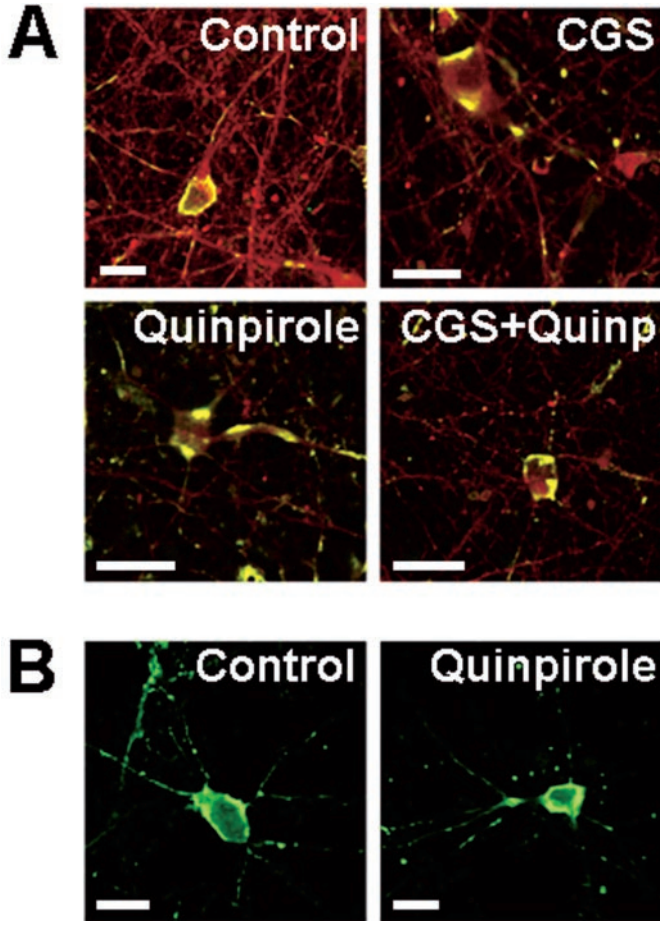

FIG. 7. **Double immunofluorescence staining and confocal images of striatal neurons in culture.** *Panel A*, cells were exposed for 6 h to either 100 nM CGS-21680, 10 μM quinpirole, or both and were processed for immunostaining using fluorescein (*green*)-conjugated rabbit anti-A_{2A}R antibodies and rhodamine (*red*)-conjugated rabbit anti-D_2R antibodies. The cells were analyzed by confocal microscopy. Superimposition of images reveals the colocalization of A_{2A}R and D_2R in *yellow*. *Panel B*, staining of adenosine A_1R with fluorescein (*green*)-conjugated anti-A_1R antibodies. Note the lack of effect of 10 μM quinpirole (6 h). Representative images from four to five independent experiments/treatment are shown; *scale bar*, 10 μm.

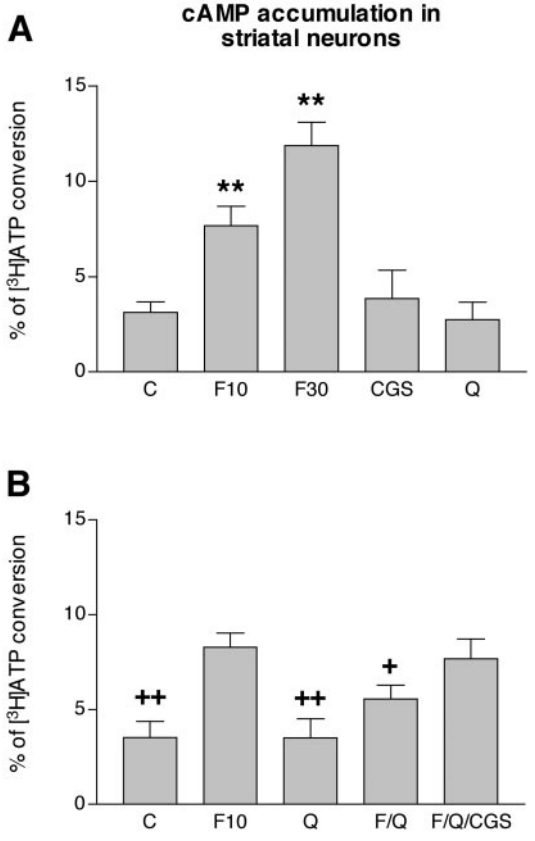

FIG. 8. **cAMP accumulation experiments in striatal neurons in culture.** Results represent means ± S.E. and are expressed as percentage of conversion of total [^{3}H]ATP to [^{3}H]cAMP (n = 10–14). *A*, effects of 10 and 30 μM forskolin (*F10* and *F30*, respectively), 1 μM CGS 21680 (*CGS*), and 1 μM quinpirole (*Q*). Forskolin, but not CGS 21680, significantly increased cAMP accumulation. **, $p < 0.01$ compared with control (*C*); one-way ANOVA. *B*, effects of 10 μM forskolin (*F*), 1 μM CGS 21680 (*CGS*), and 1 μM quinpirole (*Q*), alone or in combination. CGS 21680 counteracted the inhibitory effect of quinpirole on forskolin-induced cAMP accumulation. + and ++, $p < 0.05$ and $p < 0.01$, respectively, compared with forskolin; one-way ANOVA and *post hoc* Scheffe's multiple comparison test.

but significantly reduced forskolin (10 μM)-induced cAMP accumulation (Fig. 8*B*). Finally, CGS 21680 (1 μM) counteracted the effect of quinpirole on forskolin-induced cAMP accumulation (Fig. 8*B*). These results provide a functional demonstration of the antagonistic A_{2A}R/D_2R interactions in striatal neurons in culture.

DISCUSSION

The main findings of the present work are first that A_{2A}R and D_2R are colocalized and form heteromers in untreated neuronal cells and that they coaggregate upon long term exposure to either agonist. The formation of A_{2A}R/D_2R heteromers and aggregates is receptor subtype-specific because co-expression of A_{2A}R/D_1R (present study) or A_1R/D_2R (6) does not lead to formation of heteromers. Furthermore, A_{2A}R did not form heteromeric complexes with A_1R (present study). This phenomenon may therefore constitute the molecular basis for the selective A_{2A}R/D_2R interactions observed *in vitro*, like A_{2A}R modulation of D_2 binding characteristics (7, 8, 22, 23), counteraction of D_2R-mediated intracellular [Ca^{2+}i] responses (7), and inhibition of cAMP accumulation (see Ref. 23 and present paper). The same type of antagonism was observed *in vivo* with the A_{2A}R inhibition of D_2R-mediated regulation of GABA release in the globus pallidus and of D_2R-mediated increases in motor activity (1, 5). Besides acute antagonistic actions, the A_{2A}R/D_2R heteromers may be involved in receptor trafficking, because long term exposure to either A_{2A}R or D_2R agonists induces aggregation and cotreatment with these agonists induces internalization of both receptors. Moreover, prior exposure to A_{2A}R or D_2R agonists can produce a desensitization of the A_{2A}R in terms of cAMP accumulation associated with coaggregation. In contrast, co-exposure to A_{2A}R and D_2R agonists, but not to any of the two agonists alone, causes desensitization of D_2R-mediated inhibition of cAMP accumulation, which is associated with cointernalization. The present observation that A_{2A}R and D_2R functions are simultaneously altered after long exposure to agonists can aid in understanding behavioral findings involving cross-tolerance and cross-sensitization between dopamine agonists and compounds active at adenosine receptors (such as caffeine) (24, 25). Together with other recently reported findings, the present results suggest that changes in A_{2A}R function may be involved in the secondary effects observed after chronic intermittent treatment with L-DOPA such as reduced antiparkinsonian activity and dyskinesia (26). Adenosine is a feedback detector of neuronal activation, in view of the fact that it allows the neuronal network to return into a resting state (27). Adenosine is therefore expected to increase in the striatal extracellular fluid from patients with Parkinson's disease mainly after chronic intermittent L-DOPA

treatment and in agreement with the evidence of increased striatal glutamate drive (28). Hence, striatal extracellular levels of adenosine have been found to increase in the 1-methyl-4-phenyl-1,2,3,6-tetrahydropyridine model of Parkinson's disease (29). Thus, the wearing off of the antiparkinsonian action of L-DOPA treatment may in part be caused by the simultaneous chronic activation of $A_{2A}R$ and D_2R that, according to the present results, may lead to substantial cointernalization of both receptors. The coadministration of $A_{2A}R$ antagonists together with L-DOPA or dopamine D_2R agonists may therefore provide a new therapeutic approach lacking the secondary effects of chronic L-DOPA treatment (30, 31). Overall, the present and previous (1, 5) data implicate that the membrane interactions taking place between $A_{2A}R$ and D_2R via heteromeric complexes represent a crucial mechanism influencing D_2R-mediated transmission. This prompts development of adenosine and dopamine antagonists/agonists compounds preferentially active on $A_{2A}R/D_2R$ heteromers as new drugs for the treatment of neuropsychiatric diseases, such as Parkinson's disease (30, 31), schizophrenia (32, 33), Huntington's disease (34), and dystonia (35), in which D_2R have been implicated.

REFERENCES

1. Ferré, S., Fredholm, B. B., Morelli, M., Popoli, P., and Fuxe, K. (1997) *Trends Neurosci.* **20,** 482–487
2. Schiffmann, S. N., Jacobs, O., and Vanderhaeghen, J.-J. (1991) *J. Neurochem.* **57,** 1062–1067
3. Fink, J. S., Weaver, D. R., Rivkees, S. A, Peterfreund, R. A., Pollack, A. E., Adler, E. M., and Reppert, S. M. (1992) *Mol. Brain Res.* **14,** 186–195
4. Ferré, S., O'Connor, W. T., Svenningsson, P., Bjorklund, L., Lindberg, J., Tinner, B., Stromberg, I., Goldstein, M., Ogren, S. O., Ungerstedt, U., Fredholm, B. B., and Fuxe, K. (1996) *Eur. J. Neurosci.* **8,** 1545–1553
5. Fuxe, K., Ferré, S., Zoli, M., and Agnati, L. F. (1998) *Brain Res. Rev.* **26,** 258–273
6. Ginés, S., Hillion, J., Torvinen, M., Le Crom, S., Casado, V., Canela, E. I., Rondin, S., Lew, J. Y., Watson, S., Zoli, M., Agnati, L. F., Vernier, P., Lluis, C., Ferré, S., Fuxe, K., and Franco, R. (2000) *Proc. Natl. Acad. Sci. U. S. A.* **97,** 8606–8611
7. Salim, H., Ferré, S., Dalal, A., Peterfreund, R. A., Fuxe, K., Vincent, J. D., and Lledo, P. M. (2000) *J. Neurochem.* **74,** 432–439
8. Dasgupta, S., Ferré, S., Kull, B., Hedlund, P. B., Finnman, U. B., Ahlberg, S., Arenas, E., Fredholm, B. B., and Fuxe, K. (1996) *Eur. J. Pharmacol.* **316,** 325–331
9. Ferré, S., Torvinen, M., Antoniou, K., Irenius, E., Civelli, O., Arenas, E., Fredholm, B. B., and Fuxe, K. (1998) *J. Biol. Chem.* **273,** 4718–4724
10. Sarrio, S., Casado, V., Escriche, M., Ciruela, F., Mallol, J., Canela, E. I., Lluis, C., and Franco, R. (2000) *Mol. Cell. Biol.* **20,** 5164–5174
11. Bjelke, B., Goldstein, M., Tinner, B., Andersson, C., Sesack, S. R., Steinbusch, H. W., Lew, J. Y., He, X., Watson, S., Tengroth, B., and Fuxe, K. (1996) *J. Chem. Neuroanat.* **12,** 37–50
12. Saura, C. A., Mallol, J., Canela, E. I., Lluis, C., and Franco, R. (1998) *J. Biol. Chem.* **273,** 17610–17617
13. Ciruela, F., Casado, V., Mallol, J., Canela, E. I., Lluis, C., and Franco, R. (1995) *J. Neurosci. Res.* **42,** 818–828
14. Duncan, O. D. (1977) in *The Measurement of Population* (Smith, D., and Keyfitz, N., eds) pp. 349–363, Springer Verlag, London
15. Agnati, L. F., Fuxe, K., Zini, I., Calza, L., Benfenati, F., Zoli, M., Hokfelt, T., and Goldstein, M. (1982) *Neurosci. Lett.* **32,** 253–258
16. Olah, M. E. (1997) *J. Biol. Chem.* **272,** 337–344
17. Salomon, Y., Londos, C., and Rodbell, M. (1974) *Anal. Biochem.* **58,** 541–548
18. Palmer, T. M., Gettys, T. W., Jacobson, K. A., and Stiles, G. L. (1994) *Mol. Pharmacol.* **45,** 1082–1094
19. Mundell, S. J., and Kelly, E. (1998) *Br. J. Pharmacol.* **125,** 1594–1600
20. Ng, G. Y., Varghese, G., Chung, H. T., Trogadis, J., Seeman, P., O'Dowd, B. F., George, S. R. (1997) *Endocrinology* **138,** 4199–4206
21. Fishburn, C. S., Elazar, Z., and Fuchs, S. (1995) *J. Biol. Chem.* **270,** 29819–29824
22. Ferré, S., von Euler, G., Johansson, B., Fredholm, B. B., and Fuxe, K. (1991) *Proc. Natl. Acad. Sci. U. S. A.* **88,** 7238–7241
23. Kull, B., Ferré, S., Arslan, G., Svenningsson, P., Fuxe, K., Owman, C., and Fredholm, B. B. (1999) *Biochem. Pharmacol.* **58,** 1035–1045
24. Fenu, S., Cauli, O., and Morelli, M. (2000) *Behav. Brain. Res.* **114,** 97–105
25. Garrett, B. E., and Holtzman, S. G. (1994) *Eur. J. Pharmacol.* **262,** 65–75
26. Zeng, B. Y., Pearce, R. K., MacKenzie, G. M., and Jenner, P. (2000) *Eur. J. Neurosci.* **12,** 1096–1104
27. Ferré, S., and Fuxe, K. (2000) *Prog. Brain Res.* **125,** 353–361
28. Chase, T. N., and Oh J. D. (2000)*Trends Neurosci.* **23,** S86–S91
29. Nomoto, N., Kaseda, S., Iwata, S., Shimizu, T., Fukuda, T., and Nakagawa, S. (2000) *J. Neurol.* **247,** V16-V22
30. Kanda, T., Jackson, M. J., Smith, L. A., Pearce, R. K., Nakamura, J., Kase, H., Kuwana, Y., and Jenner, P. (1998) *Ann. Neurol.* **43,** 507–513
31. Stromberg, I., Popoli, P., Muller, C. E., Ferré, S., and Fuxe, K. (2000) *Eur. J. Neurosci.* **12,** 4033–4037
32. Ferré, S. (1997) *Psychopharmacology* **133,** 107–120
33. Akhondzadeh, S., Shasavand, E., Jamilian, H., Shabestari, O., and Kamalipour, A. (2000) *J. Clin. Pharmacol. Ther.* **25,** 131–137
34. Popoli, P., Pezzola, A., Reggio, R., Caporali, M. G., and Scotti de Carolis, A. (1994) *Eur. J. Pharmacol.* **257,** R5–R6
35. Richter, A., Hamann, M., and Bartling, C. (2000) *Eur. J. Pharmacol.* **404,** 299–302.(2000)

II-. Canals, M., Marcellino, D., Fanelli, F., Ciruela, F., Benedetti, P., Goldberg, S., Neve, K., Fuxe, K., Agnati, L., Woods, A., Ferré, S., Lluís, C., Bouvier, M. and Franco, R., 2003, "Adenosine A_{2A}-dopamine D_2 receptor-receptor heteromerization. Qualitative and quantitative assessment by fluorescence and bioluminescence energy transfer". *Journal of Biological Chemistry*, 47, 46741-46749.

THE JOURNAL OF BIOLOGICAL CHEMISTRY Vol. 278, No. 47, Issue of November 21, pp. 46741–46749, 2003
Printed in U.S.A.

Adenosine A_{2A}-Dopamine D_2 Receptor-Receptor Heteromerization

QUALITATIVE AND QUANTITATIVE ASSESSMENT BY FLUORESCENCE AND BIOLUMINESCENCE ENERGY TRANSFER*[S]

Received for publication, June 18, 2003, and in revised form, August 20, 2003
Published, JBC Papers in Press, August 21, 2003, DOI 10.1074/jbc.M306451200

Meritxell Canals,[a,b] Daniel Marcellino,[a,b] Francesca Fanelli,[c,d] Francisco Ciruela,[a] Piero de Benedetti,[d] Steven R. Goldberg,[e] Kim Neve[j], Kjell Fuxe,[f] Luigi F. Agnati,[g] Amina S. Woods,[e] Sergi Ferré,[e] Carme Lluis,[a] Michel Bouvier,[h] and Rafael Franco[a,i]

From the [a]Department of Biochemistry and Molecular Biology of the University of Barcelona E-08028, Spain, the [c]Dulbecco Telethon Institute, the [d]Department of Chemistry, and the [g]Department of Biomedical Sciences, University of Modena and Reggio Emilia, 41100 Modena, Italy, the [e]National Institute on Drug Abuse, DHHS, NIH, Intramural Research Program, Baltimore, Maryland 21224, the [f]Department of Neuroscience, Division of Cellular and Molecular Neurochemistry, Karolinska Institutet, S-171 77 Stockholm, Sweden, the [h]Department of Biochemistry, University of Montreal, Montreal, Quebec H3C 3J7, Canada, and [j]the Department of Veterans Affairs Medical Center, Portland, Oregon 97239

There is evidence for strong functional antagonistic interactions between adenosine A_{2A} receptors (A_{2A}Rs) and dopamine D_2 receptors (D_2Rs). Although a close physical interaction between both receptors has recently been shown using co-immunoprecipitation and co-localization assays, the existence of a A_{2A}R-D_2R protein-protein interaction still had to be demonstrated in intact living cells. In the present work, fluorescence resonance energy transfer (FRET) and bioluminescence resonance energy transfer (BRET) techniques were used to confirm the occurrence of A_{2A}R-D_2R interactions in co-transfected cells. The degree of A_{2A}R-D_2R heteromerization, measured by BRET, did not vary after receptor activation with selective agonists, alone or in combination. BRET competition experiments were performed using a chimeric D_2R-D_1R in which helices 5 and 6, the third intracellular loop (I3), and the third extracellular loop (E3) of the D_2R were replaced by those of the dopamine D_1 receptor (D_1R). Although the wild type D_2R was able to decrease the BRET signal, the chimera failed to achieve any effect. This suggests that the helix 5-I3-helix 6-E3 portion of D_2R holds the site(s) for interaction with A_{2A}R. Modeling of A_{2A}R and D_2R using a modified rhodopsin template followed by molecular dynamics and docking simulations gave essentially two different possible modes of interaction between D_2R and A_{2A}R. In the most probable one, helix 5 and/or helix 6 and the N-terminal portion of I3 from D_2R approached helix 4 and the C-terminal portion of the C-tail from the A_{2A}R, respectively.

Heptaspanning membrane receptors (HSMRs)[1] or G protein-coupled receptors (GPCRs) were initially considered monomeric proteins that only interact with G proteins. However, it has become clear that HSMRs are oligomeric structures formed by receptor homodimers, heterodimers, and multimers and a variety of proteins interacting at the plane of the membrane (horizontal level) or across the plane of the membrane (vertical level) (1–6). Current investigation of these macromolecular complexes offers great potential for functional proteomics and offers deeper insight into information handling at the cellular level. The occurrence of oligomeric complexes involving GPCRs and intracellular and extracellular proteins indicates that conformational changes in response to ligand binding to a receptor may be transmitted to other protein molecules within the multimolecular complex. The conformational changes transmitted by direct protein-protein interactions constitute a first level of regulation of a receptor (6). Heteromeric complexes are not distributed randomly in the membrane and form clusters following agonist-induced activation. The intercommunication between heteromeric receptor complexes within clusters represents a second level of regulation (6). It should also be considered that the plasma membrane is not an isomorphic structure, but a structure made by patches with various chemical-physical characteristics (*e.g.* lipid rafts). Therefore, multimeric complexes and agonist-induced clusters may follow preferential routes (owing, for example, to the low viscosity of the membrane) to make contact in the membrane or may be kept as isolated multimeric complexes or clusters within a patch (6).

An example of intercommunicating receptors is that formed by adenosine A_{2A} receptors (A_{2A}Rs) and dopamine D_2 receptors (D_2Rs). Important experimental evidence has accumulated in relation to the existence of functional interactions between A_{2A}Rs and D_2Rs in the basal ganglia (5, 7, 8). These two receptors are specifically localized in one subtype of neurons,

* This work was supported by European Union Grant QLG3-CT-2001-01056; Ministerio de Ciencia y Tecnología Grants BIO1999-0601-C02-02, SAF2002-03293, and SAF2001-3474; Fundacio la Caixa Grant 02/056-00; Fundació Marató of Catalonian Telethon Grant 01/012710; Telethon-Italy Grant TCP00068 and a fellowship for European Advanced Light Microscope Facility short term program at the European Molecular Biology Laboratory in Heidelberg, Germany (to D. M.). The costs of publication of this article were defrayed in part by the payment of page charges. This article must therefore be hereby marked "*advertisement*" in accordance with 18 U.S.C. Section 1734 solely to indicate this fact.

[S] The on-line version of this article (available at http://www.jbc.org) contains Figs. 11 and 12.

[b] These authors contributed equally to this work.

[i] To whom correspondence should be addressed: Dept. of Biochemistry and Molecular Biology, University of Barcelona, Martí i Franquès 1, 08028 Barcelona, Spain. Tel.: 34-93-402-12-08; Fax: 34-93-402-12-19; E-mail: r.franco@bq.ub.es.

[1] The abbreviations used are: HSMR, heptaspanning membrane receptor; GPCR, G protein-coupled receptor; YFP, yellow fluorescent protein; BRET, bioluminescence resonance energy transfer; FRET, fluorescence resonance energy transfer; E_n, extracellular loop n; I_n, intracellular loop n; Mes, 4-morpholineethanesulfonic acid; ANOVA, analysis of variance; Rluc, *Renilla* luciferase; EYFP enhanced yellow fluorescent protein; CHO, Chinese hamster ovary; GFP, green fluorescent protein; PDB, Protein Data Bank; GABA, γ-aminobutyric acid; PBS, phosphate-buffered saline; CH, channel; A_{2A}R, adenosine A_{2A} receptor; D_nR, dopamine D_n receptor.

the striatopallidal γ-aminobutyric acid (GABA)-containing neurons, on which both receptors express their highest density in the brain. The striatopallidal GABAergic neurons play a key role in the pathophysiology of basal ganglia disorders, including Parkinson's disease, and it is a common pathway for the rewarding effects in drug abuse, as well as the antipsychotic effects of neuroleptics. Relationships between $A_{2A}R$ and D_2R have been demonstrated at the biochemical, functional, and behavioral levels, where it has been suggested that the adenosine/dopamine cross-talk in the central nervous system may provide new therapeutic approaches for Parkinson's disease, schizophrenia and drug addiction (5, 7, 8). At the biochemical level, two kinds of antagonistic $A_{2A}R$-D_2R interaction have been discovered, which can explain the $A_{2A}R$-D_2R interaction observed at both the functional and behavioral levels. In the first place, by means of their intramembrane interaction, the stimulation of $A_{2A}R$ decreases the affinity of D_2R for agonists (9). Second, the stimulation of D_2R, a $G_{i/o}$ protein-coupled receptor, inhibits cAMP accumulation induced by the stimulation of the $G_{s/olf}$ protein-coupled $A_{2A}R$ (10). The intramembrane $A_{2A}R$-D_2R interaction implies a close physical interaction between the two receptors. In fact, the pharmacology of D_2R is affected by adenosine analogs activating $A_{2A}R$. Also, co-immunoprecipitation, co-aggregation, and co-internalization of $A_{2A}R$ and D_2R have been recently reported in co-transfected cell lines (10). The existence of a heterologous, *i.e.* D_2R-mediated, desensitization of $A_{2A}R$ (10) is further evidence of the $A_{2A}R$-D_2R cross-talk. However, the demonstration of protein-protein interactions between both receptors in living cells remains to be demonstrated. In the present study, $A_{2A}R$-D_2R heterodimerization in a heterologous mammalian expression system has been investigated by both fluorescence resonance energy transfer (FRET) and bioluminescence resonance energy transfer (BRET). The influence of receptor density and agonist binding on the degree of $A_{2A}R$-D_2R heteromerization was assessed. The results indicate that the two receptors heteromerize and that changes in heteromerization do not occur in response to agonists. Based on the results of biochemical, biophysical, and computational experiments, insights have been gained into $A_{2A}R$-D_2R heterodimer interface.

EXPERIMENTAL PROCEDURES

Cell Lines—HEK-293T cells (American Type Tissue Culture, Manassas, VA) were grown in Dulbecco's modified Eagle's medium supplemented with 2 mM L-glutamine, 100 units/ml penicillin/streptomycin, and 10% (v/v) fetal bovine serum (FBS) at 37 °C and in an atmosphere of 5% CO_2. Cells were passaged when they were 80–90% confluent. All cell culture reagents were from Invitrogen.

Expression Vectors—The human cDNA for Flag-$A_{2A}R$ without its stop codon was amplified using sense and antisense primers harboring unique EcoRI and BamHI sites. The fragment then was subcloned to be in-frame with either *Rluc* or EYFP into the EcoRI and BamHI restriction site of a *Renilla* luciferase-expressing vector (pcDNA3.1-Rluc) or the enhanced yellow variant of GFP (pEYFP-N1; Clontech, Heidelberg, Germany), respectively, to give the two plasmids, $pA_{2A}R$-Rluc and $pA_{2A}R$-EYFP, that express *Rluc* or EYFP on the C-terminal ends of the receptor. The human $D_{2L}R$ was also cloned in the pGFP2-N3(h) and pEYFP-N1 vectors in a similar fashion, however, subcloned into the EcoRI and KpnI site of each respective vector to be in-frame with the GFP fluorescent protein variants, GFP2 and EYFP, respectively. The previously characterized chimeric D_2R-D_1R, in which helices 5 and 6 and third intracellular (I3) and third extracellular (E3) loops of the D_2R have been swapped by the corresponding sequence from the D_1R, was described previously (11). The positive control vector used for the FRET experiments, pGFP2-EYFP, was a gift from the laboratory of R. Pepperkok (EMBL, Heidelberg, Germany) (described in Ref. 12).

Transient Transfections—HEK-293T cells growing on coverslips in 6-well dishes were transiently transfected with 10 μg of DNA encoding the indicated proteins by calcium phosphate precipitation (13). For FRET experiments the LipofectAMINE transfection reagent, FuGENE 6™ (Roche Molecular Biochemicals), was utilized following the product protocol. In both cases and to maintain the ratio of DNA in co-transfections, the empty vector, pcDNA3.1, was used to equilibrate the amount of total DNA transfected. 24 h after transfection, the medium was replaced and cells were then cultured in the same medium until harvested 32, 48, or 72 h after transfection. For FRET experiments cells were fixed with a 3.5% paraformaldehyde solution in PBS for 15 min at room temperature, before washing in PBS and mounting onto slides.

cAMP Determination—The accumulation of cAMP was measured by a [^{3}H]cAMP assay system (Amersham Biosciences) as described in the manual from the manufacturer. Transfected HEK-293 cells (2×10^6 cells/sample) were serum-starved, preincubated with 50 mM Ro 20-1724, a phosphodiesterase inhibitor (Calbiochem, St. Diego, CA) for 10 min, and then stimulated with the indicated concentrations of agonists, CGS21680 ($A_{2A}R$), quinpirole (D_2R), and forskolin (all from Sigma), for 15 min prior to the determination of cAMP levels.

FRET-based Acceptor Photo-bleaching Experiments Analyzed by Confocal Microscopy—Transiently transfected HEK-293T cells were plated onto 15-mm glass coverslips and mounted onto slides using Mowiol mounting medium. Confocal laser scanning microscopy was performed using a Leica SP2 microscope (Leica Microsystems, Mannheim, Germany) equipped with an acousto-optical beamsplitter, a 100-milliwatt argon laser for excitation at 514 nm, and a 20-milliwatt blue diode laser for excitation at 405 nm. GFP2 was excited with the 405 nm laser, YFP was excited with the 514 nm laser, and images were acquired in the following sequence. (i) A pre-photo-bleach YFP (acceptor) image was acquired by scanning while exciting with the 514 nm laser line. (ii) A pre-photo-bleach GFP2 (donor) image was acquired by scanning while exciting with 405 nm laser line. (iii) A region of interest was selected and the acceptor (YFP) was subsequently photo-bleached by scanning repeatedly with the 514 nm laser line until fluorescence signals were at background levels. (iv) A post-photo-bleach image for GFP2 was acquired by scanning with the 405 nm laser line. (v) a second post-photo-bleach image for EYFP was acquired by scanning with the 514 nm laser. In all cases, the spectral imaging was obtained at three fluorescence detection channels (Ch) set to the following ranges: Ch 1: 490–510 nm, Ch 2: 520–540 nm, Ch 3: 545–565 nm. Settings for gain and offset of the detectors were identical for all experiments to keep the relative contribution of the fluorophores to the detection channels constant for spectral un-mixing (see below). The contributions of the GFP variants, GFP2 and YFP, to each of the three detection channels (spectral signature) were measured in experiments with cells expressing only one of these proteins and normalized to the sum of the signal obtained in the three detection channels

FRET Experiments Analyzed by Fluorimetry—Forty-eight hours after transfection, cells were rapidly washed twice in PBS, detached, and resuspended in the same buffer. To control the number of cells, the protein concentration of the samples was determined using a Bradford assay kit (Bio-Rad) using bovine serum albumin dilutions as standards. Cell suspension (20 μg of protein) was distributed in duplicate into 96-well microplates (black plates with a transparent bottom). Plates were read in a Fluostar Optima Fluorimeter (BMG Labtechnologies, Offenburg, Germany) equipped with a high energy xenon flash lamp, using a 10-nm bandwidth excitation filter at 400 nm (393–403 nm), and 10-nm bandwidth emission filters corresponding to 506–515 nm filter (Ch 1) and 527–536 nm filter (Ch 2). Gain settings were identical for all experiments to keep the relative contribution of the fluorophores to the detection channels constant for spectral un-mixing. The contributions of the GFP variants, GFP2 and YFP proteins alone, to the two detection channels (spectral signature) were measured in experiments with cells expressing only one of these proteins and normalized to the sum of the signal obtained in the two detection channels. The spectral signatures of the different receptors fused to either GFP2 or YFP did not significantly vary from the determined spectral signatures of the fluorescent proteins alone.

Quantitation of FRET—Linear un-mixing was done as described by Zimmermann *et al.* (12) to separate the two emission spectra. To determine the fluorescence emitted by each of two individual fluorophores (FluoA corresponding to the donor and FluoB corresponding to the acceptor) in FRET experiments analyzed by confocal microscopy, the following formula was applied for every image pixel i,

$$\mathrm{FluoA}(i) = \frac{S(i)}{1 + \frac{1}{R(i)}} \quad \text{and} \quad \mathrm{FluoB}(i) = \frac{S(i)}{1 + R(i)} \qquad \text{(Eq. 1)}$$

where

$$S(i) = \sum_{k=1}^{n} Ch_k(i) \quad \text{(Eq. 2)}$$

$$R(i) = \frac{\text{FluoA}(i)}{\text{FluoB}(i)} = \frac{B_y Q(i) - B_x}{A_x - A_y Q(i)} \quad \text{(Eq. 3)}$$

and

$$Q(i) = \frac{Ch_x(i)}{Ch_y(i)} \quad \text{(Eq. 4)}$$

where Ch_x and Ch_y represent the signals in detection channels x and y, and A_x, B_x and A_y, B_y represent the normalized contributions of FluoA or FluoB to channels x and y, as they are known from the spectral signatures of the fluorescent proteins. For the fluorimetric experiments, the same equations were applied. By these equations the fluorophore signals, FluoA and FluoB, were calculated using the processing routines written (and generously provided) by T. Zimmermann (EMBL, Heidelberg, Germany) in Interactive Data Language (IDL, Research Systems Inc., Boulder, CO).

According to Zimmermann *et al.* (12), apparent FRET efficiencies E_A in acceptor photo-bleaching experiments were calculated for each pixel i according to Equation 5.

$$E_A(i) = 1 - \frac{F^D(i)}{F^D_{pb}(i)} \quad \text{(Eq. 5)}$$

F^D represents the emitted donor fluorescence (FluoA) before and F^D_{pb} after photo-bleaching of the acceptor. For the fluorimetric experiments, FRET efficiency was calculated as direct sensitization of the acceptor corresponding to acceptor fluorescence (FluoB) after excitation at 400 nm.

BRET Experiments—Forty-eight hours after transfection, cells were rapidly washed twice in PBS, detached, and resuspended in the same buffer. To control the number of cells, sample protein concentration was determined using a Bradford assay kit (Bio-Rad, Munich, Germany) using bovine serum albumin dilutions as standards. To quantify A_{2A}R-*Rluc* and D2-YFP expression, cell suspension (20 μg of protein) was distributed in duplicate into 96-well microplates (Corning 3604, white plates with transparent bottom). The fluorescence was measured using a Packard FluoroCount™ with an excitation filter of 485 nm and an emission filter of 530 nm using the following parameters: gain of 1, photomultiplier fixed at 1100 V, and read time of 1 s. Fluorescence was quantified as in-fold over the background (mock-transfected cells). The same samples were incubated for 10 min with 5 μM coelenterazine H (Molecular Probes, Eugene, OR), and the luminescence was measured using a Packard LumiCount™ with the following parameters: gain of 1, photomultiplier fixed at 700 V, and a read time of 1 s. For BRET measurement, 20 μg of cell suspension were distributed in duplicates in 96-well microplates (Corning 3600, white opaque plates) and 5 μM coelenterazine H was added. After 1 min the readings were collected using a Fusion microplate analyzer (Packard, Meriden, CT) that allows the integration of the signals detected in the 440–500- and the 510–590-nm windows using filters with the appropriate band pass. The BRET ratio is defined as [(emission at 510–590)/(emission at 440–500)] − *Cf* where *Cf* corresponds to (emission at 510–590)/(emission at 440–500) for the -*Rluc* construct expressed alone in the same experiment.

Subcellular Membrane Isolation—HEK-293T cells transiently co-transfected with the A_{2A}R-*Rluc* and D_2RYFP were grown in 100-mm dishes to 80–90% confluence. Cells were washed twice with ice-cold PBS and lysed with 2 ml of ice-cold hypotonic lysis buffer (20 mM HEPES, pH 7.4, 2 mM EDTA, 2 mM EGTA, 6 mM $MgCl_2$, 1 mM phenylmethylsulfonyl fluoride, and 1:100 dilution of a protease inhibitor mixture). Lysate was then sonicated for 30 s, (3 strokes with 1-min delay between strokes) followed by two 10-s bursts in a Polytron tissue grinder. Cellular debris and unlysed cells were removed by centrifuging at 1500 rpm for 5 min at 4 °C. Sucrose was added to achieve a final concentration of 0.2 M, and 2 ml were applied to the top of a discontinuous step gradient (5 ml/step) made at 0.5, 0.9, 1.2, 1.35, 1.5, and 2.0 M sucrose in lysis buffer. The samples were then centrifuged for 16 h at 27,000 rpm at 4 °C in a Beckman SW28 rotor. The plasma membrane was recovered in the sucrose gradient at the interface between 0.5 and 0.9 M. The endoplasmic reticular membrane samples were recovered at the interface between 1.35 and 1.5 M, and luminescence was detected. For the verification of isolated membranes as either plasma or endoplasmic reticulum membranes, fractions were then precipitated with cold acetone overnight and analyzed by Western blotting using monoclonal antibodies against Na^+K^+-ATPase pump (1:250 dilution, Sigma) and calnexin (1:500 dilution, BD Transduction Laboratories).

Raft Disruption—HEK-293T cells were serum-starved overnight 24 h after transfection. Cholesterol depletion was achieved by incubation for 1 h at 37 °C with 2% 2-hydroxypropyl-β-cyclodextrin (β-CD, Sigma) in Dulbecco's modified Eagle's medium. Cholesterol repletion was done, after washing twice with fresh medium, by incubation for 1 h at 37 °C with 0.4% β-CD and 16 mg/ml cholesterol (Sigma). Complete raft disruption was assessed as caveolin-1 displacement in a discontinuous sucrose gradient. For this, confluent control or depleted cells were washed twice with ice-cold PBS, scraped, and resuspended into 2 ml of 500 mM Na_2CO_3, pH 11.0. Cells were sequentially homogenized using a Polytron (3 times, 10 s), a syringe (20 times) and a sonicator (3 times, 30 s), placed at the bottom of an ultracentrifuge tube and adjusted to 45% sucrose in Mes-buffered saline (25 mM Mes, 0,15 M NaCl, pH 6.5). A discontinuous 5–35% sucrose gradient was formed above in Mes-buffered saline containing 250 mM Na_2CO_3, pH 6.5. After centrifugation at 105,000 × *g* for 18 h at 4 °C in a SW41.Ti rotor (Beckman), fractions were collected and analyzed by Western blot using an antibody against caveolin-1 (BD Transduction Laboratories, Lexington, KY). β-CD effects were also tested by mitogen-activated protein kinase phosphorylation analysis; treated cells were directly resuspended in loading buffer and analyzed by Western blot using the antibodies against phosphorylated or total extracellular signal-regulated kinase-1/2 (Sigma).

Three-dimensional Model Building of the Human D_2R and Human A_{2A}R—For the D_2R, the whole sequence of the human short variance (SWISS-PROT entry P14416) was modeled. The intracellular loops 1, 2, and 3 and the extracellular loops 1, 2, and 3 will be, respectively, abbreviated as I1, I2, I3, E1, E2, and E3. Building of I3 (sequence 215–334) was carried out by comparative modeling (by means of MODELER; Ref. 14) by using the domain A2 of Glycyl-TRNA synthetase (PDB entry 1ati; sequence 393–505) as a template, according to the results of fold recognition by means of THREADER (15). This template, characterized by a three-layer ($\alpha\beta\alpha$) sandwich architecture and a Rossmann fold, resulted to be the top hit, holding a reliable z-score (*i.e.* 3.65). Indeed, secondary structure predictions made by four different methods agree acceptably well with the secondary structures computed on the I3 in the selected average minimized structure of D_2R. Similarly, E2 was separately obtained by Molecular Dynamics simulations. A chimeric rhodopsin template (PDB entry 1F88; Ref. 16) was built by introducing the E2 and I3 models after deleting the rhodopsin segments 176–201, 229–235, and 240–243. This template was employed to generate 25 different models of the D_2R according to the sequence alignment shown in Fig. 11 (available as supplementary material in the on-line version of this article). Among these models, the one showing the lowest degree of violation of the structural restraints was used to generate the input structures for Molecular Dynamics simulations. Automatic rotation of the side chains when in bad conformation was performed, leading to different input arrangements. These arrangements were subjected to energy minimization and 150-ps runs of Molecular Dynamics simulations, by means of the program CHARMM (17). Minimizations were carried out by using 1500 steps of steepest descent followed by a conjugate gradient minimization, until the root mean square gradient was less than 0.001 kcal/mol Å. A distance dependent dielectric term ($\epsilon = 4r$) was chosen. The "united atom approximation" was used. The systems were heated to 300 K with 5-K rise, every 100 steps per 6000 steps, by randomly assigning velocities from the Gaussian distribution. After heating, the system was allowed to equilibrate for 34 ps. The lengths of the bonds involving the hydrogen atoms were constrained according to the SHAKE algorithm, allowing an integration time step of 0.001 ps. A disulfide bridge was imposed to form between Cys-107 (3.25) (in parentheses, the numbering from Ballesteros and Weinstein (Ref. 18) for the amino acids in the helix-bundle is reported) and Cys-182 in E2. The secondary structure of the seven helix-bundle was preserved by using the nuclear Overhauser effect constraints. These constraints were applied between the backbone oxygen atoms of residue i and the backbone nitrogen atom of residue $i + 4$, excluding prolines. Different combinations of intra-helix distance constraints were also probed. The non-canonical α-helical structure in the extracellular half of helix 7 was preserved by nuclear Overhauser effect constraints. The structures averaged over the 200 structures collected during the last 100 ps of the equilibrated trajectories and minimized were comparatively analyzed. One of the average arrangements obtained was then considered for docking simulations.

Also for the human A_{2A}R, the whole sequence was modeled (SWISS-PROT entry P29274). Building of the C-tail (*i.e.* the 303–412 segment) was primarily achieved by comparative modeling (14). Two different models of this receptor portion were achieved: (*a*) **model 1**, obtained by

using the domain A3 of transketolase (PDB entry 1trk; sequence 544–680) as a template and (*b*) **model 2**, obtained by using the domain 2 of the cytidine deaminase (PDB entry 1ctt; sequence 180–294) as a template, according to the results of fold recognition (15). Indeed, both 1trkA3 and 1ctt02 domains, which share a three-layer ($\alpha\beta\alpha$) sandwich architecture, were the top hits of the THREADER run, characterized by comparable *z*-scores (*i.e.* 3.17 and 3.14, respectively). The agreement between the secondary structures predicted on the $A_{2A}R$ C-tail sequence and that computed on the C-tail models in the average minimized structures of the receptor is acceptable, especially for the C-tail based upon 1ctt02. Three modified rhodopsin templates (PDB entry 1F88; Ref. 16) were built in which the segments 227–235, 240–246, and 321–348 were deleted and either **model 1** or **model 2** of the C-tail from the human $A_{2A}R$ sequence was added. In particular, one template holds "model 1 C-tail," whereas the other two templates hold "model 2 C-tail," but in a slightly different orientation. Each of these templates was used to generate 50 models according to alignment reported in Fig. 12 (available as supplementary material in the on-line version of this article). α-Helical restraints were applied to the amino acid stretches 198–209, 221–228, 224–227, and 299–306. The best $A_{2A}R$ models obtained from each of the three MODELLER runs were subjected to refinement of I3 by means of MODELLER, leading to other three sets of structures. From each of these three sets of structures, one model was finally selected and subjected to automatic rotation of the side chains when in bad conformation, leading to different input arrangements. For the $A_{2A}R$ model holding the "**model 1**" C-tail and for that holding the "**model 2**" C-tail, 19 and 17 different input structures were, respectively, subjected to energy minimization and Molecular Dynamics simulations. The same computational protocol as that employed for the D_2R was followed. A disulfide bridge was imposed to form between Cys-77 (3.25) and Cys-159 in E2. The structures averaged over the 200 structures collected during the last 100 ps of the equilibrated trajectories and minimized were then analyzed. Eleven average arrangements were finally considered for docking simulations.

Computations: Rigid Body Docking Simulations—One selected average arrangement for the human D_2R was subjected to rigid body docking simulations with 11 different average arrangements of the human $A_{2A}R$. Docking simulations were carried out by means of two different rigid body docking programs, ZDOCK 2.1 (19) and ESCHER (20). Default conditions were used. Each ZDOCK run provided 2000 solutions filtered according to the shape complementarity score. On the other hand, each ESCHER run produced 30,000 solutions that were then filtered according to both shape and electrostatic complementarity, by using bump and charge cutoffs of 200 and −200, respectively. The filtered ZDOCK and ESCHER solutions were then subjected to a filter made in-house that discharged all the solutions that violated the membrane topology requirements. A few selected D_2R-$A_{2A}R$ complexes, representatives of the most populated docking solutions, were then subjected to manual relief of the steric conflicts followed by energy minimization.

RESULTS

Functionality of Modified $A_{2A}Rs$ and D_2Rs—The formation of $A_{2A}R$-D_2R heterodimers was demonstrated by BRET and FRET techniques in cells transfected with fusion proteins consisting of each receptor and either a fluorescent protein (GFP2, YFP) or *Renilla* luciferase (*Rluc*). Expression of fusion proteins and or the chimeric D_2R-D_1R protein was assessed by Western blot and immunocytochemistry (data not shown). The functionality of the receptor-*Rluc*, -GFP2, or -YFP constructs was assessed by the determination of cAMP levels produced in transfected cells in response to ligand binding. According to the positive coupling of $A_{2A}R$ to the adenylyl cyclase, the $A_{2A}R$ agonist CGS21680 properly induced cAMP accumulation in cells transfected with $A_{2A}R$-YFP or $A_{2A}R$-*Rluc* (Fig. 1*A*). On the other hand, in agreement with the inhibitory role of D_2R on adenylyl cyclase activity, the D_2R agonist quinpirole was able to reduce forskolin-induced cAMP levels in cells transfected with either D_2R-YFP or D_2R-GFP2 (Fig. 1*B*).

FRET Experiments—FRET and BRET approaches have been used in several studies to assess GPCR homo- and heterodimerization as reviewed by Angers *et al.* (21). By using the FRET approach with the D_2R-GFP2 and $A_{2A}R$-YFP pair, it was possible to confirm the heteromerization between $A_{2A}R$ and D_2R and to estimate the distance between the fluorophores. Using the acceptor photobleaching technique and confocal microscopy on cells expressing both receptors in the plasma membrane, a direct interaction was demonstrated between $A_{2A}R$ and D_2R (Fig. 2). FRET efficiency was determined to be in the range of 23–25%. Similar FRET efficiencies were obtained using a fluorescence plate reader as described under "Experimental Procedures" (Fig. 3). The low FRET efficiency of a negative control constituted by the pair D_2R-GFP2 and CD4-YFP demonstrated the specificity in the energy transfer between D_2R-GFP2 and $A_{2A}R$-YFP (Fig. 3). Using the theoretical curve of FRET efficiency correlated to the distance between the donor and acceptor fluorophores while assuming only a dimeric interaction, an efficiency in the range of 23–25%, indicates that the distance between fluorophores (GFP2 and YFP), both located at the C terminus of either $A_{2A}R$ or D_2R, is ~6–6.5 nm (Fig. 4).

BRET Experiments—In BRET experiments, little attention has been paid to the ratio of donor to acceptor molecules; thus, the interpretation of the data has remained rather qualitative. Indeed, the level of energy transfer detected for a given concentration of donor should increase with higher concentrations of acceptor until all of the donor molecules are bound to an acceptor molecule. This follows the theory that the energy transfer will reach a plateau therefore giving rise to a saturation curve. The maximum level reached will be a function of the total number of dimers formed and of the distance between the donor and acceptor while considering the relative orientation of the proteins within the dimers. The concentration of acceptor, giving 50% of the maximum energy transfer ($BRET_{50}$), will

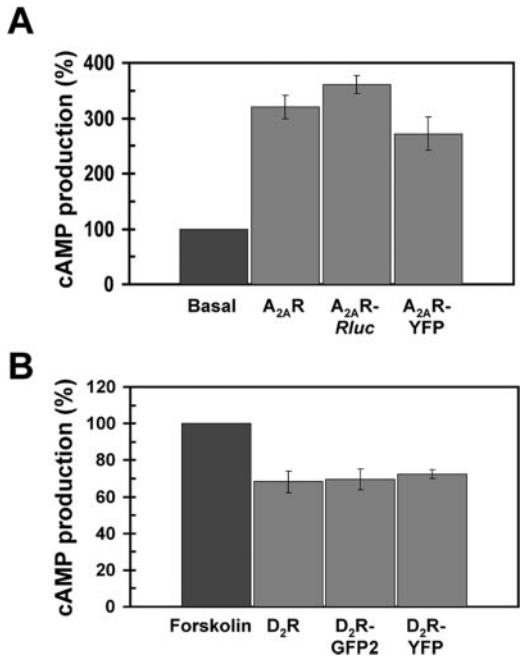

FIG. 1. **Functionality test of receptors fused to GFP variants or *Renilla* luciferase (*Rluc*).** HEK-293T cells transiently transfected with the corresponding constructs were stimulated with either 200 nM CGS21680 for $A_{2A}R$ (*panel A*), or 10 μM quinpirole in the presence of 10 μM forskolin for D_2R (*panel B*). $A_{2A}R$ induction of cAMP production is presented as percentage over basal levels (100%). As D_2R inhibits the production of cAMP, results are presented as its ability to inhibit forskolin induced cAMP production (100%). Results are a mean ± S.D. of four independent experiments performed in triplicate. One-way ANOVA showed a significant increase of cAMP production with CGS 21680 with wild-type $A_{2A}R$ and the $A_{2A}R$ fused to *Rluc* or YFP. Similarly, one-way ANOVA showed a significant decrease in forskolin-induced cAMP production with quinpirole with wild-type D_2R and the D_2R fused to GFP2 or YFP (*post hoc* Newman-Keuls test; $p < 0.05$ in all cases).

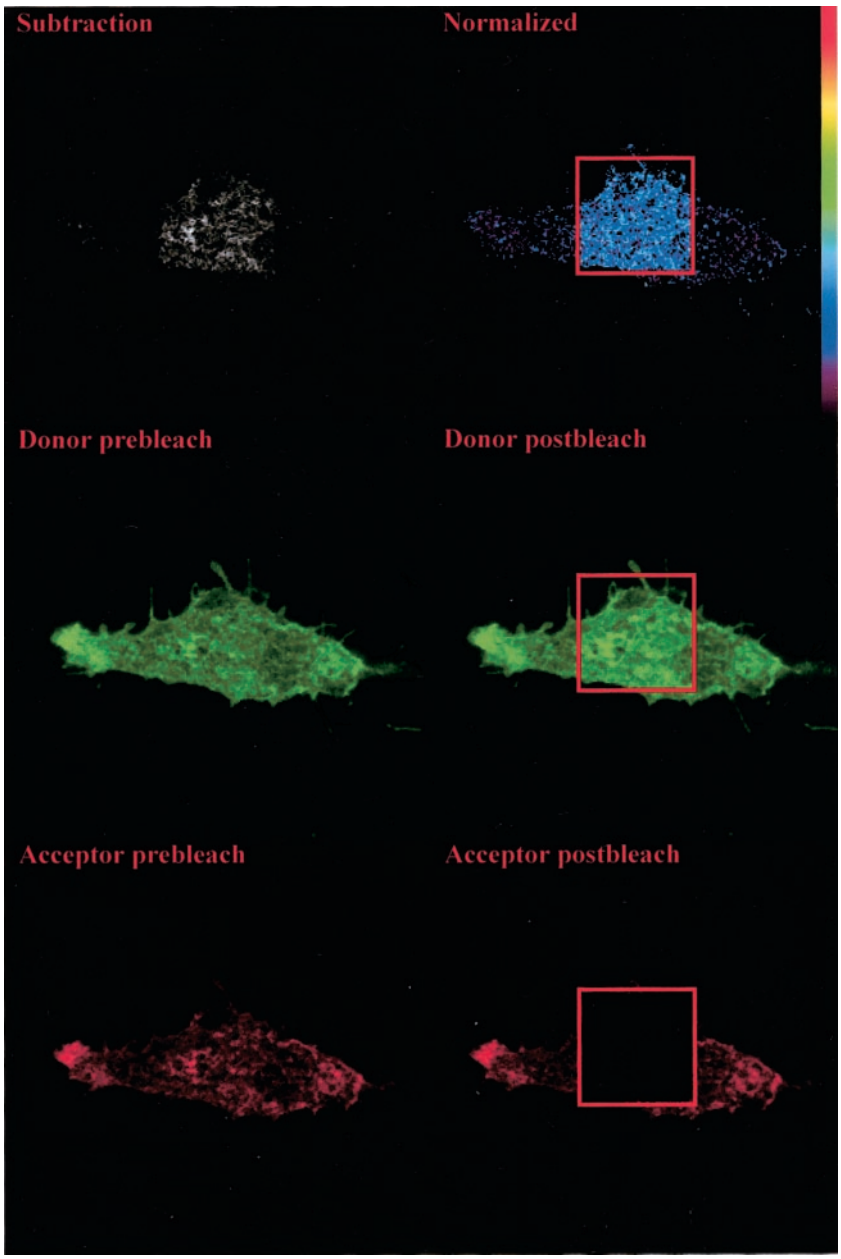

FIG. 2. **Imaging FRET efficiency of the D_2R-GFP2 and A_{2A}R-YFP pair by acceptor photo-bleaching.** HEK-293T cells were transiently transfected with the plasmid DNA for the D_2R-GFP2 and A_{2A}R-YFP constructs using a ratio of donor to acceptor DNA of 1:2 and fixed 48 h after transfection. Central panels are images of the D_2R-GFP2 donor before (*Donor prebleach*) and after (*Donor postbleach*) photo-bleaching of the A_{2A}R-YFP acceptor obtained in a central region of the lowest plane of the cell by spectral imaging and subsequent liner un-mixing as described under "Experimental Procedures." The extent of the photo-bleaching is shown in the *bottom panels* as a lack of acceptor fluorescence in the selected region after photo-bleaching (*Acceptor postbleach*) with respect to the image of the acceptor before photo-bleaching (*Acceptor prebleach*). The *top panels* represent donor un-quenching following acceptor photo-bleaching as donor postbleach − donor prebleach (subtraction) and a color representation of the FRET efficiency (normalized) calculated as indicated under "Experimental Procedures" and normalized to a scale from 0 to 1.

reflect the relative affinity of an acceptor and a donor to dimerize (22).

Here, we applied this theoretical framework to study A_{2A}R and D_2R heteromerization by constructing a BRET saturation curve in cells co-transfected with a constant amount of the A_{2A}R-*Rluc* construct while increasing concentrations of the D_2R-YFP plasmid. A positive BRET signal for the transfer of energy between A_{2A}R-*Rluc* and D_2R-YFP was obtained (Fig. 5). The BRET signal increased as a hyperbolic function of the concentration of the YFP-fusion construct added (assessed by the fluorescence emitted upon direct excitation at 480 nm) reaching an asymptote. As the pair A_{2A}R-*Rluc* and $GABA_BR2$-YFP led to an undetectable BRET signal (Fig. 5), the hyperbolic BRET signal found for the A_{2A}R-*Rluc*-D_2R-YFP indicates that the interaction between A_{2A}R and D_2R is specific.

Energy transfer between closely located receptor molecules can occur even in the absence of direct interaction (23). In fact, receptors located within specific plasma membrane microdomains, such as membrane rafts, may give rise to FRET or BRET signals not caused by real heteromerization. Raft localization of overexpressed membrane fluorescent proteins could allow a close enough proximity (<10 nm) to permit the transfer of energy. To explore this possibility, membrane rafts were disrupted by cyclodextrin treatment, and BRET assays were performed in these cells. As indicated in Fig. 3*A*, cyclodextrin did not lead to any change in the BRET signal for A_{2A}R-*Rluc*-D_2R-YFP. In addition, no change in the BRET signal was noted when cells were repleted with cholesterol after cyclodextrin treatment (Fig. 6*A*). The efficacy of the treatment was assessed by cyclodextrin-mediated extracellular signal-regulated kinase-1/2 phosphorylation, as indicated by Furuchi and Anderson (24). Raft disruption was also assessed by the redistribution of caveolin-1 from raft-enriched light fractions to heavier fractions after sucrose gradient separation (Fig. 6*B*). Taken together, this indicates that the energy transfer between A_{2A}R-*Rluc* and D_2R-YFP is the result of the formation of true heterodimers.

Stimulation with the A_{2A}R agonist CGS21680 or the D_2R agonist quinpirole, individually or in combination, did not promote any consistent change in either maximal BRET (data not shown) or $BRET_{50}$ (Fig. 7). An analysis of the subcellular distribution of the fusion proteins indicated that the lack of ago-

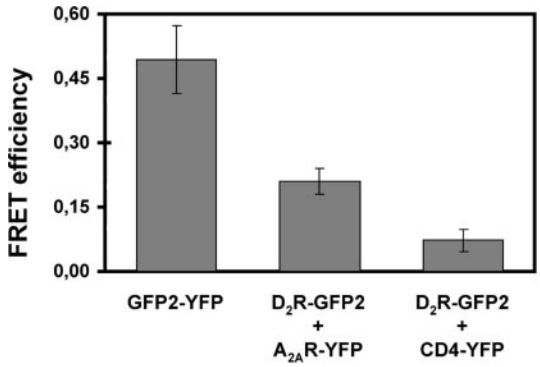

FIG. 3. **FRET efficiency of the D_2R-GFP2 and A_{2A}R-YFP pair by sensitized emission in living cells.** HEK-293T cells were transiently transfected with the plasmid DNA corresponding to D_2R-GFP2 (donor) and A_{2A}R-YFP (acceptor) proteins using a ratio of donor to acceptor DNA of 1:2, or with the positive control plasmid GFP2-YFP. Fluorescence readings were performed 48 h after transfection as described under "Experimental Procedures." Linear un-mixing of the emission signals was applied to the data (see "Experimental Procedures"), and the results are shown as the sensitized emission of the acceptor when the cells were excited at 400 nm. CD4-YFP was used as a negative control. Data are the mean ± S.D. of five independent experiments performed in duplicate. One-way ANOVA followed by Newman-Keuls test shows significant differences between GFP2-YF2 and D_2R-GFP2+A_{2A}R-YFP and between D_2R-GFP2+A_{2A}R-YFP and D_2R-GFP2+CD4-YFP ($p < 0.01$ in all cases).

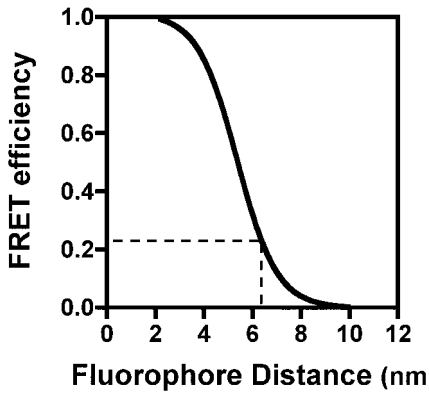

FIG. 4. **FRET efficiencies related to the distance between the fluorescent proteins.** FRET efficiencies of the GFP2 and YFP pair derived from their spectral properties were plotted as a function of the distance between the fluorescent proteins as described by Zimmermann *et al.* (12). *Dotted lines* show the relation between the determined FRET efficiency for the D_2R-GFP2-A_{2A}R-YFP pair and the approximate distance between the fluorescent proteins in this pair.

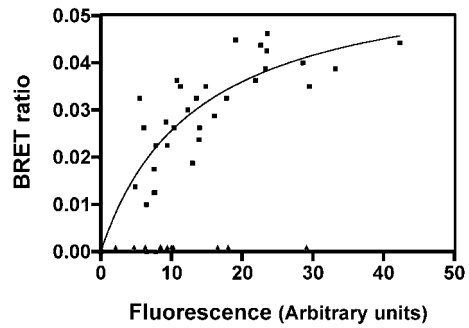

FIG. 5. **BRET saturation curve.** BRET was measured in HEK-293T cells co-expressing A_{2A}R-*Rluc* and D_2R-YFP (*squares*) or A_{2A}R-*Rluc* and $GABA_B$R2-YFP (*triangles*) constructs. Co-transfections were performed with increasing amounts of plasmid DNA for the YFP construct whereas the DNA for the *Rluc* construct was maintained constant. Both fluorescence and luminescence of each sample were measured prior to every experiment to confirm equal expression of *Rluc* while monitoring the increase of YFP expression.

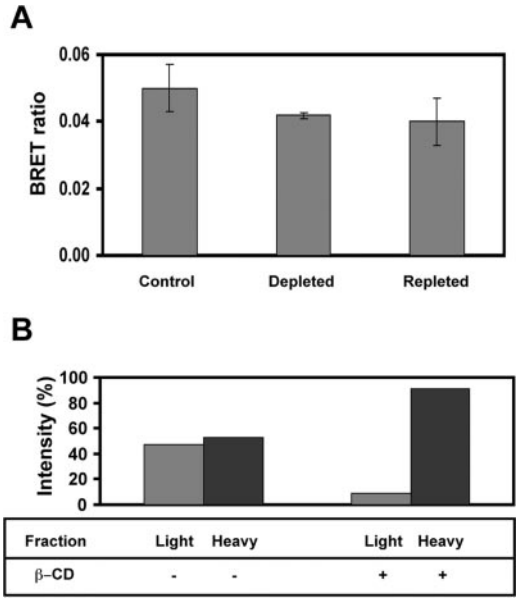

FIG. 6. ***β*-CD treatment.** BRET experiments were performed in HEK-293T cells co-transfected with the amount of plasmid DNA for the A_{2A}R-*Rluc* and D_2R-YFP constructs to give $BRET_{50}$. Cells were not treated (*Control*) or treated with 2% β-CD for 1 h (*Depleted*). Cholesterol repletion was achieved by incubating depleted cells for 1 h with 0.4% β-CD and 16 mg/ml cholesterol (*Repleted*). No differences in BRET were observed after depletion or repletion treatment (*panel A*) (analyzed with one-way ANOVA). For immunoblotting of caveolin-1 in cells treated with β-CD (*panel B*), extracts from control and treated cells were fractionated by a discontinuous sucrose gradient to obtain the light and heavy membrane fractions. Caveolin-1 was detected by Western blot in both membrane fractions. Densitometry of the bands was performed, and results are expressed as the percentage of the total intensity.

nist modulation of the BRET signal occurred in cells expressing A_{2A}-*Rluc* and D_2R-YFP in the plasma membrane (Fig. 8). These results indicate that receptor activation does not affect their oligomerization state and that the heteromers are, most probably, constitutively pre-formed. However, one cannot exclude the possibility that agonist stimulation may promote assembly/disassembly cycles that do not affect the steady-state proportion of receptors engaged in dimers.

To gain some insight into the putative heterodimer interface, a chimeric D_2R-D_1R in which helices 5, 6, I3, and E3 of the D_2R have been swapped by the corresponding sequence from the D_1R (11) was used as a competitor in BRET experiments. Although the wild-type D_2R was able to decrease the BRET signal between A_{2A}R-*Rluc* and D_2R-YFP, the D_2R-D_1R chimeric receptor failed to decrease the BRET signal even at high amounts of competitor cDNA (Fig. 9). These results are in agreement with previous studies, where we have shown that A_{2A}R does not modulate the agonist binding characteristics of this chimeric D_2R-D_1R (25). This suggests somewhere in the region of the D_2R containing helices 5, 6, I3, and E3 of the D_2R lies a critical site necessary for the heteromerization with A_{2A}R.

Computational Experiments—Further insight into the D_2R-A_{2A}R heterodimer interface was obtained by docking simulations on theoretical models of D_2R and A_{2A}R. The whole sequences of both receptors were modeled, because dimerization and/or oligomerization might also involve the cytosolic and/or the extracellular domains as recently suggested for rhodopsin (26). We are aware that structural errors might reside particularly in these receptor portions. Additionally, for this reason, we have used nine different average minimized structures of the A_{2A}R, differing in the conformations of the intracellular and extracellular domains as well as in the topology of the huge

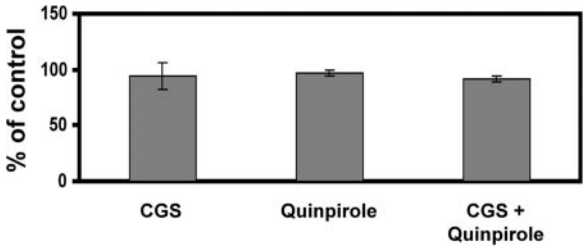

FIG. 7. **Effect of ligands on A_{2A}R-D_2R dimerization.** BRET measurements were performed after 1 h of treatment with 200 nM A_{2A}R agonist CGS21680 (*CGS*), 10 μM D_2R agonist quinpirole, or both ligands simultaneously in HEK-293T cells co-transfected with the A_{2A}R-*Rluc*-D_2R-YFP pair at the $BRET_{50}$ ratio. Data are mean ± S.D. of three independent experiments. Results are expressed as the percentage of the $BRET_{50}$ value of untreated (control) cells. No significant differences were observed between the three different groups (one-way ANOVA).

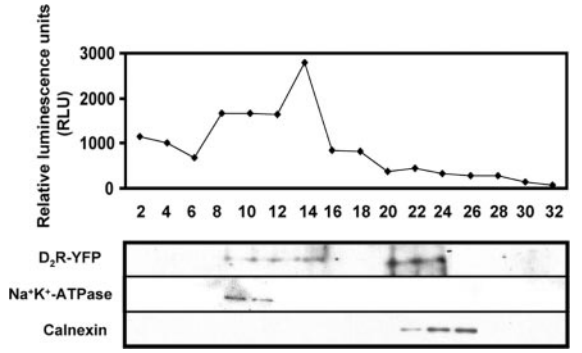

FIG. 8. **Subcellular distribution of A_{2A}R-*Rluc* and D_2R-YFP constructs.** Lysates of co-transfected HEK-293T cells as described in Fig. 7 were applied and separated on a discontinuous sucrose gradient. Fractions were subsequently analyzed for luminescence (*top panel*) and by immunoblotting (*bottom panel*). As a result of high levels of fluorescence in fractions with large concentrations of sucrose, the distribution of D_2R-YFP was analyzed by Western blot with an anti-GFP antibody. Fractions rich in plasma membrane and ER were detected by Western blot using either Na^+K^+-ATPase or calnexin antibodies, respectively.

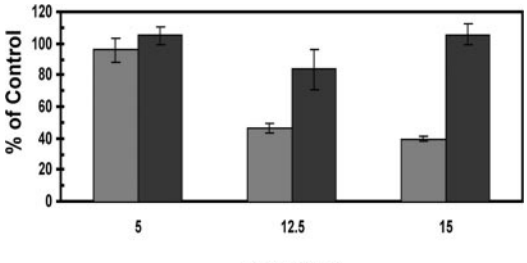

FIG. 9. **BRET competition.** HEK-293T cells were transfected with the appropriate amount of plasmid DNA for the A_{2A}R-*Rluc* and D_2R-YFP constructs corresponding to the previously determined $BRET_{50}$ (control) and with increasing amounts of D_2R cDNA (*gray bars*) or the cDNA of the dopamine D_2R-D_1R chimera (*black bars*). The BRET ratio was determined and values are expressed as a percentage of the control. Data are the mean ± S.D. of five experiments in duplicate. One-way ANOVA (with post-hoc Newman-Keuls comparisons) shows significant BRET competition with 12.5 and 15 μg of D_2R cDNA ($p < 0.001$ in both cases) and no significant differences with 12.5 or 15 μg of D_2R-D_1R cDNA.

C-tail, to probe the effect of such structural differences on the results of docking simulations. The A_{2A}R structures include four structures holding the "**model 1** C-tail" (see "Experimental Procedures") and seven structures holding the "**model 2** C-tail." Each of these structures has been docked with the selected average minimized structure of D_2R. Two different rigid-body docking programs, ZDOCK (19) and ESCHER (20), were employed. A total amount of 32,000 and 9400 filtered solutions (see "Experimental Procedures") was obtained by means of different runs of ZDOCK 2.1 and ESCHER, respectively. These solutions were subjected to an additional filter that discharged those arrangements that significantly violate the membrane topology requirements. In the majority of the more realistic (*i.e.* dimers with lower interacting enthalpy) docking solutions, the D_2R portions that participate in the heterodimer interface include the C-terminal half of helix 5, the N-terminal portion of I3 that contains a solvent-exposed stretch of positively charged amino acids (*i.e.* 217–220), helix 6, helix 7, and the segment that corresponds to helix 8 of rhodopsin (16). Among these solutions, a highly populated one (population 1, Fig. 10) is characterized by the following contacts: (*a*) **helix 5**(D_2R)-**helix 4**(A_{2A}R) and **I3$_{N\text{-term}}$**(D_2R)-**C-tail$_{C\text{-term}}$**-(A_{2A}R) and (*b*) **helix 5$_{C\text{-term}}$**(D_2R)-**helix 3$_{C\text{-term}}$**(A_{2A}R), **helix 6**(D_2R)-**helix 4**(A_{2A}R) and **I3$_{N\text{-term}}$**(D_2R)-**C-tail$_{C\text{-term}}$**(A_{2A}R); **helix 7**(D_2R) may also participate together with helix 6 in the contacts with **helix 4**(A_{2A}R). To estimate the putative interfluorophore distances in selected members of population 1, the structures of GFP and YFP (PDB entries 2emn and 1huy, respectively), have been approached to D_2R and A_{2A}R, respectively, in selected dimmers, the first amino acid of the fluorescent proteins being close to the last amino acid of the receptors. The distance between the C1 atoms of the GFP and YFP chromophores in the different complexes ranges between 6 and 8 nm, very similar to that deduced from FRET experiments.

In a less populated solution (population 2, Fig. 10), almost two different sets of contacts characterize the D_2R-A_{2A}R dimers. The first set of contacts includes: (*a*) **I2**(D_2R)-**I2**(A_{2A}R), (*b*) **helix 4$_{C\text{-teminal half}}$**(D_2R)-**helix 3$_{C\text{-terminal half}}$**($A_{2A}$R), (*c*) **helix 4$_{N\text{-terminal half}}$**($D_2$R)-**helix 5$_{N\text{-terminal half}}$**($A_{2A}$R), and (*d*) **helix 5**(D_2R)-**helix 4**(A_{2A}R). The second set of contacts includes: (*a*) **helix 3$_{C\text{-terminal half}}$**($D_2$R)-**helix 4$_{C\text{-terminal half}}$**-($A_{2A}$R), (*b*) **helix 4$_{N\text{-terminal half}}$**($D_2$R)-**helix 5$_{N\text{-terminal half}}$**-($A_{2A}$R), (*c*) **helix 5**($D_2$R)-**helix 4**($A_{2A}$R), and (*d*) **I3**(D2R)-**C-tail**(A_{2A}R) (only a few contacts).

DISCUSSION

Adenosine-dopamine interactions play a very important role in basal ganglia function and dysfunction. This is the result of the existence of specific antagonistic interactions between different adenosine and dopamine receptor subtypes co-localized in different neurons of the striatum, the main input structure of the basal ganglia. Two subtypes of GABAergic efferent neurons, the striatonigral and the striatopallidal neurons, constitute more than 90% of the striatal neuronal population. The interaction of A_1Rs and D_1Rs modulates the function of striatonigral neurons, whereas the interactions of A_{2A}R and D_2R modulates the function of striatopallidal neurons (5, 7, 8). The existence of functional A_1R-D_1R and A_{2A}R-D_2R heteromeric complexes has recently been demonstrated in mammalian cell lines (10, 27). However, the techniques used in previously reported data, including co-immunoprecipitation and confocal laser microscopy co-localization studies, could not discard the possibility of a third protein acting as scaffolding to bring the two receptors together.

In the present work, we have used FRET and BRET techniques to demonstrate that, in fact, A_{2A}R and D_2R form heteromers in living cells. This interaction was found to be specific where no BRET or FRET signals were detected when other receptors were assayed (see "Results"). The estimated distance between the fluorophores fused to C-terminal tails of A_{2A}R and D_2R resulted to be ~6.3 nm. Receptor molecules with very close proximity in small membrane microdomains can lead to artifactual BRET results, as with proteins targeted to cholesterol-rich plasma membrane domains by lipid anchoring clusters in rafts (23). This was ruled out by the unmodified BRET signal between A_{2A}R-*Rluc* and D_2R-YFP in the presence of cyclodex-

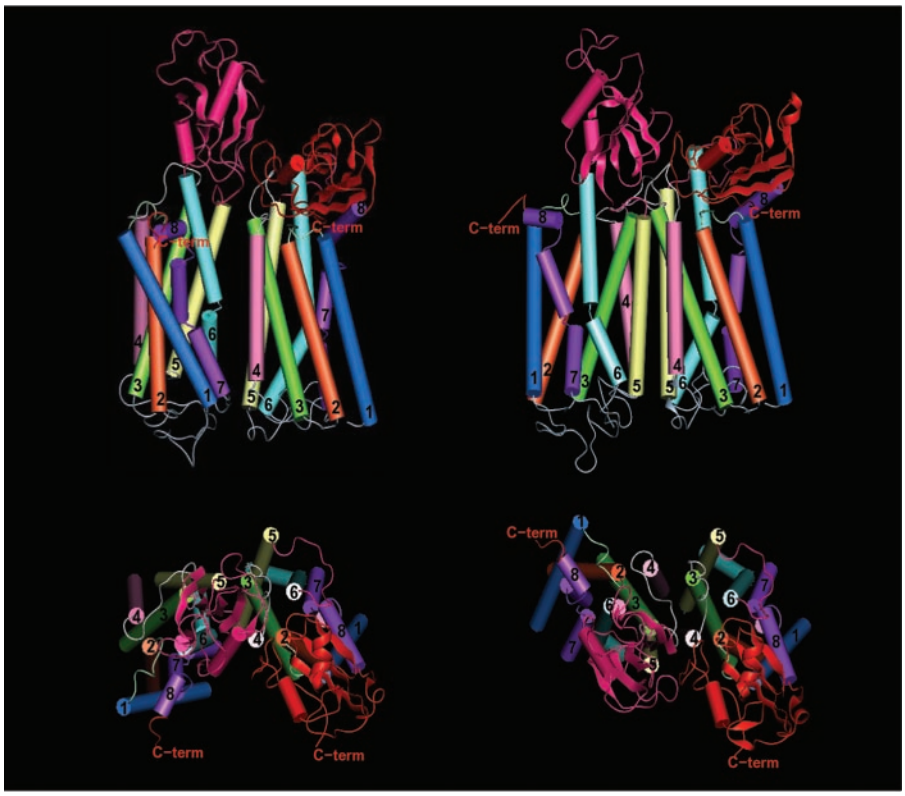

FIG. 10. **Examples of the D_2R-$A_{2A}R$ heterodimers belonging to population 1 (*top* and *bottom left*) and to population 2 (*top* and *bottom right*).** In the *top views*, the helix bundles are seen in a direction parallel to the membrane surface, the intracellular side being at the *top*. In the *bottom views*, the helix bundles are seen from the intracellular side in a direction almost perpendicular to the membrane surface. Helices 1, 2, 3, 4, 5, 6, and 7 are, respectively, *blue*, *orange*, *green*, *pink*, *yellow*, *cyan*, and *violet*. The amino acid stretch corresponding to helix 8 of rhodopsin is *violet* as well. The extracellular domains are *gray*, whereas the intracellular loops 1, 2 and 3 and the C-tail (*C-term*) are, respectively, *light green*, *white*, *purple*, and *red*.

trin, which disrupts rafts and prevents the eventual accumulation of receptors in these structures (Fig. 6).

Homomerization and heteromerization of GPCRs have been suggested to involve different receptor domains. The C-terminal tail of the GABA receptors is involved in $GABA_BR1$-$GABA_BR2$ heteromerization by a coiled-coil interaction (28, 29). X-ray studies performed with the metabotropic glutamate receptor $mGlu_1R$ have shown that its extracellular N-terminal ligand-binding region forms disulfide-linked homodimers (30). There is also evidence for the transmembrane domains in mediating the formation of homo- or heterodimers (for review, see Ref. 1). The sixth and seventh helices of D_2R have been implicated in its homodimerization, because synthesized peptides encoding sequences in these regions inhibit dimer formation (31). Furthermore, Guo *et al.* (32) have recently reported that D_2R homodimers are stabilized by cross-linking through a cysteine residue located at the extracellular end of helix 4. The present results using the previously characterized chimeric D_2R-D_1R containing helices 5 and 6, I3, and E3 of the dopamine D_1R (9), demonstrate that these portions of the D_2R are directly involved in the formation of $A_{2A}R$-D_2R heteromers. Thus, differing from the wild-type D_2R, the chimeric D_2R-D_1R was not able to compete for the specific BRET between $A_{2A}R$-*Rluc* and D_2R-YFP.

To gain insight into the potential D_2R-$A_{2A}R$ heterodimer interfaces, rigid-body docking simulations have been done between an average minimized structure of D_2R and nine different average minimized structures of $A_{2A}R$. From docking simulations two sets of dimers sharing (within each set) similar interdimer interfaces have been obtained (population 1 and population 2, see Fig. 10). In particular, in the most populated one (population 1), helix 5 and/or helix 6 and the N-terminal portion of I3 from D_2R approach helix 4 and the C-terminal portion of the C-tail from the $A_{2A}R$, respectively. Helix 7(D_2R) may also participate together with helix 6 in the contacts with helix 4($A_{2A}R$) (Fig. 10, *left side*). The interface contacts in population 1 are consistent with the results of BRET experiments done in this work on the chimeric D_2R-D_1R and $A_{2A}R$. Population 2 has a reduced number of structures if compared with population 1. However, structures in population 2 display high docking scores and resemble the intradimer contact model proposed for rhodopsin (26).

The analysis of the BRET signal in $A_{2A}R$-D_2R-expressing cells indicated that the activation of $A_{2A}R$ or D_2R by their corresponding agonist did not affect the degree of heteromerization. Similar results were obtained when the two agonists were used simultaneously (Fig. 7). The lack of modulation by agonists has also been reported for other homo- and heterodimeric partners (3, 33, 34). In carefully controlled BRET studies, it has been demonstrated that a number of heteromerizing receptors are pre-assembled in the ER and the dimers that reach the plasma membrane are not affected, in terms of the degree of dimerization, after receptor activation by their corresponding ligands (33–36). In contrast to this recently reported data, detailed studies by Patel *et al.* (37) in stable CHO-K1 cells expressing somatostatin receptors suggest that the receptors are monomeric in their basal state and oligomerize only upon agonist activation. For the somatostatin receptor subtype R5, the same authors report that ligand-induced homomerization extends beyond dimers to higher order oligomers (39). For our experimental data, the unchanged BRET signal reported in cells treated with agonists is not necessarily in contradiction to the known clustering of these receptors when they are activated by agonists. In fact, the $A_{2A}R$ agonist CGS21680 leads to the clustering of $A_{2A}R$ receptors in neuroblastoma SH-SY5Y cells or in primary neuronal cell cultures, and similar clustering occurs with D_2R receptors when D_2R-expressing cells are treated with the D_2R agonist quinpirole (10). It should also be noted that co-clustering of $A_{2A}R$ and D_2R occurs when either agonist is added, alone or simultaneously, to cells co-expressing both receptors (10). Taken together these results indicate that $A_{2A}R$ or D_2R agonists lead to the reorganization of receptors within the plasma membrane while not affecting their degree of heterodimerization. Considering the

data, it appears as if ligand-induced activation of the receptors leads to target pre-existing $A_{2A}R$-D_2R heterodimers to membrane microdomains. Ligand modulation of heteromers may also be dependent upon the nature of the receptors involved and their level of expression. It should not be ruled out that other factors might also contribute to this modulation. Further research is required to understand whether ligand regulation is dependent on the particular expression of scaffold or chaperone proteins in cell models where ligand modulation of receptor oligomerization is studied.

Receptor-receptor heteromerization serves a variety of purposes in receptor function. For instance, assembly of heterodimers is required for targeting $GABA_B$ receptors to the cell surface (38). $GABA_BR1$-$GABA_BR2$ heterodimerization is necessary for $GABA_B$ receptor signaling, because one of the receptors within the heterodimer binds the ligand whereas the other is linked to the signaling machinery. Moreover, $GABA_BR2$ is required to provide high affinity for agonists to the $GABA_BR1$ subunit (39). We have previously postulated that heterodimerization may be necessary for intramembrane receptor-receptor interactions, where the stimulation of one receptor changes the binding characteristics of another receptor in tissue or cell membrane preparations (5, 40–42). An intramembrane $A_{2A}R$-D_2R antagonistic interaction has been repeatedly demonstrated in both rat and human striatum as well as in transfected mammalian cell lines, where the stimulation of $A_{2A}R$ decreases the affinity of D_2R receptor for agonists (9, 43–47). In CHO-transfected cells, the $A_{2A}R$ agonist CGS 21680 decreased the affinity of the D_2R but not of the chimeric D_2R-D_1R for tritiated dopamine (25). Taken together with the above-mentioned results, this strongly suggests that the intramembrane $A_{2A}R$-D_2R interaction depends on the heteromerization between $A_{2A}R$ and D_2R. It is very probable that the loss of affinity to dopamine binding of the D_2R when the $A_{2A}R$ is activated is a result of conformational changes transmitted through the heteromeric interaction. Interestingly, there is an increase in the agonist binding affinity for D_2R with an enhancement of G protein and effector coupling to adenylyl cyclase when the D_2R and somatostatin SSTR5 receptors heteromerize in response to agonist treatment (48). Therefore, the increase or decrease in the affinity of agonist binding to D_2R would depend on the nature of the heteromeric partner; SSTR5 receptors leading to an increase in its affinity (*i.e.* synergy) and $A_{2A}R$ leading to a decrease (*i.e.* antagonism). This and other potential roles of the $A_{2A}R$-D_2R heteromers are important to fully understand the molecular basis of the adenosine-dopamine antagonism within the central nervous system, thus allowing for the design of novel strategies to combat basal ganglia disorders (like Parkinson's disease), schizophrenia, and drug addiction.

REFERENCES

1. Bouvier, M. (2001) *Nat. Rev. Neurosci.* **2,** 274–286
2. Milligan, G., and White, J. H. (2001) *Trends Pharmacol. Sci.* **22,** 513–518
3. Rios, C. D., Jordan, B. A., Gomes, I., and Devi, L. A. (2001) *Pharmacol. Ther.* **92,** 71–87
4. George, S. R., O'Dowd, B. F., and Lee, S. P. (2002) *Nat. Rev. Drug Discov.* **1,** 808–820
5. Agnati, L. F., Ferré, S., Lluis, C., Franco, R., and Fuxe, K. (2003) *Pharmacol. Rev.* **55,** 509–550
6. Franco, R., Canals, M., Marcellino, D., Ferré, S., Agnati, L. F., Mallol, J., Casadó, V., Ciruela, F., Fuxe, K., Lluis, C., and Canela, E. I. (2003) *Trends Biochem. Sci.* **28,** 238–243
7. Ferré, S., Fredholm, B. B., Morelli, M., Popoli, P., and Fuxe, K. (1997) *Trends Neurosci.* **20,** 482–487
8. Ferré, S., Ciruela, F., Woods, A. S., Canals, M., Burgueno, J., Marcellino, D., Karcz-Kubicha, M., Hope, B. T., Morales, M., Popoli, P., Goldberg, S. R., Fuxe, K., Lluis, C., Franco, R., and Agnati, L. F. (2003) *Curr. Med. Chem.* **3,** 1–26
9. Ferré, S., von Euler, G., Johansson, B., Fredholm, B. B., and Fuxe, K. (1991) *Proc. Natl. Acad. Sci. U. S. A.* **88,** 7238–7241
10. Hillion, J., Canals, M., Torvinen, M., Casado, V., Scott, R., Terasmaa, A., Hansson, A., Watson, S., Olah, M. E., Mallol, J., Canela, E. I., Zoli, M., Agnati, L. F., Ibanez, C. F., Lluis, C., Franco, R., Ferré, S., and Fuxe, K. (2002) *J. Biol. Chem.* **277,** 18091–18097
11. Kozell, L. B., and Neve, K. A. (1997) *Mol. Pharmacol.* **52,** 1137–1149
12. Zimmermann, T., Rietdorf, J., Girod, A., Georget, V., and Pepperkok, R. (2002) *FEBS Lett.* **531,** 245–249
13. Jordan, M., Schallhorn, A., and Wurm, F. M. (1996) *Nucleic Acids Res.* **24,** 596–601
14. Sali, A., and Blundell, T. L. (1993) *J. Mol. Biol.* **234,** 779–815
15. Jones, D. T., Taylor, W. R., and Thornton, J. M. (1992) *Nature* **358,** 86–89
16. Palczewski, K., Kumasaka, T., Hori, T., Behnke, C. A., Motoshima, H., Fox, B. A., Le Trong, I., Teller, D. C., Okada, T., Stenkamp, R. E., Yamamoto, M., and Miyano, M. (2000) *Science* **289,** 739–745
17. Brooks, B. R., Bruccoleri, R. E., Olafson, B. D., States, D. J., Swaminathan, S., and. Karplus, M. (1983) *J. Comput. Chem.* **4,** 187–217
18. Ballesteros, J. A., and Weinstein, H. (1995) *Methods Neurosci.* **25,** 366–428
19. Chen, R., Li L., and Weng, Z. (2003) *Proteins* **52,** 80–87
20. Ausiello, G., Cesareni, G., and Helmer-Citterich, M. (1997) *Proteins* **28,** 556–567
21. Angers, S., Salahpour, A., and Bouvier, M. (2002) *Annu. Rev. Pharmacol. Toxicol.* **42,** 409–435
22. Mercier, J. F., Salahpour, A., Angers, S., Breit, A., and Bouvier, M. (2002) *J. Biol. Chem.* **277,** 44925–44931
23. Zacharias, D. A., Violin, J. D., Newton, A. C., and Tsien, R. Y. (2002) *Science* **296,** 913–916
24. Furuchi, T., and Anderson, R. G. (1998) *J. Biol. Chem.* **273,** 21099–21104
25. Torvinen, M., Liu, Y., Kozell, L. B., Neve, K. A., Ferré, S., Ibañez, C., and Fuxe, K. (2001) *Soc. Neurosci. Abstr.* **27,** 379
26. Liang, Y., Fotiadis, D., Filipek, S., Saperstein, D. A., Palczewski, K., and Engel, A. (2003) *J. Biol. Chem.* **278,** 21655–21662
27. Ginés, S., Hillion, J., Torvinen, M., Le Crom, S., Casado, V., Canela, E. I., Rondin, S., Lew, J. Y., Watson, S., Zoli, M., Agnati, L. F., Vernier, P., Lluis, C., Ferré, S., Fuxe, K., and Franco, R. (2000) *Proc. Natl. Acad. Sci. U. S. A.* **97,** 8606–8611
28. Kuner, R., Kohr, G., Grunewald, S., Eisenhardt, G., Bach, A., and Kornau, H. C., (1999) *Science* **283,** 74–77
29. Kammerer, R. A., Frank, S., Schulthess, T., Landwehr, R., Lustig, A., and Engel, J. (1999) *Biochemistry* **38,** 13263–13269
30. Kunishima, N., Shimada, Y., Tsuji, Y., Sato, T., Yamamoto, M., Kumasaka, T., Nakanishi, S., Jingami, H., and Morikawa, K. (2000) *Nature* **407,** 971–977
31. Ng, G. Y., O'Dowd, B. F., Lee, S. P., Chung, H. T., Brann, M. R., Seeman, P., and George, S. R. (1996) *Biochem. Biophys. Res. Commun.* **227,** 200–204
32. Guo, W., Shi, L., and Javitch, J. A. (2003) *J. Biol. Chem.* **278,** 4385–4388
33. Issafras, H., Angers, S., Bulenger, S., Blanpain, C., Parmentier, M., Labbe-Jullie, C., Bouvier, M., and Marullo, S. (2002) *J. Biol. Chem.* **277,** 34666–34673
34. Terrillon, S., Durroux, T., Mouillac, B., Breit, A., Ayoub, M. A., Taulan, M., Jockers, R., Barberis, C., and Bouvier, M. (2003) *Mol. Endocrinol.* **17,** 677–691
35. Jensen, A. A., Hansen, J. L., Sheikh, S. P., and Brauner-Osborne, H. (2002) *Eur. J. Biochem.* **269,** 5076–5087
36. Ramsay, D., Kellet, E., McVey, M., Rees, S., and Milligan, G. (2002) *Biochem. J.* **365,** 429–440
37. Patel, R. C., Kumar, U., Lamb, D. C., Eid, J. S., Rocheville, M., Grant, M., Rani, A., Hazlett, T., Patel, S. C., Gratton, E., and Patel, Y. C. (2002) *Proc. Natl. Acad. Sci. U. S. A.* **99,** 3294–3299
38. White, J. H., Wise, A., Main, M. J., Green, A., Fraser, N. J., Disney, G. H., Barnes, A. A., Emson, P., Foord, S. M., and Marshall, F. H. (1998) *Nature* **396,** 679–682
39. Kniazeff, J., Galvez, T., Labesse, G., and Pin, J. P. (2002) *J. Neurosci.* **22,** 7352–7361
40. Agnati, L. F., Fuxe K., Zini I., Lenzi P., and Hökfelt T. (1980) *Med. Biol.* **58,** 182–187
41. Fuxe, K., and Agnati, L. F. (1985) *Med. Res. Rev.* **5,** 441–482
42. Zoli, M., Agnati, L. F., Hedlund, P. B., Li, X.-M., Ferré, S., and Fuxe, K. (1993) *Mol. Neurobiol.* **7,** 293–334
43. Dasgupta, S., Ferré, S., Kull, B., Hedlund, P. B., Finnman, U. B., Ahlberg, S., Arenas, E., Fredholm, B. B., and Fuxe, K. (1996) *Eur. J. Pharmacol.* **316,** 325–331
44. Dixon, A. K., Widdowson, L., and Richardson, P. J. (1997) *J. Neurochem.* **69,** 315–321
45. Kull, B., Ferré, S., Arslan, G., Svenningsson, P., Fuxe, K., Owman, C., and Fredholm, B. B. (1999) *Biochem. Pharmacol.* **58,** 1035–1045
46. Salim, H, Ferré, S., Dalal, A., Peterfreund, R. A., Fuxe, K., Vincent, J. D., and Lledo, P. M. (2000) *J. Neurochem.* **74,** 432–439
47. Díaz-Cabiale, Z., Hurd, Y., Guidolin, D., Finnman, U.-B., Zoli, M., Agnati, L. F., Vanderhaeghen, J.-J., Fuxe, K., and Ferré, S. (2001) *Neuroreport* **12,** 1831–1834
48. Rocheville, M., Lange, D. C., Kumar, U., Patel, S. C., Patel, R. C., and Patel, Y. C. (2000) *Science* **288,** 154–157

Supplementary material

Figure 11 Sequence alignment between a modified rhodopsin template (see methods) and the human D_2R. This alignment has been used for comparative modelling.

Figure 12 Sequence alignment between a modified rhodopsin template (see methods) and the human $A_{2A}R$. This alignment has been used for comparative modelling.

N-TERM

Rhodchim	M N G T E G P N F Y V P F S N K T G V V R S P F E A P Q Y Y L A E P	**36**
D_2R	M D P L N L S W Y D D D L E - R Q N W S R - P F N G S D G K - A D R	**33**

HELIX 1

Rhodchim	W Q F S M L A A Y M F L L I M L G F P I N F L T L Y V T V Q	**64**
D_2R	P H Y N Y Y A T L L T L L I A V I V F G N V L V C M A V S R	**61**

I1

Rhodchim	H K K L R T	**70**
D_2R	E K A L Q T	**67**

HELIX 2

Rhodchim	P L N Y I L L N L A V A D L F M V F G G F T T T L Y T S L H	**100**
D_2R	T T N Y L I V S L A V A D L L V A T L V M P W V V Y L E V V	**97**

E1

Rhodchim	G Y F V F G	**106**
D_2R	G E W K F S	**103**

HELIX 3

Rhodchim	P T G C N L E G F F A T L G G E I A L W S L V V L A I E R Y V V V	**139**
D_2R	R I H C D I F V T L D V M M C T A S I L N L C A I S I D R Y T A V	**136**

I2

Rhodchim	C K P M - S N F R F G E N -	**151**
D_2R	A M P M L Y N T R Y S S K R	**150**

HELIX 4

Rhodchim	H A I M G V A F T W V M A L A C A A P P L V G W -	**175**
D_2R	R V T V M I S I V W V L S F T I S C P L L F G L N	**175**

E2

Rhodchim	- - - - - - - - - - - -	
D_2R	N A D Q N E C I I A N P	**187**

HELIX 5

Rhodchim	S F V I Y M F V V H F I I P L I V I F F C Y G Q L V F	**228**
D_2R	A F V V Y S S I V S F Y V P F I V T L L V Y I K I Y I	**214**

I3

Rhodchim	- -	
D_2R	V L R R R R K R V N T K R S S R A F R A H L R A P L K E A A R R A Q E L E M E M	**254**
Rhodchim	- -	
D_2R	L S S T S P P E R T R Y S P I P P S H H Q L T L P D P S H H G L H S T P D S P A	**294**
Rhodchim	- -	
D_2R	K P E K N G H A K D H P K I A K I F E I Q T M P N G K T R T S L K T M S R R K L	**334**

HELIX 6

Rhodchim	T Q K A E K E V T R M V I I M V I A F L I C W L P Y A G V A F Y I F	**276**
D_2R	S Q Q K E K K A T Q M L A I V L G V F I I C W L P F F I T H I L N I	**368**

E3

Rhodchim	T H Q G S D F G P	**285**
D_2R	- H C D C N I P P	**376**

HELIX 7

Rhodchim	I F M T I P A F F A K T S A V Y N P V I Y I M M N K Q F R N C - M V T T L C	**322**
D_2R	V L Y S A F T W L G Y V N S A V N P I I Y T T F N I E F R K A F L K I L H C	**414**

C-TAIL

Rhodchim	C G K N P S T T V S K T E T S Q V A P A	**348**
D_2R	- - - - - - - - - - - - - - - - - - - -	

Figure 11

	N-TERM	
Rhodchim	M N G T E G P N F Y V P F S N K T G V V R S P F E A P Q Y Y L A E P	**36**
$A_{2A}R$	- M P I	**3**
	HELIX 1	
Rhodchim	W Q F S M L A A Y M F L L I M L G F P I N F L T L Y V T V Q	**64**
$A_{2A}R$	M G S S V Y I T V E L A I A V L A I L G N V L V C W A V W L	**33**
	I1	
Rhodchim	H K K L R T	**70**
$A_{2A}R$	N S N L Q N	**39**
	HELIX 2	
Rhodchim	P L N Y I L L N L A V A D L F M V F G G F T T T L Y T S L	**99**
$A_{2A}R$	V T N Y F V V S L A A A D I A V G V L A I P F A I T I S T	**68**
	E1	
Rhodchim	H G Y F V F G	**106**
$A_{2A}R$	- G - F C A A	**73**
	HELIX 3	
Rhodchim	P T G C N L E G F F A T L G G E I A L W S L V V L A I E R Y V V V	**139**
$A_{2A}R$	C H G C L F I A C F V L V L T Q S S I F S L L A I A I D R Y I A I	**106**
	I2	
Rhodchim	C K P M - S N F R F G E N	**151**
$A_{2A}R$	R I P L R Y N G L V T G T	**119**
	HELIX 4	
Rhodchim	H A I M G V A F T W V M A L A C A A P P L V G W S -	**176**
$A_{2A}R$	R A K G I I A I C W V L S F A I G L T P M L G W N N	**145**
	E2	
Rhodchim	R Y I P - E G M Q - C S - C G I D Y Y T P H - E E T - N N E	**201**
$A_{2A}R$	C G Q P K E G K N H S Q G C G E G Q V A C L F E D V V P M N	**175**
	HELIX 5	
Rhodchim	S F V I Y M F V V H F I I P L I V I F F C Y Q L - - - - - - - - - -	**226**
$A_{2A}R$	Y M V Y F N F F A C V L V P L L L M L G V Y L R I F L A A R R Q L K	**209**
	I3	
Rhodchim	- - - - - - - - - - - - - - -	
$A_{2A}R$	Q M E S Q P L P G E R A R S	**223**
	HELIX 6	
Rhodchim	- - - - E K E V T R M V I I M V I A F L I C W L P Y A G V A F Y I F	**228**
$A_{2A}R$	T L Q K E V H A A K S L A I I V G L F A L C W L P L H I I N C F T F	**257**
	E3	
Rhodchim	T H Q G S D F G P -	**285**
$A_{2A}R$	F C P D C S H A P L	**267**
	HELIX 7	
Rhodchim	I F M T I P A F F A K T S A V Y N P V I Y I M M N K Q F R N C M V T T	**320**
$A_{2A}R$	W L M Y L A I V L S H T N S V V N P F I Y A Y R I R E F R Q T F R K I	**302**
	C-TAIL	
Rhodchim	- -	
$A_{2A}R$	I R S H V L R Q Q E P F K A A G T S A R V L A A H G S D G E Q V S L R L N G H P	**342**
Rhodchim	- -	
$A_{2A}R$	P G V W A N G S A P H P E R R P N G Y A L G L V S G G S A Q E S Q G N T G L P D	**382**
Rhodchim	- -	
$A_{2A}R$	V E L L S H E L K G V C P E P P G L D D P L A Q D G A G V S	**412**

Figure 12

III-. Canals, M., Burgueño, J., Marcellino, D., Cabello, N., Canela, E.I., Mallol, J., Agnati, L., Ferré, S., Bouvier, M., Fuxe, K., Ciruela, F., Lluís, C. and Franco, R., 2004, "Homodimerization of adenosine A_{2A} receptors: qualitative and quantitative assessment by fluorescence and bioluminescence energy transfer". *Journal of Neurochemistry*, 88, 726-734.

Journal of Neurochemistry, 2004, **88**, 726–734 doi:10.1046/j.1471-4159.2003.02200.x

Homodimerization of adenosine A_{2A} receptors: qualitative and quantitative assessment by fluorescence and bioluminescence energy transfer

Meritxell Canals,* Javier Burgueño,* Daniel Marcellino,* Núria Cabello,* Enric I. Canela,* Josefa Mallol,* Luigi Agnati,† Sergi Ferré,‡ Michel Bouvier,§ Kjell Fuxe,¶ Francisco Ciruela,* Carmen Lluis* and Rafael Franco*

**Department of Biochemistry and Molecular Biology of the University of Barcelona, Barcelona, Spain*

†*Department of Biomedical Sciences, University of Modena and Reggio Emilia, Modena, Italy*

‡*Behavioural Neuroscience Branch, National Institute on Drug Abuse, Intramural Research Program, National Institutes of Health, Department of Health and Human Services, Baltimore, Maryland, USA*

§*Department of Biochemistry, University of Montreal, Montreal, Quebec, Canada*

¶*Department of Neuroscience, Division of Cellular and Molecular Neurochemistry, Karolinska Institutet, Stockholm, Sweden*

Abstract

The results presented in this paper show that adenosine A_{2A} receptor ($A_{2A}R$) form homodimers and that homodimers but not monomers are the functional species at the cell surface. Fluorescence resonance energy transfer (FRET) and bioluminescence resonance energy transfer (BRET) techniques have been used to demonstrate in transfected HEK293 cells homodimerization of $A_{2A}R$, which are heptaspanning membrane receptors with enriched expression in striatum. The existence of homodimers at the cell surface was demonstrated by time-resolved FRET. Although agonist activation of the receptor leads to the formation of receptor clusters, it did not affect the degree of $A_{2A}R$–$A_{2A}R$ dimerization. Both monomers and dimers were detected by immunoblotting in cell extracts. However, cell surface biotinylation of proteins has made evident that more than 90% of the cell surface receptor is in its dimeric form. Thus, it seems that homodimers are the functional form of the receptor present on the plasma membrane. A deletion mutant version of the A_{2A} receptor, lacking its C-terminal domain, was also able to form both monomeric and dimeric species when cell extracts from transfected cells were analyzed by immunoblotting. This suggests that the C-terminal tail does not participate in the dimerization. This is relevant as the C-terminal tail of $A_{2A}R$ is involved in heteromers formed by $A_{2A}R$ and dopamine D2 receptors. BRET ratios corresponding to $A_{2A}R$–$A_{2A}R$ homodimers were higher than those encountered for heterodimers formed by $A_{2A}R$ and dopamine D2 receptors. As $A_{2A}R$ and dopamine D2 receptors do indeed interact, these results indicate that $A_{2A}R$ homodimers are the functional species at the cell surface and that they coexist with $A_{2A}R$/D2 receptor heterodimers.

Keywords: 7TM receptors, dopamine receptors, G protein-coupled receptors, heteromerization, homomerization, receptor–receptor interactions.

J. Neurochem. (2004) **88,** 726–734.

Heptaspanning membrane receptors (HSMRs) also known as G protein-coupled receptors (GPCRs) were previously considered to be monomeric proteins which only interacted with G proteins. However it has become clear that HSMRs are oligomeric structures formed by receptor homodimers, heterodimers and multimers and a variety of proteins interacting at the horizontal and the vertical level (Agnati *et al*. 2002, 2003; Bouvier, 2001; Milligan and White 2001; Rios *et al*. 2001; Franco *et al*. 2003). Adenosine A_1 and A_{2A} receptors (A_1R and $A_{2A}R$) can be considered as a paradigm

Received August 26, 2003; revised manuscript received September 30, 2003; accepted October 13, 2003.

Address correspondence and reprint requests to Rafael Franco, Department of Biochemistry and Molecular Biology of the University of Barcelona, Marti Franquès 1, Barcelona E-08028, Spain.
E-mail: rfranco@ub.edu

Abbreviations used: $A_{2A}R$, adenosine A_{2A} receptor; BRET, bioluminescence resonance energy transfer; D_2R, dopamine D_2 receptor; FRET, fluorescence resonance energy transfer; GABAergic neuron, gamma-amino butyric acid neuron; GPCR, G protein-coupled receptor; HSMR, heptaspanning membrane receptor; PBS, phosphate-buffered saline; SDS–PAGE, sodium dodecyl sulfate–polyacrylamide gel electrophoresis.

of HSMRs involved in receptor–receptor interactions. In fact, the existence of heteromeric complexes leads to the demonstration that in cells coexpressing adenosine A_1 and dopamine D_1 receptors A_1R agonists inhibit the binding of dopamine to D_1 receptors (Ferré *et al*. 1998; Ginés *et al*. 2000). A synergism in signaling via A_1 receptors and metabotropic glutamate 1α receptors has been demonstrated in cells expressing heteromeric complexes formed by A_1 and metabotropic 1α receptors (Ciruela *et al*. 2001). These antagonisms or agonisms can in part be caused by cross-talk at the level of second messengers. However, the effect on pharmacological profile and on binding kinetics can be attributed almost exclusively to the conformational changes transmitted within the intercommunicating receptor molecules when they are activated by agonists. Important experimental evidence has accumulated in relation to the existence of reciprocal interactions between $A_{2A}R$ and metabotropic glutamate receptor mGlu5 (mGluR5) and between $A_{2A}R$ and D_2 receptors (D_2R) in the basal ganglia (Ferré *et al*. 2002; Hillion *et al*. 2002) that can again be attributed to the existence of heteromers between $A_{2A}R$ and mGluR5 or between $A_{2A}R$ and D_2R. $A_{2A}R$ and D_2R are specifically localized in one subtype of neuron, the striatopallidal gamma-amino butyric acid neuron (GABAergic neuron), on which both receptors express their highest density in the brain. The striatopallidal GABAergic neurons play a key role in the pathophysiology of basal ganglia disorders, including Parkinson's disease, and it is a common pathway for the rewarding effects in drug abuse, as well as for the antipsychotic effects of neuroleptics. $A_{2A}R$–D_2R interactions have been demonstrated at the biochemical, functional, and behavioral level leading to the suggestion that this interaction may provide new therapeutic approaches for Parkinson's disease, schizophrenia and drug addiction (reviewed in Ferré *et al*. 2003 and Agnati *et al*. 2003). Recently, fluorescence resonance energy transfer (FRET) and bioluminescence resonance energy transfer (BRET) approaches demonstrated the occurrence of $A_{2A}R$–D_2R heterodimerization in a heterologous mammalian expression system (Canals *et al*. 2003).

In contrast to heteromerization, homomerization of adenosine receptors has not been extensively studied. Using a sodium dodecyl sulfate–polyacrylamide gel electrophoresis (SDS–PAGE) strategy and immunoblotting, Ciruela *et al*. (1995) demonstrated the existence of A_1 homodimers in brain tissue from different species. This article was among the first describing homodimers of HSMRs and it was the first to report homodimers of HSMRs in a native tissue. In this paper FRET and BRET techniques have been used to study the homodimerization of $A_{2A}R$. The influence of receptor density, of agonist activation and of the presence of D_2R on the degree of $A_{2A}R$–$A_{2A}R$ homomerization was also assessed showing that $A_{2A}R$ undergoes constitutive homodimerization and that the active molecule at the cell surface is the dimer. Furthermore, it was analyzed whether the C-terminal tail of $A_{2A}R$, which is important for $A_{2A}R$-D_2R heteromerization (Canals *et al*. 2003), is involved in homodimerization.

Experimental procedures

Plasmids

The HA epitope was introduced between amino acids six and seven of the human adenosine $A_{2A}R$ receptor using the same PCR mutagenesis approach as for the $A_{2A}R$-Flag construct (Ferré *et al*. 2002). The human $A_{2A}R$-Flag without its stop codon was amplified using sense and antisense primers harboring unique *Eco*RI and *Bam*HI sites. The fragment was then subcloned to be in-frame with either *Rluc,* EYFP, or GFP^2 into the *Eco*RI and *Bam*HI restriction site of a *Renilla luciferase* expressing vector (pcDNA3.1-Rluc) and the enhanced variant of GFP (pEYFP-N1; Clontech, Heidelberg, Germany), respectively. The positive control vector used for the FRET experiments, pGFP2-EYFP, was a gift from R. Pepperkok's laboratory, EMBL, Heidelberg (described in Zimmermann *et al*. 2002). A mutant lacking the C-terminal domain of adenosine A_{2A} receptor was generated using $A_{2A}R$-Flag as the template (Burgueño *et al*. 2003).

Antibodies, cell culture and transfection

An antiserum against the GST fusion protein containing amino acids 322–412 (SA2A) of the adenosine A_{2A} receptor was used in this study, designated as anti-CTA2A. The immunization of rabbits and affinity purification of the antisera were performed as described previously (Ciruela and McIlhinney 1997). Other primary antibodies used were: anti-Flag monoclonal antibody (Clone M2, Sigma-Aldrich Chemical Co., St. Louis, MO, USA), anti-Flag monoclonal antibody europium cryptate labeled and anti-HA monoclonal antibody allophycocyanin (APC) labeled (CIS bio internacional, Bagnols/Cèze, France). The secondary antibodies used were: horseradish-peroxidase (HRP)-conjugate goat anti-rabbit IgG and HRP-conjugate goat anti-mouse IgG (Pierce, Rockford, IL, USA).

Cells

HEK-293 and HeLa were grown in Dulbecco's modified Eagle's medium, DMEM (Sigma-Aldrich Chemical Co., St. Louis, MO, USA) supplemented with 2 mM L-glutamine, 100 U/mL penicillin/streptomycin and 10% (v/v) fetal bovine serum (FBS) at 37°C and in an atmosphere of 5% CO_2. HEK-293 cells growing in 25 cm^2 flasks or 3 cm^2 coverslips were transiently transfected with 3 μg or 1 μg, respectively, of DNA encoding for the proteins specified in each case by calcium phosphate precipitation (Jordan *et al*. 1996). The cells were harvested at either 24 or 48 h after transfection.

Determination of total protein in transfected cells and control of fusion-protein expression

Forty-eight hours post-transfection, cells were rapidly washed twice in PBS, detached, and resuspended in the same buffer. To control the amount of cells in the assays, protein concentration was determined in the samples using a Bradford assay kit (Bio-Rad, Munich, Germany) using bovine serum albumin dilutions as a standard. To quantify $A_{2A}R$-GFP^2, $A_{2A}R$-YFP or D2-YFP expression, the cell suspension (20 μg of protein) was distributed in duplicate into 96-well

microplates (Corning #3604, U.S.A, white plates with transparent bottom). The fluorescence was measured using a Packard Fluoro-Count™ with an excitation filter of 400 nm (for A_{2A}R-GFP^2) or 485 nm (for A_{2A}R-YFP or D2-YFP) and an emission filter of 510 (for A_{2A}R-GFP^2) or 530 nm for (A_{2A}R-YFP or D2-YFP) using the following parameters: Gain of 1, PMT fixed at 1100 V, and read time of 1 s. Fluorescence was quantified as fold over the background (mock transfected cells). For assessing the expression of A_{2A}R-Rluc, the same samples were incubated for 10 min with 5 μM coelenterazine H (Molecular Probes) and the luminescence was measured using a Packard LumiCount™ with the following parameters: Gain of 1, PMT fixed at 700 V, and a read time of 1 s.

BRET experiments

For BRET measurement, the equivalent of 20 μg of cell suspension (see above) were distributed in duplicates in 96-well microplates (Corning #3600, USA, white opaque plates) and 5 mM coelenterazine H was added. After 1 min, the readings were collected using a Fusion microplate analyzer (Packard, Meriden, CT) that allows the integration of the signals detected in the 440–500 nm and the 510–590 nm windows using filters with the appropriate band pass. The BRET ratio is defined as

$$[(\text{emission at } 510-590)/(\text{emission } 440-500)] - \text{Cf}$$

where Cf corresponds to (emission at 510–590)/(emission at 440–500) for the -Rluc construct expressed alone in the same experiment.

Subcellular membrane isolation

HEK-293T cells transiently cotransfected with the A_{2A}R-Rluc and D_2R-YFP were grown in 100 mm dishes to 80–90% confluency. Cells were washed twice with ice-cold PBS and lysed with 2 mL of ice-cold hypotonic lysis buffer (20 mM HEPES, pH 7.4, 2 mM EDTA, 2 mM EGTA, 6 mM $MgCl_2$, 1 mM phenylmethylsulfonyl fluoride and 1 : 100 dilution of a protease inhibitor cocktail). Lysate was then sonicated for 30 s (three strokes with a delay of 1 min between strokes) followed by two 10 s bursts in a Polytron tissue grinder. Cellular debris and unlysed cells were removed by centrifuging at 1000 *g* for 5 min at 4°C. Sucrose was added to achieve a final concentration of 0.2 M and 2 mL was applied to the top of a discontinuous step gradient (5 mL/step) made at 0.5, 0.9, 1.2, 1.35, 1.5 and 2.0 M sucrose in lysis buffer. The samples were then centrifuged for 16 h at 105 000 *g* at 4°C in a Beckman SW28 rotor. The plasma membrane was recovered in the sucrose gradient at the interface between 0.5 and 0.9 M. The endoplasmic reticular membrane samples were recovered at the interface between the 1.35 and 1.5 M and luminescence was measured. For the verification of isolated membranes as either plasma or endoplasmic reticulum membranes, fractions were then precipitated with cold acetone overnight and analyzed by immunoblotting using monoclonal antibodies against the Na^+K^+-ATPase pump (1 : 250 dilution, Sigma-Aldrich, St. Louis, MO, USA) and calnexin (1 : 500 dilution, BD Transduction Laboratories, Lexington, CY, USA).

Raft disruption

HEK-293T cells were serum-starved overnight 24 h post-transfection. Cholesterol depletion was achieved by incubation for 1 h at 37°C with 2% 2-hydroxypropyl-β-cyclodextrin (β-CD, Sigma-Aldrich) in Dulbecco's modified Eagle's medium. Cholesterol repletion was carried out after washing twice with fresh medium, by incubation for 1 h at 37°C with 0.4% β-CD and 16 mg/mL of cholesterol (Sigma-Aldrich). Complete raft disruption was assessed as caveolin-1 displacement in a discontinuous sucrose gradient. For this, confluent control or depleted cells were washed twice with ice-cold phosphate-buffered saline (PBS), scraped and resuspended into 2 mL of 500 mM Na_2CO_3, pH 11.0. Cells were sequentially homogenized using a Polytron (three times, 10 s), a syringe (20 times) and a sonicator (three times, 30 s), placed at the bottom of an ultracentrifuge tube and adjusted to 45% sucrose in MBS (25 mM Mes, 0,15 M NaCl, pH 6,5). A discontinuous 5–35% sucrose gradient was formed above in MBS containing 250 mM Na_2CO_3 pH 6,5. After centrifugation at 105 000 × *g* for 18 h at 4°C in a SW41.Ti rotor (Beckman) fractions were collected and analyzed by western blot using an antibody against caveolin-1 (BD Transduction Laboratories). β-CD effects were also tested by MAPK phosphorylation analysis. Treated cells were directly resuspended in loading buffer and analyzed by western blot using the antibodies against phosphorylated or total ERK1, 2 (Sigma-Aldrich).

FRET experiments analyzed by fluorimetry

Forty-eight hours post-transfection, HeLa cells were rapidly washed twice in PBS, detached, and resuspended in the same buffer. Cell suspension (20 μg of protein) was distributed in duplicate into 96-well microplates (black plates with a transparent bottom). Plates were read in a Fluostar Optima Fluorimeter (BMG Labtechnologies, Offenburg, Germany) equipped with a high-energy xenon flash lamp, using a 10-nm bandwidth excitation filter at 400 nm (393–403 nm), and 10 nm bandwidth emission filters corresponding to 506–515 nm filter (Ch 1), 527–536 nm filter (Ch 2). Gain settings were identical for all experiments to keep the relative contribution of the fluorophores to the detection channels constant for spectral unmixing. The contributions of the GFP variants, GFP^2 and YFP proteins alone, to the two detection channels (spectral signature) were measured in experiments with cells expressing only one of these proteins and normalized to the sum of the signal obtained in the two detection channels. The spectral signatures of the different receptors fused to either GFP^2 or YFP did not significantly vary from the determined spectral signatures of the fluorescent proteins alone. FRET quantitation was performed as described previously (Zimmermann *et al*. 2002; Canals *et al*. 2003).

Time-resolved FRET

Time-resolved FRET was performed as described by McVey *et al*. (2001). Transiently transfected HEK cells (1×10^6) were detached, washed twice with PBS and fixed in 4% paraformaldehyde for 15 min, and washed with PBS containing 20 mM glycine to quench the remaining free aldehyde groups. Blocking was carried out using PBS containing 50% fetal bovine serum (buffer A) during 30 min. An over-night incubation was performed at 4°C in a total volume of 100 μL containing 3 nM Eu^{3+}-labeled anti-Flag antibody and 45 nM APC-labeled anti-HA antibody in buffer A. After incubation cells were washed once with buffer A and once with PBS containing 400 mM KF. Cells were resuspended in 50 μL of PBS/KF before placing into wells of a 96-well microtiter plate for FRET analysis using a Victor^2 (Perkin-Elmer, Boston, MA, USA) configured for time-resolved fluorescence. The Eu^{3+}-labeled anti-Flag antibody

was excited at 340 nm and emissions monitored at 615 nm (Eu^{3+} emission) and 665 nm (FRET). A 400-μs reading was taken after a 50-μs delay to allow for decay of short-lived endogenous fluorescence signals.

Immunoprecipitation and immunoblotting

Transiently transfected HEK cells were solubilized in ice-cold lysis buffer (PBS, pH 7.4, containing 1% (v/v) Nonidet P-40) for 30 min on ice. The solubilized preparation was then centrifuged at 13.000 × *g* for 30 min. The supernatant (1 mg/mL) was processed for immunoprecipitation, each step of which was conducted with constant rotation at 0–4°C. The supernatant was incubated with a monoclonal anti-Flag antibody (2 μg/mL) for 2 h. Then 40 μL of a suspension of protein G cross linked to agarose beads were added and the mixture was incubated overnight. The beads were washed twice with ice-cold lysis buffer, twice with ice-cold lysis buffer containing 0.1% (v/v) Nonidet P-40, once with ice-cold Tris buffered saline, pH 7.4, and aspirated to dryness with a 28-gauge needle. Subsequently, 30 μL of SDS–PAGE sample buffer (8 M Urea, 2% SDS, 100 mM DTT, 375 mM Tris, pH 6.8) was added to each sample. Immune complexes were dissociated by heating to 37°C for 2 h and resolved by SDS–PAGE in 10% gels. Proteins were transferred to polyvinylidene difluoride membranes (Immobilon-P, Millipore, Watford, UK) using a semidry transfer system and immunoblotted using the anti-CTA2A antiserum (1 : 2000), the anti-Flag monoclonal antibody (8 μg/mL) and then horseradish–peroxidase(HRP)-conjugated goat anti-rabbit IgG (1 : 60 000). The immunoreactive bands were developed with the SuperSignal chemiluminescent detection kit (Pierce, Rockford, IL, USA).

Biotinylation of cell surface proteins

HEK-293 cells transiently transfected with A_{2A}R-Flag were washed three times in borate buffer (10 mM H_3BO_3, pH 8.8; 150 mM NaCl) and then incubated with 50 μg/mL sulfo-NHS-LC-biotin (Pierce) in borate buffer for 5 min at room temperature. Cells were washed three times in borate buffer and again incubated with 50 μg/mL sulfo-NHS-LC-biotin in borate buffer for 10 min at room temperature, and then 100 mM NH_4Cl was added for 5 min to quench the remaining biotin. Cells were washed in PBS, disrupted with three 10-s strokes in a polytron and centrifuged at 13 000 *g* for 30 min The pellet was solubilized in ice-cold lysis buffer [PBS, pH 7.4, containing 1% (v/v) Nonidet P-40] for 30 min and centrifuged at 13 000 *g* for 30 min. The supernatant was incubated with 80 μL streptavidin–agarose beads (Sigma) for 1 h with constant rotation at 4°C. Beads were washed twice with ice-cold lysis buffer, twice with 1 : 10 ice-cold lysis buffer and once with ice-cold PBS. The complexes were dissociated by adding 50 μL of SDS/PAGE sample buffer (see above), heated at 37°C for 2 h, and then resolved by SDS–PAGE on 10% gels. The gels were run and immunoblotted as described above.

Results and discussion

Although it has been shown by FRET and BRET that A_{2A}R form heterodimers with D_2R in HEK293 cells (Canals *et al*. 2003), the ability of A_{2A}R to form homodimers has not been described. To investigate A_{2A}R-A_{2A}R homodimerization, BRET and FRET techniques were applied in cells transfected with fusion proteins consisting of the receptor and either a fluorescent protein (GFP2, YFP) or *Renilla luciferase* (*Rluc*). Expression of chimeric proteins was assessed by western blot and immunocytochemistry (data not shown). The functionality of the receptor-*Rluc*, -GFP[2] or -YFP constructs was assessed by the determination of cAMP levels produced in transfected cells in response to ligand binding. According to the positive coupling of A_{2A}R to the adenylyl cyclase, the A_{2A}R agonist CGS21680 properly induced the same cAMP accumulation in cells transfected with A_{2A}R-YFP or A_{2A}R-*Rluc* or in cells transfected with A_{2A}R (Canals *et al*. 2003 and data not shown).

BRET saturation curve in cells cotransfected with a constant amount of the A_{2A}R-*Rluc* construct while increasing concentrations of the A_{2A}R-YFP plasmid was analyzed. A positive BRET signal for the transfer of energy between A_{2A}R-*Rluc* and A_{2A}R-YFP was obtained (Fig. 1). The BRET signal increased as a hyperbolic function of the concentration of the YFP-fusion construct added (assessed by the fluorescence emitted upon direct excitation at 480 nm) reaching an asymptote. As the pair A_{2A}R-*Rluc* and $GABA_BR2$-YFP led to an undetectable BRET signal (Fig. 1), the hyperbolic BRET signal found for the A_{2A}R-*Rluc*-A_{2A}R-YFP indicates that the interaction between two A_{2A}R molecules is specific. These results agree with those provided recently by Kamiya *et al*. (2003) showing a BRET ratio of 0.10 at a given ratio of A_{2A}R-*Rluc* and A_{2A}R-GFP[2]. In heterologous expression systems positive BRET or FRET signals are not sufficient to invoke A_{2A}R homodimer formation. In fact, receptors located within specific plasma membrane microdomains, such as membrane rafts, may give rise to FRET or BRET

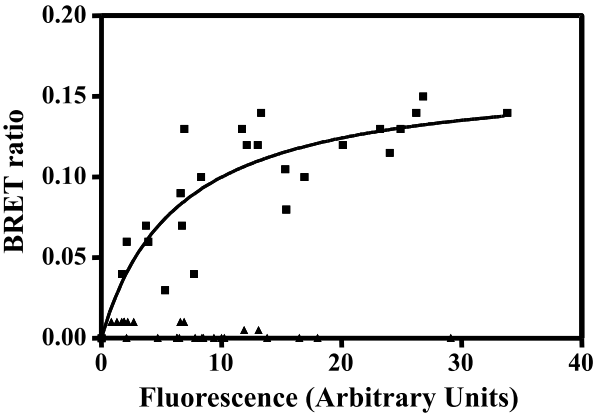

Fig. 1 BRET saturation curve. BRET was measured in HEK-293T cells coexpressing A_{2A}R-*Rluc* and A_{2A}R-YFP (■) or A_{2A}R-*Rluc* and $GABA_BR2$-YFP (▲) constructs. Co-transfections were performed with increasing amounts of plasmid DNA for the YFP construct whereas the DNA for the *Rluc* construct was maintained constant. Both fluorescence and luminescence of each sample were measured prior to every experiment to confirm equal expression of *Rluc* while monitoring the increase of YFP expression (see Methods).

signals not due to homodimerization. $A_{2A}R$ are not expected to be in caveolae in HEK cells. However from the report by Zacharias *et al*. 2002, energy transfer between closely located receptor molecules can occur in heterologous expression systems even in the absence of a direct interaction. The cyclodextrin assay is therefore performed to be sure that overexpression of receptors does not lead to their accumulation in rafts. Localization of overexpressed membrane fluorescent proteins in rafts could allow a close enough proximity of receptors (< 10 nm) to permit the transfer of energy. To explore this possibility, membrane rafts were disrupted by cyclodextrin treatment, and BRET assays were performed in these cells. As indicated in Fig. 2(a), cyclodextrin did not lead to any change in the BRET signal. In addition, no change in the BRET signal was noted when cells were repleted with cholesterol after cyclodextrin treatment (Fig. 2a). The efficacy of the treatment was assessed by cyclodextrin-mediated ERK1/2 phosphorylation (Fig. 2b), as indicated by Furuchi and Anderson (1998). Raft disruption was also assessed by the redistribution of caveolin-1 from raft enriched light fractions to heavier fractions after sucrose gradient separation (Fig. 2c). Taken together, this indicates that the energy transfer between $A_{2A}R$-*Rluc* and $A_{2A}R$-YFP is due to the formation of true homodimers.

Stimulation with the agonist CGS21680 did not promote any consistent change in the $BRET_{50}$ signal and similar results were obtained at maximum BRET and at low BRET ratio (Fig. 3). These results agree with those reported by Kamiya *et al*. (2003) and suggest that receptor activation does not affect its oligomerization state and, that the homodimers are, most probably, constitutively preformed. The lack of modulation by agonists has also been reported for other homo- and heterodimeric partners (Rios *et al*. 2001; Issafras *et al*. 2002; Terrillon *et al*. 2003). In carefully controlled BRET studies, it has been demonstrated that a number of heteromerizing receptors are preassembled in the ER and the dimers that reach the plasma membrane are not affected, in terms of the degree of dimerization, after receptor activation by their corresponding agonists (Jensen *et al*. 2002; Issafras *et al*. 2002; Ramsay *et al*. 2002 Terrillon *et al*. 2003). In contrast, detailed studies by Patel *et al*. (2002) in stable CHO-K1 cells expressing somatostatin receptors suggest that the receptors are monomeric in their basal state and oligomerize only upon agonist activation. For the somatostatin receptor subtype R5, the same authors report that agonists-induced homomerization extends beyond dimers to higher order oligomers (Patel *et al*. 2002). It should be also noted that D_2R homodimers are not modulated by ligands whereas there is an agonist-mediated oligomerization of a shorter splice variant of the receptor (D_{2s}) that is found presynaptically as an autoreceptor (Wurch *et al*. 2001). From our experimental data, the unchanged BRET signal reported in cells treated with agonists, is not necessarily in contradiction to the known clustering of these receptors when they are activated by agonists (Hillion *et al*. 2002). Taken together these results indicate that $A_{2A}R$ agonists leads to the reorganization of receptors within the plasma membrane while not affecting their degree of homodimerization. Considering the data, it appears as if ligand activation of

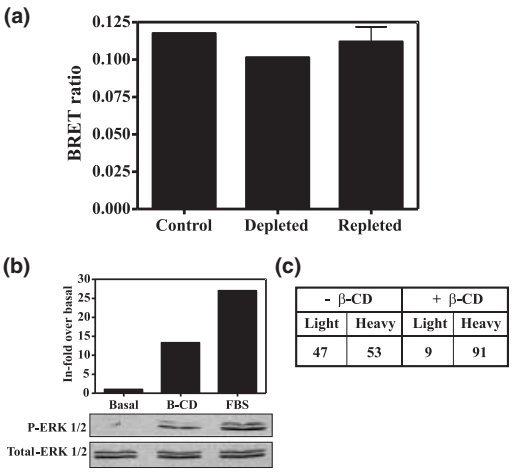

Fig. 2 β-Cyclodextrin (β-CD) treatment. (a) BRET experiments were performed in HEK-293T cells cotransfected with the amount of plasmid DNA for the $A_{2A}R$-Rluc and $A_{2A}R$-YFP constructs to give the maximum BRET. Cells were not treated (control) or treated with 2% β-CD for 1 h (depleted). Cholesterol repletion was achieved by incubating depleted cells for 1 h with 0.4% β-CD and 16 mg/mL cholesterol (repleted). No differences in BRET were observed after depletion or repletion treatment. (b) β-CD-induced phosphorylation of ERK1,2. A2AR-Rluc-A2AR-YFP cotransfected HEK-293T cells treated with 2% β-CD for 1 h were then lysed and analyzed for western blot against phoshorylated or total ERK1,2 while FBS-induced phosphorylation was used as a control. (c) Densitometry of the bands of an immunoblotting of caveolin-1 in cells treated with β-CD. Extracts from control and treated cells were fractionated by a discontinuous sucrose gradient to obtain the light and heavy membrane fractions. Caveolin-1 was detected by western blot in both membrane fractions. Results are expressed as the percentage of the total intensity.

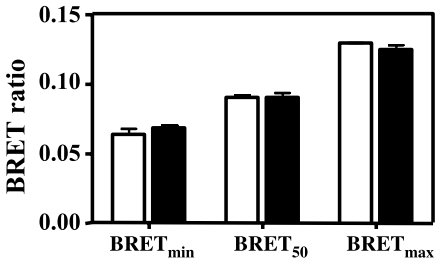

Fig. 3 Effect of ligands on $A_{2A}R$-$A_{2A}R$ dimerization. BRET measurements were performed after 2 h of treatment with (black bars) or without (white bars) 200 nM of $A_{2A}R$ agonist CGS21680 in HEK-293T cells cotransfected with the $A_{2A}R$-*Rluc*/$A_{2A}R$-YFP pair at the $BRET_{min}$, $BRET_{50}$, $BRET_{max}$ ratios. Data are mean ± SD of three independent experiments.

the receptors leads to targeting of pre-existing $A_{2A}R$ homodimers to membrane microdomains. Using the FRET approach with the $A_{2A}R$-GFP^2 and $A_{2A}R$-YFP pair (see Experimental procedures), it was possible to confirm the homodimerization between $A_{2A}R$ molecules and to estimate a FRET efficiency of 0.28 (Fig. 4a). Cells expressing a chimeric GFP^2-YFP protein (see Experimental procedures) were used as positive control and gave a FRET efficiency of 0.52, whereas the cotransfection with the vectors coding for GFP^2 and YFP gave a very low FRET efficiency signal (Fig. 4a).

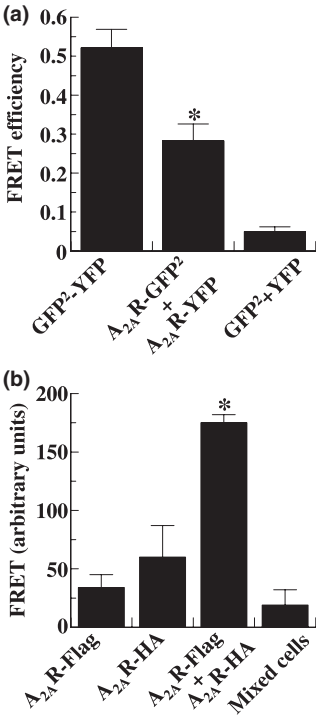

Fig. 4 FRET assays. (a) FRET efficiency of the $A_{2A}R$-GFP^2 and $A_{2A}R$-YFP pair by sensitized emission in living cells. HeLa cells were transiently transfected with the plasmid DNA corresponding to $A_{2A}R$-GFP^2 (donor) and $A_{2A}R$-YFP (acceptor) proteins using a ratio of donor to acceptor DNA of 1 : 2, with the positive control plasmid GFP^2-YFP, or with the two fluorescent proteins GFP^2 and YFP. Fluorescence readings were performed 48 h post-transfection as described in Materials and methods. Linear un-mixing of the emission signals was applied to the data (see Materials and methods) and the results are shown as the sensitized emission of the acceptor when the cells were excited at 400 nm. Similar results were found in HEK-293 cells. Data are the mean ± SD of three independent experiments performed in triplicate. Significance was evaluated using paired Student's *t*-test. $^*p < 0.01$ versus the two fluorescent proteins GFP^2 and YFP co-transfected in the same cells. (b) Time-resolved FRET detection of cell surface $A_{2A}R$ homodimers. HEK cells were transfected with $A_{2A}R$-Flag, $A_{2A}R$-HA or both Flag and HA tagged $A_{2A}R$ and were processed for time-resolved FRET (see Experimental procedures). A mixture of separately transfected cells with either $A_{2A}R$-Flag or $A_{2A}R$-HA (mixed cells) were used as a negative control. $^*p < 0.01$ versus single transfected cells.

BRET and FRET are powerful techniques to demonstrate protein–protein interactions in living cells. However, neither the above described FRET and BRET data nor the BRET data given by Kamiya *et al*. (2003) give insights about the functionality of the homodimers. This is due to the fact that FRET, using fluorescent fusion proteins, or BRET, cannot distinguish between interactions occurring at the cell surface or in intracellular compartments. Functionality of G protein coupled receptors is closely related with their expression at the plasma membrane, i.e. the functional species will be the ones which predominate at the cell surface. It would be then very relevant to know whether homo or heterodimers or both are present at the plasma membrane. In this paper the demonstration of the existence of homodimers at the cell surface has been approached by two different techniques: time-resolved FRET and the biotinylation of cell surface proteins. Time-resolved FRET was assayed in cells transfected with $A_{2A}R$-flag and/or $A_{2A}R$-hemagglutinin detected with a fluorescent FRET pair of antibodies against flag or hemagglutinin (see protocol in Experimental procedures). Cotransfected cells gave a significant and strong FRET signal compared with cells singly transfected with one vector. When cells were transfected with different vectors separately and then mixed prior to the assays the signal was very weak (Fig. 4b). This indicates that $A_{2A}R$ homodimers are formed in the cotransfected cells but do not form *in vitro* after mixing this singly transfected cells. Overall these results demonstrate that $A_{2A}R$-$A_{2A}R$ homodimers are present on the cell surface of cotransfected cells.

To confirm whether these homodimeric structures were expressed on the cell surface, biotinylation experiments were performed in cells expressing $A_{2A}R$-flag. In crude lysates it was possible to detect both the dimer and the monomer of $A_{2A}R$ when using an anti-$A_{2A}R$ antibody (Fig. 5a). The ratio of dimer versus monomer in the crude cell extract is less than two (Fig. 2b). In contrast, using streptavidin to precipitate the biotinylated proteins it was possible to detect a higher ratio of the dimer versus the monomer (9 : 1) on the cell surface (Fig. 5b). In the conditions described in Experimental procedures, which constitute standard protocols for sample preparation and immunoblotting, the receptor dimers are preserved even in a SDS-containing denaturing buffer (Fig. 5a). Biotinylated species existing on the cell surface were also analyzed by immunoprecipitation using an anti-flag antibody. In these assays more than 90% of the total labeled proteins, corresponded to biotinylated-$A_{2A}R$-dimers (Fig. 5c). As a control, the blot developed using an anti-$A_{2A}R$ antibody showed in the immunoprecipitate the presence of both $A_{2A}R$ monomers and $A_{2A}R$ dimers. These results indicate again that $A_{2A}R$ dimers are the major species present on the cell surface. In intracellular compartments, a certain amount of monomeric species exists and, probably, assemble into dimers prior to cell surface expression of

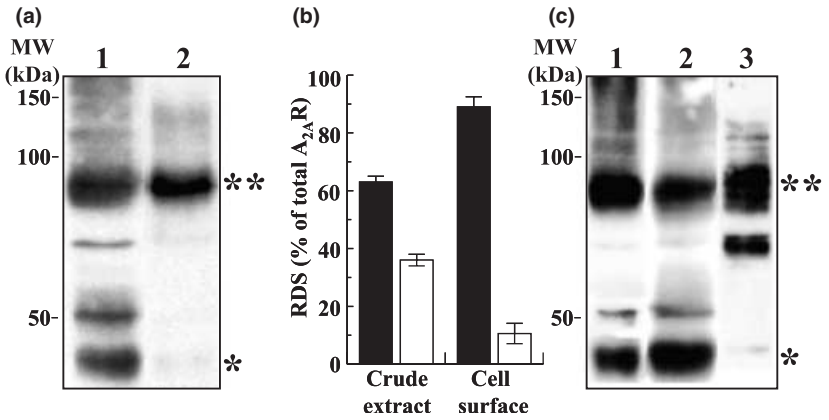

Fig. 5 Cell surface detection of $A_{2A}R$ homodimers. (a) HEK-293 cells were transiently transfected with $A_{2A}R$-Flag and cell surface labeling was performed as described in Experimental procedures. Crude extracts (lane 1) and biotinylated proteins (lane 2) were subsequently analyzed by SDS-PAGE and immunoblotted using anti-$CT_{A2}A$ polyclonal antibody (1/2000). **Band corresponding to the $A_{2A}R$ dimmer; *band corresponding to the $A_{2A}R$ monomer. (b) Relative densitometric scans (RDS) of immunoblot in (a). The amount of $A_{2A}R$ dimer (black bars) and monomer (white bars) are normalized using the total sum of $A_{2A}R$ (dimer plus monomer) in each lane. The crude extract corresponds to lane 1 in (a) and cell surface fraction to lane 2 in (a). The data are the mean ± SD of three independent experiments. (c) HEK-293 cells were transiently transfected with $A_{2A}R$-Flag and cell surface labeling was performed as described in Experimental procedures. Cells solubilized in ice-cold lysis buffer (lane 1) were immunoprecipitated with an anti-Flag monoclonal antibody (2 μg/mL) (lane 2 and 3). The soluble extract and immunoprecipitates were analyzed by SDS–PAGE and immunoblotted using anti-CTA_{2A} polyclonal antibody (1 : 2000) (lanes 1 and 2) or HRP-conjugate streptavidin (Amersham, 1/1000) (lane 3). **Band corresponding to the $A_{2A}R$ dimmer; *band corresponding to the $A_{2A}R$ monomer.

$A_{2A}R$. Alternatively, these monomeric species could be targeted for degradation and this may be a reason for their failure to reach the cell surface. In any case the time-resolved FRET and the biotinylation data confirm that homodimers are the functionally relevant $A_{2A}R$ species. Demonstration of both molecular interactions between $A_{2A}R$ and $A_{2A}R$ to form homodimers in this paper and between $A_{2A}R$ and D_2R to form heterodimers (Canals *et al*. 2003) leads to the question which of them is the most favored interaction. BRET experiments performed using cells cotransfected with either $A_{2A}R$-*Rluc* and $A_{2A}R$-YFP or $A_{2A}R$-*Rluc* and D_2R-YFP implies that the homodimerization is more favored than heterodimerization (Fig. 6). Although the level of expression of the fluorescent acceptor in the assays was similar for $A_{2A}R$-YFP and D_2R-YFP, these results should be taken with some caution due to intrinsic differences in fluorescence emission for a given amount of $A_{2A}R$-YFP and D_2R-YFP and to differences in the distance between donor and acceptor in the homo- or the heterodimer. On the other hand, the formation of homo-oligomers by interaction of homodimers of each receptor may not predispose to generation of an efficient BRET signal. As the C-terminal tail of $A_{2A}R$ is probably involved in $A_{2A}R$-D_2R heteromerization (Canals *et al*. 2003), the role of this domain of the receptor in homodimerization has been investigated. Western blot and co-immunoprecipitation assays were performed in cells transfected with a cDNA encoding for an $A_{2A}R$-deletion mutant-flag which lacks the C-terminal region of the molecule ($A_{2A\Delta CT}R$-flag, see Experimental procedures). Immunoblots obtained using an antibody against the flag epitope confirmed coexpression of monomers and dimers of $A_{2A\Delta CT}R$-flag in transfected cells (Fig. 7). Co-immunoprecipitation using anti-flag antibodies also revealed the

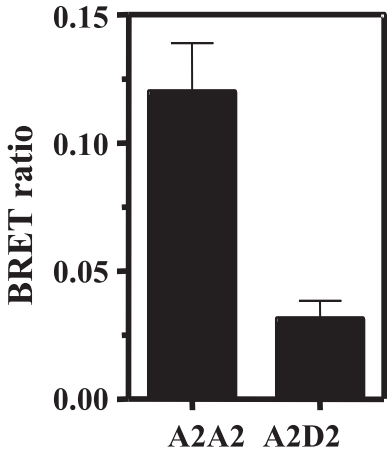

Fig. 6 Comparison of the BRET ratio between the $A_{2A}R$-$A_{2A}R$ homodimer (A2A2) and the $A_{2A}R$-D_2R (A2D2) heterodimer. BRET was measured in HEK-293T cells coexpressing $A_{2A}R$-*Rluc* and $A_{2A}R$-YFP or $A_{2A}R$-*Rluc* and D_2-YFP constructs. Measurements were performed at maximum BRET keeping constant the amount of *Rluc* construct. Fluorescence of the samples was assessed for similar expression of $A_{2A}R$-YFP and D_2-YFP.

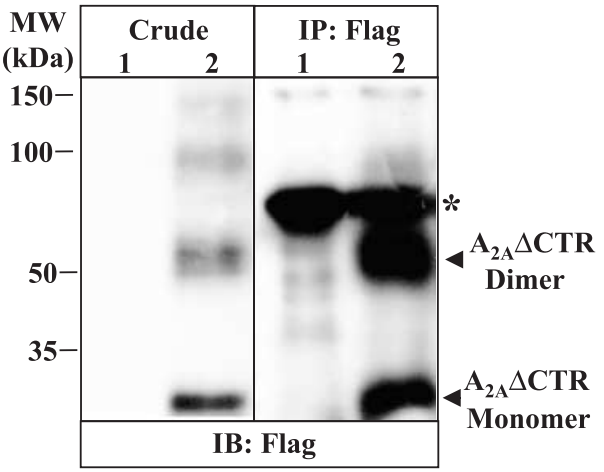

Fig. 7 Dimerization of $A_{2A}\Delta_{CT}R$ in HEK-293 cells. Mock transfected cells (lane 1) or expressing $A_{2A}\Delta_{CT}R$-Flag (lane 2) were washed, solubilized and processed for immunoprecipitation using anti-Flag monoclonal antibody (2 μg/mL). Solubilized membranes (Crude) and immunoprecipitates (IP, Flag) were analyzed by SDS–PAGE and immunoblotted using an anti-Flag monoclonal antibody (IB, Flag) band corresponding to the immunoglobulins.

presence of both, monomers and dimers of the deletion mutant (Fig. 7). The results indicate that a receptor lacking the C-terminal domain is also able to form homodimers and this suggests that different domains are involved in the formation of $A_{2A}R$-$A_{2A}R$ homodimers versus $A_{2A}R$-D_2R heterodimers.

On the other hand, indirect evidence shown by confocal microscopy indicates that a high colocalization of $A_{2A}R$ and D_2 receptor occurs in primary cultures of striatal neurons (Hillion *et al*. 2002). It would then be predicted that in striatal neurons, which express high amounts of both $A_{2A}R$ and D_2 receptors, homodimers (of $A_{2A}R$ and also of D_2R, Guo *et al*. 2003) and heterodimers would coexist and their proportion would vary depending on the level of expression of each of the receptors, i.e. their stoichiometry, in individual striatal neurons. Although agonist modulation of the homodimers and the heterodimers has been ruled out for $A_{2A}R$ homodimers and for $A_{2A}R/D_2$ receptor heterodimers (Canals *et al*. 2003; Kamiya *et al*. 2003), the search of other possible mechanisms of modulation of the interconversion among homo and heterodimers would be of interest to understand the exact role of these species in striatal function and to design novel therapeutical strategies to treat basal ganglia disorders such as Parkinson's disease.

Acknowledgements

This study was supported by grants: QLG3-CT-2001–01056 from the European Union; SAF2001-5357-E (RF), SAF2002-03293 (R.F), and SAF2001-3474 (EIC) from Ministerio de Ciencia y Tecnología, 02/056–00 (RF) from Fundacio la Caixa and 01/012710 (RF) from Fundació Marató of Catalonian Telethon. F. Ciruela is currently holding a Ramón y Cajal research contract signed with the Ministerio de Ciencia y Tecnología.

References

Agnati L. F., Santarossa L., Benfenati F., Ferri M., Morpurgo A., Apolloni B. and Fuxe K. (2002) Molecular basis of learning and memory: modelling based on receptor mosaics, in *From Synapses to Rules* (Apolloni, B. and Kurfes, F., eds), pp. 165–195. Kluwer Academic/Plenum Publishers, New York.

Agnati L., Ferré S., Lluis C., Franco R. and Fuxe K. (2003) Molecular mechanisms and therapeutical implications of intramembrane receptor–receptor interactions among heptahelical receptors with examples from the striato-pallidal GABA neurons. *Pharmacol Rev.* **55**, 509–550.

Bouvier M. (2001) Oligomerization of G-protein-coupled transmitter receptors. *Nat. Rev. Neurosci.* **2**, 274–286.

Burgueño J., Blake D. J., Benson M. A., Tinsley C. L., Esapa C. T., Canela E. I., Penela P., Mallol J., Mayor F., Lluis C. *et al.* (2003) Adenosine A2 receptor interacts with actinin-binding protein α-actinin. *J. Biol. Chem.* **278**, 37545–37552.

Canals M., Marcellino D., Fanelli F., Ciruela F., de Benedetti P., Goldberg S., Fuxe K., Agnati L., Woods A. S., Ferré S. *et al.* (2003) Adenosine A_{2A}-dopamine D_2 receptor-receptor heteromerization: qualitative and quantitative assessment by fluorescence and bioluminiscence energy transfer. *J. Biol. Chem.* **278**, 46741–46749.

Ciruela F. and McIlhinney R. A. J. (1997) Differential internalisation of mGluR1 splice variants in response to agonist and phorbol esters in permanently transfected BHK cells. *FEBS Lett.* **418**, 83–86.

Ciruela F., Casadó V., Mallol J., Canela E. I., Lluis C. and Franco R. (1995) Immunological identification of A1 adenosine receptors in brain cortex. *J. Neurosc. Res.* **42**, 818–828.

Ciruela F., Escriche M., Burgueno J. *et al.* (2001) Metabotropic glutamate 1alpha and adenosine receptors assemble into functionally interacting complexes. *J. Biol. Chem.* **276**, 18345–18351.

Ferré S. J., Torvinen M., Antoniou K., Irenius E., Civelli O., Arenas E., Fredholm B. B. and Fuxe K. (1998) Adenosine A1 receptor-mediated modulation of dopamine D1 receptors in stably cotransfected fibroblast cells. *J. Biol. Chem.* **273**, 4718–4724.

Ferré S., Karcz-Kubicha M., Hope B. T., Popoli P., Burgueno J., Gutierrez M. A., Casado V., Fuxe K., Goldberg S. R., Lluis C. *et al.* (2002) Synergistic interaction between adenosine A1 and glutamate mGlu5 receptors: Implications for striatal neuronal function. *Proc. Natl Acad. Sci. USA* **99**, 11940–11945.

Ferré S., Ciruela F., Woods A. S., Canals M., Burgueno J., Marcellino D., Karcz-Kubicha M., Hope B. T., Morales M., Popili P. *et al.* (2003) Glutamate mGlu5-adenosine A2A–dopamine D2 receptor interactions in the striatum: implications for drug therapy in neuropsychiatric disorders and drug abuse. *Curr. Med. Chem.-Central Nervous System Agents* **3**, 1–26.

Franco R., Canals M., Marcellino D., Ferré S., Agnati A., Mallol J., Casadó V., Ciruela F., Fuxe K., Lluis C. *et al.* (2003) Regulation of heptaspanning membrane receptor function by dimerization and clustering. *TIBS* **28**, 238–243.

Furuchi T. and Anderson R. G. (1998) Cholesterol depletion of caveolae causes hyperactivation of extracellular signal-related kinase (ERK). *J. Biol. Chem.* **273**, 21099–21104.

Ginés S., Hillion J., Torvinen M., Le Crom S., Casado V., Canela E. I., Rondin S., Lew J. Y., Watson S., Zoli M. *et al.* (2000) Dopamine D_1 and adenosine A_1 receptors form functionally interacting heteromeric complexes. *Proc. Natl Acad. Sci. USA* **97**, 8606–8611.

Guo W., Shi L. and Javitch J. A. (2003) The fourth transmembrane segment forms the interface of the dopamine D2 receptor homodimer. *J. Biol. Chem.* **27**, 4385–4388.

Hillion J., Canals M., Torvinen M., Casadó V., Scott R., Terasmaa A., Hansson A., Watson S., Olah M. E., Mallol J. *et al.* (2002) Coaggregation, cointernalization, and codesensitization of adenosine A2A receptors and dopamine D2 receptors. *J. Biol. Chem.* **277**, 18091–18097.

Issafras H., Angers S., Bulenger S., Blanpain C., Parmentier M., Labbe-Jullie C., Bouvier M. and Marullo S. (2002) Constitutive agonist-independent CCR5 oligomerization and antibody-mediated clustering occurring at physiological levels of receptors. *J. Biol. Chem.* **277**, 34666–34673.

Jensen A. A., Hansen J. L., Sheikh S. P. and Brauner-Osborne H. (2002) Probing intermolecular protein–protein interactions in the calcium-sensing receptor homodimer using bioluminescence resonance energy transfer (BRET). *Eur. J. Biochem.* **269**, 5076–5087.

Jordan M., Schallhorn A. and Wurm F. M. (1996) Transfecting mammalian cells: optimization of critical parameters affecting calcium-phosphate precipitate formation. *Nucleic Acid Res.* **24**, 596–601.

Kamiya T., Saitoh O., Yoshioka K. and Nakata H. (2003) Oligomerization of adenosine A2A and dopamine D2 receptors in living cells. *Biochem. Biophys. Res. Commun.* **306**, 544–549.

McVey M., Ramsay D., Kellett E., Rees S., Wilson S., Pope A. J. and Milligan G. (2001) Monitoring receptor oligomerization using time-resolved fluorescence resonance energy transfer and bioluminescence resonance energy transfer: the human delta-opioid receptor displays constitutive oligomerization at the cell surface, which is not regulated by receptor occupancy. *J. Biol. Chem.* **276**, 14092–14099.

Milligan G. and White J. H. (2001) Protein–protein interactions at G-protein-coupled receptors. *TIPS* **22**, 513–518.

Patel R. C., Kumar U., Lamb D. C., Eid J. S., Rocheville M., Grant M., Rani A., Hazlett T., Patel S. C., Gratton E. *et al.* (2002) Ligand binding to somatostatin receptors induces receptor-specific oligomer formation in live cells. *Proc. Natl Acad. Sci. USA* **99**, 3294–3299.

Ramsay D., Kellet E., McVey M., Rees S. and Milligan G. (2002) Homo- and hetero-oligomeric interactions between G-protein-coupled receptors in living cells monitored by two variants ofbioluminescence resonance energy transfer (BRET): hetero-oligomers between receptor subtypes form more efficiently than between less closely related sequences. *Biochem. J.* **365**, 429–440.

Rios C. D., Jordan B. A., Gomes I. and Devi L. A. (2001) G-protein-coupled receptor dimerization: modulation of receptor function. *Pharmacol. Ther.* **92**, 71–87.

Terrillon S., Durroux T., Mouillac B., Breit A., Ayoub M. A., Taulan M., Jockers R., Barberis C. and Bouvier M. (2003) Oxytocin and vasopressin V1a, and V2 receptors form constitutive homo- and hetero-dimers during biosynthesis. *Mol. Endocrino.* **1**, 677–691.

Wurch T. A., Matsumoto A. and Pauwels P. J. (2001) Agonist-independent and -dependent oligomerization of dopamine D2 receptors by fusion to fluorescent proteins. *FEBS Lett.* **507**, 109–113.

Zacharias D. A., Violin J. D., Newton A. C. and Tsien R. Y. (2002) Partitioning of lipid-modified monomeric GFPs into membrane microdomains of live cells. *Science* **296**, 913–916.

Zimmermann T., Rietdorf J., Girod A., Georget V. and Pepperkok R. (2002) Spectral imaging and linear un-mixing enables improved FRET efficiency with a novel GFP^2-YFP FRET pair. *FEBS Lett.* **531**, 245–249.

IV-. Canals, M., Angulo, E., Casadó, V., Canela, E.I., Mallol, J., Viñals, F., Staines, W., Tinner, B., Hillion, J., Agnati, L., Fuxe, K., Ferré, S., Lluís, C. and Franco, R., 2004, "Molecular mechanisms involved in the adenosine A_1 and A_{2A} receptor-induced neuronal differentiation in neuroblastoma cells and striatal primary cultures". *Submitted manuscript*.

MOLECULAR MECHANISMS INVOLVED IN THE ADENOSINE A_1 AND A_{2A} RECEPTORS-INDUCED NEURONAL DIFFERENTIATION IN NEUROBLASTOMA CELLS AND STRIATAL PRIMARY CULTURES.

Meritxell Canals†, Ester Angulo†, Vicent Casadó†, Enric I. Canela†, Josefa Mallol†, Francesc Viñals%, William Staines††, Babben Tinner††, Joelle Hillion||, Luigi Agnati&, Kjell Fuxe$, Sergi Ferré#, Carmen Lluis*†. Rafael Franco*†,

From the †Department of Biochemistry and Molecular Biology of the University of Barcelona E-08028, Spain, †† Department of Cellular and Molecular Medicine, University of Ottawa, 451 Smyth Rd, Ottawa, Ontario. Canada. Canada K1H 8M5, || National Institute of Neurological Disorders and Stroke, NIH, DHHS, Bethesda, MD 20892, USA, # National Institute on Drug Abuse, NIH, DHHS, Baltimore, MD 21224, USA, & Section of Physiology, Department of Biomedical Sciences, University of Modena, 41100 Modena, Italy $Department of Neuroscience, Division of Cellular and Molecular Neurochemistry, Karolinska Institutet, S-171 77 Stockholm, Sweden

% Departament de Ciències Fisiològiques II, University of Barcelona, Campus de Bellvitge, Spain.

* These authors contributed equally to this paper.

Address for correspondence: Rafael Franco, Department of Biochemistry and Molecular Biology of the University of Barcelona, Marti Franquès 1, Barcelona E-08028, Spain. Tel 34-934021208 FAX 34-934021219. e-mail: rfranco@ub.edu

Acknowledgements: This study was supported by grants: QLG3-CT-2001-01056 from the European Union; SAF2002-03293 (R.F.), SAF2001-5357-E (RF) and SAF2001-3474 (E.I.C.) from Ministerio de Ciencia y Tecnología, 02/056-00 (RF) from Fundacio la Caixa and 01/012710 (RF) from Fundació Marató of Catalonian Telethon.

We are grateful to the personnel from *Serveis Científic-Tècnics* from the University of Barcelona for their excellent technical assistance.

ABSTRACT

Adenosine A_1 receptors (A_1Rs) and adenosine A_{2A} receptors (A_{2A}Rs) are the major mediators of the neuromodulatory actions of adenosine in the brain. In the striatum A_1Rs and A_{2A}Rs are mostly colocalized in the GABAergic striatopallidal neurons. In this paper we show that agonist-induced stimulation of A_1Rs and A_{2A}Rs induces neurite outgrowth processes in the human neuroblastoma SH-SY5Y cell line and also in striatal neuronal precursor cells in primary cultures. The kinetics of adenosine-mediated neuritogenesis was faster than that triggered by retinoic acid. The triggering of the expression of TrkB neurotrophin receptor and the arrest of cells in the G_1 phase by the activation of adenosine receptors suggest that adenosine may participate in early steps of neuronal differentiation. Furthermore, the A_1R- and A_{2A}R-mediated ERK-1/2 pathway activation is involved in the morphological differentiation of neuroblastoma cells as well as PKC activation, which is necessary to induce a full neuritogenesis. Inhibition of PKA activity results in a total inhibition of neuritogenesis induced by A_{2A}R agonists but not by A_1R agonists. PKA activation is therefore necessary for A_{2A}R-mediated neurotogenesis. These results are relevant to understand the mechanisms by which adenosine receptors modulate neuronal differentiation and open new perspectives for considering the use of adenosine agonists as therapeutic agents in diseases requiring neuronal repair.

INTRODUCTION

Adenosine is a ubiquitous endogenous nucleoside that functions as a neuromodulator in the brain. Extracellular adenosine levels are dynamically regulated by various mechanisms involving enzymes and transporters (Kobayashi et al., 2000). In fact, cells with increased metabolic activity release adenosine to the extracellular milieu. It has also been demonstrated that hypoxia results in increased extracellular adenosine concentrations due to the enhanced breakdown of adenine nucleotides. Adenosine in the brain is also formed from the breakdown of extracellular ATP, which can be released as a neurotransmitter ((Braun et al., 1998), (Dunwiddie et al., 2001)) or from extracellular cAMP metabolism (Latini et al., 2001). Adenosine mediates its actions through activation of specific G protein-coupled receptors, for which four subtypes have been identified: A_1, A_{2A}, A_{2B} and A_3 receptors (Fredholm et al., 1994). A_1 and A_{2A} receptors are the major adenosine receptor subtypes in the central nervous system. A_1R interacts with the pertussis toxin-sensitive G proteins, Gi and Go, that predominantly mediate inhibition of adenylyl cyclase and activation of phospholipases. In contrast, A_{2A}R stimulates adenylyl cyclase via Gs (for review see (Fredholm et al., 1999), (Schulte G, 2003), (Haas and Selbach, 2000)). A_1Rs are widely distributed in the central nervous system, whereas A_{2A}Rs are mostly expressed in the striatum (Fredholm ·, 2000). In the striatum A_{2A}Rs are mostly localized in the GABAergic striatopallidal neurons, where they co-localize and they can potentially interact with A_1Rs (Ferre et al., 1997).

It is widely accepted that A_1Rs and A_{2A}Rs are involved in the neuroprotective role of adenosine under conditions of cerebral ischemia (Moreau et al., 1999). Moreover, there is evidence indicating that adenosine, acting through both A_1Rs and A_{2A}Rs, may influence the development of the nervous system. It has been reported that both receptors are expressed during late prenatal periods and that their levels increase after birth (Rivkees, 1995). The expression pattern of A_1Rs in the brain during the second half of gestation leads to the possibility that the activation of these receptors may influence the differentiation and migration of neurons, an event that occurs during this period of neural development (Rivkees, 1995). Similarly, time-dependent changes in A_{2A}R expression in the brain has been reported to vary during development, which suggests a role of

these receptors during neuronal differentiation and synaptogenesis (Svenningsson et al., 1999).

Controversial results have been found when investigating the role of adenosine in neurite outgrowth in a neuronal cell model. On one hand, activation of A_1Rs inhibits nerve growth factor (NGF)-induced neurite outgrowth in both A_1R-transfected PC12 cells and neurons (Thevananther et al., 2001). On the other hand, it has also been described that antisense-mediated inactivation of ecto-5'-nucleotidase, the enzyme that converts ATP to adenosine, inhibits neurite outgrowth in PC12 cells which endogenously express A_{2A}Rs. ((Heilbronn et al., 1995), (Arslan et al., 1999)). Moreover, also in PC12 cells, A_{2A}R agonist stimulation rescued the blockade of NGF-induced neurite outgrowth involving MAPK and cAMP-response element-binding protein (CREB) activation (Cheng et al., 2002). In line with these findings, Charles et al. (2003) reported that the bacterial nucleoside N^6-methyldeoxyadenosine (MDA) induces and A_{2A}R-mediated neurite outgrowth in PC12 cells which also depends on NGF-dependent MAPK activation. Despite all these previous results, the direct stimulation of adenosine receptors by their classical agonists, independent of growth or differentiation factors, and the possible role their activation may play in the neuronal differentiation process has not been explored.

In the present paper, we show that either A_1R or A_{2A}R activation leads to neuritogenesis and differentiation in a neuronal cell model and in primary cultures of rat striatal neurons. The signaling pathways involved in A_1R or A_{2A}R neurite outgrowth were studied in the neuroblastoma cell line. MAPK and PKC activation was involved in the differentiating effects of both A_1R and A_{2A}R activation. PKA activation was found necessary for A_{2A}R- but not A_1R-mediated neuritogenesis.

MATERIALS AND METHODS

Cell culture

The SH-SY5Y neuroblastoma cell line was grown in Dulbecco's Modified Eagle's medium (DMEM) supplemented with 2 mM L-Glutamine, 100 U/ml penicillin/streptomycin, 1 mM sodium pyruvate and 10% heat inactivated Foetal Calf Serum (FCS). Cells were maintained at 37ºC in an atmosphere of 5% CO_2. All culture reagents were from Invitrogen (Paisley, Scotland). Cryo-preserved primary striatal neuron were obtained from QBM Cell Science, Ottawa, Canada. The cells were stored in liquid nitrogen until use. The frozen cell suspension was rapidly thawed by placing the tube into +37 ^{o}C waterbath for 2-3 min. By using a 1 ml pipette the cells were transferred to a 15 ml sterile tube. Pre-warmed NeuroBasal Media with B27 (Invitrogen) and 2 mM L-Glutamine, was added drop by drop over a period of 2 min, continually rotating the tube. Cells were re-suspended and plated on a 6-well sterile tissue culture plate containing a round 12 mm coverslip coated with poly-D-lysine. The cells were incubated at +37 ^{o}C incubator in 5% CO_2 air atmosphere. Two hours after plating, the media was replaced with DMEM containing 10 % heat-inactivated FCS and 50 mg/ml Gentamicin. The next day the cells were washed with DMEM, and the medium replaced with serum free B27-supplemented Neurobasal medium (Invitrogen) containing 50mg/ml Gentamicin (BNG medium) in absence or presence of 100 nM of R-PIA or 100 nM of CGS21680. Cells were kept at 37 ºC in an atmosphere of 5% CO_2 for the indicated time without frequent medium change.

RNA extraction and RT-PCR.

Total RNA of SH-SY5Y cells was extracted using the QuickPrep Total RNA extraction kit from Amersham Pharmacia Biotech (Buckinghamshire, UK) and following manufacturer's instructions. For the RT-PCR assay 2 µg of total RNA was reversely transcribed using SUPERSCRIPT RNaseH Reverse Transcriptase protocol (Invitrogen). 2 µl of cDNA were used to perform PCR amplification for A_1R, $A_{2A}R$ and GADPH as an internal control. Samples were subjected to 30 cycles of 95 °C for 1 min, 58 °C for 30 s, and 72 °C for 2 min on a Techne thermal cycler, with hot start at 95 °C. Products were analyzed on 2% ethidium bromide stained gels. Primer sequences were as follows: human A_1R

forward (FhA1), GCGGTGAGGCAGGGGAGTCT; human A_1R reverse (RhA1), GGGGCGCCTACAGTCAACAC; human A_{2A}R forward (FhA2A), GGCTGCCCCTACACATCATCAACT; human A_{2A}R reverse (RhA2A); TGGGCCAGGGGGTCATCT; human GADPH forward (FhGADPH), GCGGGGCTCTCCAGAACATCAT; human GADPH reverse (RhGADPH), GGTGGTCCAGGGGTCTTACTCC.

Immunocytochemistry

SH-SY5Y cells were incubated in absence or presence of 10 µM of retinoic acid (RA), 100 nM of R-PIA or 100 nM of CGS21680 (Sigma, Saint Louis, U.S.A) for the indicated time. Treated cells were subsequently fixed in 4% paraformaldehyde for 15 min and washed with PBS containing 20 mM glycine (buffer A) to quench the aldehyde groups. Where indicated, cells were permeabilized with buffer A containing 0.2% Triton X-100 for 5 min. Cells were blocked with buffer A containing 1% BSA (buffer B) for 1 h at room temperature. Cells were labeled for 1 h with the corresponding primary antibody: rabbit anti-A_1R antibody (PC21 1:200), rabbit anti- A_{2A}R antibody (VC21 1:200), mouse anti-MAP antibody (1:200, Calbiochem, San Diego, USA) or rabbit anti-trkB antibody (1:1500, Chemicon, Temecula, USA). Subsequently, cells were washed and stained with the secondary antibody: Cy3-conjugated affinity-purified donkey anti-mouse IgG or Cy5-conjugated affinity-purified donkey anti-rabbit IgG (both at a 1:200 dilution, Jackson ImmunoResearch, West Grove, USA,). Coverslips were rinsed for 30 min in buffer B and mounted with ImmunoFluor mounting medium (ICN, Cleveland, USA). Confocal microscope observations were made with a Leica TCS-SP (Leica Lasertechnik, Heidelberg, Germany) confocal scanning laser microscope adapted to an inverted Leitz DMIRBE microscope. For primary cultures of striatal neurons, cells were directly plated in medium containing 100 nM of CGS21680 or 100 nM of R-PIA and incubated for one or two weeks. Subsequently, fixation, permeabilization and MAP labelling were performed as described above for SH-SY5Y cells.

Evaluation of neuritogenesis

SH-SY5Y cells were seeded in 10 mm poly-D-lysine coated glass cover slips and incubated with FBS containing medium in absence or presence of 10 µM of

retinoic acid, 100 nM of R-PIA, 100 nM of CGS21680, 1 μM of DPCPX (Sigma) or 1 μM of ZM241385 (Tocris, Bristol, UK) alone or in combination and for the indicated time. Treated cells were washed once with DMEM and once with PBS, fixed in 4% paraformaldehyde for 15 min, and washed with phosphate buffered saline (PBS) containing 20 mM glycine. Cover slips were mounted with Mowiol mounting medium and phase-contrast observations were made in a Leica DMIRB (Leica Microsystems) with a 0.63X lens. Cell bodies and neurites present in 15 randomly selected fields were measured using MetaMorph Imaging System (Universal Imaging Corporation, USA). Cells were considered to be differentiated if they had at least one process longer than the cell body, which would be regarded as a neurite, and the results are expressed in percentage respect to the total cell number. At least three independent experiments were conducted in each treatment and the results are expressed as mean+/-SEM.

Western blot analysis

To determine the presence of A_1Rs and A_{2A}Rs, SH-SY5Y neuroblastoma cell membranes were obtained by disrupting the cells with a Polytron homogenizer (Kinematica, PTA 20TS rotor, setting 4; Brinkmann) for three 5s-periods in 50 mM Tris-HCl, pH 7.4. Membranes were separated by centrifugation at 105,000 x *g* for 45 min at 4 °C. For the TrkB receptor expression, SH-SY5Y cells were incubated in the absence or presence of 10 μM of RA, 100 nM of R-PIA or 100 nM of CGS21680 for the indicated time. Extracts from treated cells were prepared in ice-cold RIPA buffer (1% Nonidet P-40, 0.5% sodium deoxycholate, EDTA 1mM and 0.1% SDS in PBS) containing a protease inhibitor cocktail (Sigma). In all cases, the total protein content was measured using the BCA Protein Assay Reagent (Pierce, Rockford, USA). Aliquots corresponding to 20 μg of protein were mixed with SDS loading buffer, applied to 7.5% SDS-Polyacrylamide gel electrophoresis, transferred to a PVDF membrane and analyzed by western blot for the detection of TrkB with an anti-TrkB antibody (1:1500, Chemicon). Striping of these membranes and blotting with a mouse anti-tubulin antibody (1:500, Sigma) was performed as a control for the amount of protein loaded in the gel. For the detection of adenosine receptors, anti- A_1R (PC21) or anti- A_{2A}R were used. The immunoreactive bands were visualized

using horseradish peroxidase-linked secondary anti-mouse and anti-rabbit antibodies (DAKO, Denmark) and SuperSignal West Pico Chemiluminescent Substrate (Pierce).

ERK phosphorylation assays

SH-SY5Y cells were grown to 80% confluence and rendered quiescent by serum starvation overnight prior to MAPK phosphorylation assays. An additional 2h- period of incubation in fresh serum-free medium was performed to minimize basal activity. Cells were subsequently stimulated by addition of medium with or without agonists (R-PIA for A_1R or CGS21680 for $A_{2A}R$) and/or antagonists (DPCPX for A_1R or ZM241385 for $A_{2A}R$) and/or signal transduction inhibitors (PD98059 for MEK, GF109203XX for PKC and H89 for PKA, all from Tocris). Stimulation was terminated by rapidly rinsing with ice-cold PBS and cell lysis was performed by the addition of 500 µl of ice-cold lysis buffer (50 mM Tris-HCl pH 7.4, 50 mM NaF, 150 mM NaCl, 40 mM α-Glycerophosphate, 1% Triton 100X, 20 µM phenyl-arsin oxide, 1 mM $NaVO_4$ and protease inhibitor cocktail). The cellular debris was removed by centrifugation at 13000xg for 5 min, and the total protein content was measured using BCA Protein Assay Reagent (Pierce). Aliquots corresponding to 15 µg of protein were mixed with SDS loading buffer, applied to 7.5% SDS-Polyacrylamide gel electrophoresis and analyzed by western blot. ERK1/2 activation was assayed by incubating PVDF blots with a mouse anti-phospho-ERK1/2 antibody (Sigma, 1:10000). In order to rule out that the differences observed were due to the application of unequal amounts of lysates, control blots were also run in parallel and probed with a rabbit anti-ERK1/2 antibody that recognizes both, unphosphorylated and phosphorylated forms (Sigma, 1:40000). The immunoreactive bands were visualized using horseradish peroxidase linked secondary anti-mouse and anti-rabbit antibodies (DAKO) and SuperSignal West Pico Chemiluminescent Substrate (Pierce). Quantitative analysis of detected bands was performed by densitometry scanning.

p21 Ras activation assay.

A pull-down assay reported elsewhere was used to measure the degree of activation of p21 Ras, ((de Rooij and Bos, 1997), (Ferrer et al., 2001),(Gomez-

Santos et al., 2002)). Shortly, human neuroblastoma SH-SY5Y cells were cultured in 10 cm-plates until 80-90% confluence and serum deprived for 16 h. Cells were stimulated with 100 nM of PIA or 100 nM of CGS21680 for different time periods at 37 ºC prior being washed with ice-cold PBS and lysed with buffer A (50mM Tris-HCl pH 7.5, 15mM NaCl, 20mM $MgCl_2$, 5mM EGTA, 100 µM phenyl-methylsulfonyl fluoride, 1 µg/ml of leupeptin, 1 µM pepstatin A, 1% Triton X-100, 1% N-octylglucoside) for 15 min at 4ºC. Insoluble material was removed by centrifugation at 12,000 x g for 10 min. Lysates (1.5 mg protein) were incubated for 2 h at 4ºC with 30 µg of glutathione S-transferase (GST)-RBD fusion protein (where RBD consists of amino acids 51 to 131 of Raf-1 which is the minimal domain required for the binding of Ras-GTP) preadsorbed to glutathione-sepharose beads. Precipitates were washed four times with buffer A. The presence of p21 ras was detected by resuspending the final pellet in 25 µl of Laemmli sample buffer (Laemmli, 1970), followed by protein separation on 12.5% polyacrylamide gels and Western blotting as described above using the monoclonal antibody pan-Ras-Ab3 (Calbiochem). As control, 25 µg of the supernatant were loaded to immunodetect total Ras.

Cell cycle analysis.

SH-SY5Y cells were incubated in absence or presence of 10 µM of RA, 100 nM of R-PIA or 100 nM of CGS21680 for the indicated time. Treated cells were trypsinized and rinsed twice with PBS by centrifugation at 2000 rpm. At least $4x10^5$ cells were resuspended in 150 µl PBS + 1% FBS, fixed by slow addition of absolute ethanol for 10 min at -20ºC, rinsed with PBS and then labelled with 20 µg/ml propidium iodide and 10 µg/ml of RNAse A (Sigma) on ice for 1 hour. Fluorescence-activated cell sorter (FACS) analysis was carried out using an Epics XL flow cytometer (Coulter Corporation, Hialeah, Florida). The instrument was set up with the standard configuration: excitation of the sample was done using an standard 488nm air-cooled argon-ion laser at 15 mW power. Forward scatter (FSC), side scatter (SSC) and red (620 nm) fluorescence for propidium iodide were acquired. Optical alignment was based on optimized signal from 10 nm fluorescent beads (Immunocheck, Epics Division). Time was used as a control of the stability of the instrument. Aggregates were excluded gating single cells by their area vs. peak fluorescence signal. DNA analysis (Ploidy analysis)

on single fluorescence histograms was made using Multicycle software (Phoenix Flow Systems, San Diego, USA).

RESULTS

Expression of adenosine A_1Rs and A_{2A}Rs in SH-SY5Y cells.

The expression of endogenous A_1Rs and A_{2A}Rs in SH-SY5Y cells was previously demonstrated by radioligand-binding experiments (Salim et al., 2000) and further confirmed by three different techniques. RT-PCR showed the existence of the mRNA for both receptors (**Fig 1A**) and protein expression was confirmed by western blot of cell membranes using specific anti-A_1R and anti-A_{2A}R antibodies which revealed the bands corresponding to each receptor (**Fig 1B**). The expression of the receptors on the cell surface of SH-SY5Y cells was confirmed by immunocytochemistry and confocal microscopy analysis (**Fig 1C**).

Activation of A_1R and A_{2A}R induces neurite outgrowth in SH-SY5Y cells.

The human neuroblastoma cell line SH-SY5Y is a well-characterized model system to study neuronal differentiation *in vitro*. These cells develop long neurites and express several neuronal markers when treated with different agents including neurotrophic factors (Kaplan et al., 1993), retinoic acid (RA) or phorbol esters (Pahlman et al., 1995). SH-SY5Y cells reduce their rate of growth and initialize differentiation toward a neuronal phenotype when exposed to 10 µM retinoic acid (RA, (Pahlman et al., 1984),(Encinas et al., 2000)). This reagent has therefore been used as a control treatment for neuritogenesis. The effect of adenosine on neuroblastoma in vitro differentiation was analyzed using agonists selective for A_1R (R-PIA) or A_{2A}R (CGS21680). Treatment with R-PIA or CGS21680 in complete medium induced morphological changes in the cells with the appearance of what resembled neurite outgrowth processes (**Fig 2**). Neuritogenesis was observed by immunocytochemistry and confocal microscopy analysis with an anti-MAP antibody, and by phase-contrast imaging of treated cells.

Using different concentrations (**Fig 3A**) and different incubation times (**Fig 3B**) it was found that this effect was saturable reaching a maximal neuritogenesis at 100 nM and after 24h of incubation with either R-PIA or CGS21680. To demonstrate agonist selectivity the ability of selective antagonists to prevent the

agonist-induced neurite outgrowth was analyzed. As shown in **Fig. 4**. The effects of R-PIA (100 nM) could be antagonised by the selective A_1R antagonist DPCPX (1 μM), but not by the selective A_{2A}R antagonist ZM241385 (1 μM). Conversely, ZM241385 (1 μM), but not DPCPX (1 μM), prevented the effects of CGS21680 (100 nM). Taken together these results indicate that each of the receptors, A_1R and A_{2A}R, are able to induce neurite outgrowth processes when stimulated by their corresponding agonist.

Activation of A_1Rs or A_{2A}Rs triggers the expression of TrkB and the G_1 cell cycle arresting of SH-SY5Y cells.

To determine if R-PIA or CGS21680-induced neurite outgrowth processes indicated neuronal differentiation, differentiation markers were analyzed. As previously reported, differentiation of SH-SY5Y cells leads to the expression of TrkB receptor (Kaplan et al., 1993). Western blots of cell lysates revealed that 24h of treatment with 100 nM R-PIA or 100 nM CGS21680 resulted in a significant increase in TrkB receptor levels (**Fig. 5A**). To ensure that the differences observed were not due to the application of uneven amounts of lysates, control blots were also run in parallel and probed with an anti-tubulin antibody (**Fig. 5A**). TrkB receptor expression on the cell surface was established by immunocytochemistry and confocal microscopy analysis, (**Fig. 5B**).

Since neuronal differentiation processes are usually related to cell cycle regulation we analyzed the cell cycle distribution during R-PIA and CGS21680 treatments (**Fig. 5C**). Propidium iodide was used to label cells after 48h of treatment and cell cycle distribution was measured. Untreated cells (control) displayed 30 ± 2% (mean±S.E.M.) of the cells in the S phase while 60 ± 5% (mean±S.E.M.) remained in the G_1 phase. Treatment with the differentiating agent RA increased the number of cells arrested in G_1 phase up to 70%, R-PIA and CGS21680 increased the number of cells arrested in G_1 phase to the same extent as retinoic acid (**Fig. 5C**). Taken together these results suggest that the neurite outgrowth processes induced by activation of either A_1Rs or A_{2A}Rs reflect early steps in the differentiation of the SH-SY5Y cell line toward a neuronal phenotype.

A_1R- and A_{2A}R-mediated activation of MAPK pathway in SH-SY5Y cells

Previous reports have described that the MAPK cascade is activated by adenosine receptors ((Schulte and Fredholm, 2003), (Seidel et al., 1999), (Angulo, 2003; Angulo E., 2003)). To know whether A_1Rs and A_{2A}Rs are able to trigger activation of this signalling pathway in SH-SY5Y cells, ERK-1/2 phosphorylation was determined. By the results found in both dose-response (**Fig. 6A**) and time-course (**Fig. 6B**) experiments it was found that adenosine receptors in SH-SY5Y cells are coupled to the MAPK cascade, the maximal activation being achieved at 3 min with 100 nM of R-PIA and at 5 min with 100 nM of CGS21680. The ERK-1/2 phosphorylation induced by R-PIA was inhibited by the selective antagonist of A_1R, DPCPX (1 μM), and that induced by CGS21689 was inhibited by the selective A_{2A}R antagonist ZM241385 (1 μM) (**Fig. 6C**). Activation of p21Ras occurred with the two selective agonists and the maximum of activation was found at 3 min for R-PIA (100 nM) and at 10 min when CGS21680 (100 nM) was used (**Fig. 7**).

In order to better characterize the mechanism of the signal transduction pathways involved in the ERK1/2 activation, a set of experiments were performed in the presence of PD98059, a MEK inhibitor, GF109203XX, an inhibitor of conventional and novel PKC isoforms, and H89, an inhibitor of PKA. As observed in **Fig. 8A**, R-PIA-induced phosphorylation of ERK-1/2 was only inhibited by PD98059. ERK-1/2 phosphorylation induced by CGS21680 could be inhibited by both PD98059 and H89 but not with GF109203X. These results indicate that the pathway from A_1R activation down to ERK-1/2 phosphorylation is independent of PKA and PKC whereas the pathway triggered by A_{2A}R is dependent of PKA but not PKC.

Signalling pathways involved in A_1R- and A_{2A}R-mediated differentiation.

To determine the signal transduction pathway involved in differentiation, the ability of MEK, PKC or PKA inhibitors to prevent adenosine receptors-mediated neuritogenesis was explored (**Fig. 8B**). R-PIA-induced processes were only partially inhibited when PD98059 or GF109203X were used alone but they were totally inhibited when used in combination. In contrast, the PKA inhibitor H89 had no effect. These results suggest that both, MAPK and PKC, are independently involved in the differentiation processes induced by the

stimulation of A_1Rs. Similar experiments performed using CGS21680 resulted in a partial inhibition of the differentiation pattern by PD98059 or GF109203X and a total inhibition when both reagents combined together. As in the case of A_1R, activation of A_{2A}Rs results in independent MAPK- and PKC-mediated neuritogenesis. In the case of the treatment with CGS21680, H89 was however able to inhibit the process.

A_1R or A_{2A}R activation accelerates differentiation processes in primary cultures of striatal neurons.

The effects of A_1R or A_{2A}R stimulation on the growth and differentiation of primary neuronal cell cultures was determined. R-PIA or CGS21680 were added immediately after seeding neuronal precursor cells in Neurobasal medium (see Methods) and cell morphology was followed during 14 days (see Methods). Treatment with either 100 nM of R-PIA or 100 nM of CGS21680 accelerated the neuronal differentiation process since primary neuronal precursors after 1 week of incubation with either ligand already presented a neuronal morphology, which was not observed in non-treated control plates (**Fig.9**). These results suggest that the adenosine A_1R and A_{2A}R not only induce the differentiation of the SH-SY5Y neuroblastoma cell line but also accelerate neuritogenesis in primary neuronal precursor cells.

DISCUSSION

In this study activation of A_1Rs or A_{2A}Rs is shown to induce neurite outgrowth in the SH-SY5Y neuroblastoma cell line and primary cultures of striatal neurons. Using SH-SY5Y cells as a neuronal model, the neurite outgrowth after the stimulation of A_1Rs and A_{2A}Rs was found to be mediated by the phosphorylation of ERK-1/2 and the activation of PKC. In addition, agonist stimulation of A_1Rs and A_{2A}Rs induced both the expression of TrkB receptors and the arrest of cells in the G_1 phase, which are early events in neuronal differentiation processes ((Kaplan et al., 1993; Encinas et al., 2000)).

The intracellular events triggering neurite sprouting are not well established (Da Silva et al., 2003). Some authors suggest that the MAPK pathway is involved in BDNF-mediated survival and neuritogenesis in SH-SY5Y neuroblastoma cells (Encinas et al., 1999), whereas others postulate a role for this pathway in gene

induction for differentiation but not for the neurite outgrowth (Olsson et al., 2001). Also, Miller and colleagues have demonstrated that the MAPK pathway plays no role in neural progenitor survival or proliferation but, instead, specifically regulates neurogenesis ((Menard et al., 2002), (Barnabe-Heider et al., 2003)). Interestingly, in this paper the neuronal differentiation induced by A_1R or $A_{2A}R$ activation was found to be dependent upon both the MAPK activity and PKC activity, but in an independent manner.

In agreement with the results shown in **Fig. 7**, it has been demonstrated in SH-SY5Y cells that A_1Rs mediate ERK-1/2 phosphorylation by a *ras*-dependent pathway (Angulo et al., 2003). This suggests that in these cells A_1R activate the classical *ras*/raf/MEK/ERK pathway (see (Luttrell et al., 1999) and references therein). Here it is shown that not only A_1R but also $A_{2A}R$ activates the MEK/ERK-1/2 pathway. However, while the A_1R activation of this pathway was found to be PKA independent, the $A_{2A}R$ response is mediated by PKA. In fact, $A_{2A}R$ agonists, but not A_1R agonists, are able to increase intracellular cAMP concentration, which subsequently activates PKA. In some cell types cAMP controls *ras* and, subsequently, the raf/MEK/ERK pathway (see (Luttrell et al., 1999) and references therein). In the case of SH-SY5Y neuroblastoma cells this could be a straightforward possibility since it is well known that $A_{2A}R$ is positively coupled to adenylate cyclase (Hillion et al., 2002) and in the present report we found an $A_{2A}R$ agonist-induced *ras* activation (**Fig. 7**). However, in these cells ERK1/2 phosphorylation was completely sensible to PKA inhibition thus suggesting that $A_{2A}R$-mediated ERK1/2 activation follows the classical pathway downstream of PKA (Luttrell et al., 1999) which includes Rap1/B-RAF/MEK/ERK1/2..

In agreement with previously reported data, ERK-1/2 activation may not be the only pathway involved in the morphological differentiation of SH-SY5Y neuroblastoma cells (Olsson et al., 2001)). In fact, it has been shown that PACAP-mediated neurite outgrowth results in pleiotropic stimulation of several signaling pathways acting synergistically (Bouschet et al., 2003).

The present results show that PKC activation is also necessary to induce a full neuritogenesis after stimulation of A_1R or $A_{2A}R$ (**Fig.8**). In SH-SY5Y cells the activation of different isoforms of PKC by TPA has been shown to induce neurite outgrowth processes (Zeidman et al., 1999). Based on the finding that

the inhibitors of MEK or PKC are only able to totally prevent neuritogenesis when used in combination, while only partially preventing it when used separately, it is suggested that MAPK and PKC may be two independent pathways that upon A_1R or $A_{2A}R$ activation lead to similar differentiation events. The PKC isoform activated upon treatment of cells with R-PIA has to be conventional or novel since the effect is sensitive to GF109203XX, which at the concentrations used does not inhibit atypical PKC isoforms. Most probably, conventional PKC isoforms are not involved, since they are calcium-dependent and it has previously been reported that A_1R activation in SH-SY5Y cells leads to decreases in intracellular calcium (Salim et al., 2000). Thus, a novel PKC isoform, likely different from the one activated via $A_{2A}R$ (PKCε, see below), is probably controlled by A_1R in neuroblastoma cells. A more complex picture occurs with $A_{2A}R$ activation. In pheochromocytoma PC12 cells CGS212680 can activate both novel (PKCε) and atypical (PKCζ) isoforms in a calcium-independent manner (Gardner et al., 2003). The atypical PKCζ isoform mediates the $A_{2A}R$-promoted antagonization of apoptosis in serum-deprived PC12 cells (Huang et al., 2001). Since GF109203XX, which is less efficient in inhibiting atypical isoforms such as PKCζ, partially blocked neurite outgrowth, PKCε could participate in the ERK-independent pathway of $A_{2A}R$-mediated neuritogenesis. Since inhibitors of PKA activity resulted in a total inhibition of neuritogenesis induced by CGS21680, it is postulated that in the $A_{2A}R$-mediated differentiation events, PKA is activating the MEK/ERK pathway and another pathway that in combination with a PKC-dependent pathway results in neuritogenesis. A not yet identified signaling molecule could act as a link between PKA and PKC or, eventually, a PKA-mediated activation of a component of the signaling cascade could be essential for PKC translocation to the nucleus and couple this molecule to differentiation events.

It should be noted that in PC12 cells A_1R activation inhibits NGF-induced neurite outgrowth via activation of Rho kinase (Thevananther et al., 2001) that via profillin IIa controls actin stability (Da Silva et al., 2003). This mechanism may be dependent upon the presence of NGF or may not be dominant in SH-SY5Y cells since the A_1R transduction led concomitantly to a MEK-dependent and a PKC-dependent neurite outgrowth. Activation of either A_1R or $A_{2A}R$ leads

to a quicker differentiation of neural precursor cells (**Fig. 9**) and even after 14 days of culture there is no evident damage or degradation in growing cones.

Recently, it has been described that adenosine, acting through adenosine receptors, appears to be an active axon-glial signaling molecule in the CNS, where it promotes oligodendrocyte progenitor cells differentiation into myelinating oligodendrocytes (Stevens et al., 2002). Our observation that the activation of A_1R or $A_{2A}R$ induces the differentiation of the SH-SY5Y neuroblastoma cell line as well as accelerates neuritogenesis in primary neuronal precursor cells suggests that this nucleoside plays an important role not only in myelinization processes but also during neuronal differentiation. Impairment of neurite outgrowth has been associated with Alzheimer's disease, ((Furukawa et al., 1998),(Dowjat et al., 1999)) and mutations that affect neuronal differentiation cause multiple diseases in humans, ranging from varying degrees of mental retardation to severe heteropathies that lead to early death (da Silva and Dotti, 2002). This highlights the importance of understanding the mechanisms behind the early stages of neuronal differentiation. Based on the present results adenosine receptors may be considered as targets for treatment of these diseases.

REFERENCES

Angulo E, Casado, V., Mallol, J., Canela, E.I., Viñals, F., Ferrer, I., Lluis, C., Franco, R. (2003) A1 adenosine receptors accumulate in neurodegenerative structures in Alzheimer's Disease and mediate both amyloid precursor protein processing and Tau phosphorylation and translocation. Brain Pathology In Press.

Angulo E. CV, Mallol, J., Canela, E.I., Viñals, F., Ferrer, I., Lluis, C., Franco, R. (2003) A1 adenosine receptors accumulate in neurodegenerative structures in Alzheimer's Disease and mediate both amyloid precursor protein processing and Tau phosphorylation and translocation. Brain Pathology In Press.

Arslan G, Kull B, Fredholm BB (1999) Signaling via A2A adenosine receptor in four PC12 cell clones. Naunyn Schmiedebergs Arch Pharmacol 359:28-32.

Barnabe-Heider F, Miller FD (2003) Endogenously produced neurotrophins regulate survival and differentiation of cortical progenitors via distinct signaling pathways. J Neurosci 23:5149-5160.

Bouschet T, Perez V, Fernandez C, Bockaert J, Eychene A, Journot L (2003) Stimulation of the ERK pathway by GTP-loaded Rap1 requires the concomitant activation of Ras, protein kinase C, and protein kinase A in neuronal cells. J Biol Chem 278:4778-4785.

Braun N, Zhu Y, Krieglstein J, Culmsee C, Zimmermann H (1998) Upregulation of the enzyme chain hydrolyzing extracellular ATP after transient forebrain ischemia in the rat. J Neurosci 18:4891-4900.

Cheng HC, Shih HM, Chern Y (2002) Essential role of cAMP-response element-binding protein activation by A2A adenosine receptors in rescuing the nerve growth factor-induced neurite outgrowth impaired by blockage of the MAPK cascade. J Biol Chem 277:33930-33942.

da Silva JS, Dotti CG (2002) Breaking the neuronal sphere: regulation of the actin cytoskeleton in neuritogenesis. Nat Rev Neurosci 3:694-704.

Da Silva JS, Medina M, Zuliani C, Di Nardo A, Witke W, Dotti CG (2003) RhoA/ROCK regulation of neuritogenesis via profilin IIa-mediated control of actin stability. J Cell Biol 162:1267-1279.

de Rooij J, Bos JL (1997) Minimal Ras-binding domain of Raf1 can be used as an activation-specific probe for Ras. Oncogene 14:623-625.

Dowjat WK, Wisniewski T, Efthimiopoulos S, Wisniewski HM (1999) Inhibition of neurite outgrowth by familial Alzheimer's disease-linked presenilin-1 mutations. Neurosci Lett 267:141-144.

Dunwiddie T.V. Masino SA (2001) The role and regulation of adenosine in the central nervous system. Annu Rev Neurosci 24:31-55.

Encinas M, Iglesias M, Llecha N, Comella JX (1999) Extracellular-regulated kinases and phosphatidylinositol 3-kinase are involved in brain-derived neurotrophic factor-mediated survival and neuritogenesis of the neuroblastoma cell line SH-SY5Y. J Neurochem 73:1409-1421.

Encinas M, Iglesias M, Liu Y, Wang H, Muhaisen A, Cena V, Gallego C, Comella JX (2000) Sequential treatment of SH-SY5Y cells with retinoic acid and brain-derived neurotrophic factor gives rise to fully

differentiated, neurotrophic factor-dependent, human neuron-like cells. J Neurochem 75:991-1003.

Ferre S, Fredholm BB, Morelli M, Popoli P, Fuxe K (1997) Adenosine-dopamine receptor-receptor interactions as an integrative mechanism in the basal ganglia. Trends Neurosci 20:482-487.

Ferrer I, Blanco R, Carmona M, Ribera R, Goutan E, Puig B, Rey MJ, Cardozo A, Vinals F, Ribalta T (2001) Phosphorylated map kinase (ERK1, ERK2) expression is associated with early tau deposition in neurones and glial cells, but not with increased nuclear DNA vulnerability and cell death, in Alzheimer disease, Pick's disease, progressive supranuclear palsy and corticobasal degeneration. Brain Pathol 11:144-158.

Fredholm · B.B. , Halldner ·L., Kull · B., Schulte · G., Wasserman W. (2000) Structure and function of adenosine receptors and their genes. Naunyn-Schmiedeberg's Arch Pharmacol 362:364-374.

Fredholm BB, Battig K, Holmen J, Nehlig A, Zvartau EE (1999) Actions of caffeine in the brain with special reference to factors that contribute to its widespread use. Pharmacol Rev 51:83-133.

Fredholm BB, Abbracchio MP, Burnstock G, Daly JW, Harden TK, Jacobson KA, Leff P, Williams M (1994) Nomenclature and classification of purinoceptors. Pharmacol Rev 46:143-156.

Furukawa K, Guo Q, Schellenberg GD, Mattson MP (1998) Presenilin-1 mutation alters NGF-induced neurite outgrowth, calcium homeostasis, and transcription factor (AP-1) activation in PC12 cells. J Neurosci Res 52:618-624.

Gardner AM, Olah ME (2003) Distinct protein kinase C isoforms mediate regulation of vascular endothelial growth factor expression by A2A adenosine receptor activation and phorbol esters in pheochromocytoma PC12 cells. J Biol Chem 278:15421-15428.

Gomez-Santos C, Ferrer I, Reiriz J, Vinals F, Barrachina M, Ambrosio S (2002) MPP+ increases alpha-synuclein expression and ERK/MAP-kinase phosphorylation in human neuroblastoma SH-SY5Y cells. Brain Res 935:32-39.

Haas HL, Selbach O (2000) Functions of neuronal adenosine receptors. Naunyn Schmiedebergs Arch Pharmacol 362:375-381.

Heilbronn A, Maienschein V, Carstensen K, Gann W, Zimmermann H (1995) Crucial role of ecto-5'-nucleotidase in differentiation and survival of developing neural cells. Neuroreport 7:257-261.

Hillion J, Canals M, Torvinen M, Casado V, Scott R, Terasmaa A, Hansson A, Watson S, Olah ME, Mallol J, Canela EI, Zoli M, Agnati LF, Ibanez CF, Lluis C, Franco R, Ferre S, Fuxe K (2002) Coaggregation, cointernalization, and codesensitization of adenosine A2A receptors and dopamine D2 receptors. J Biol Chem 277:18091-18097.

Huang NK, Lin YW, Huang CL, Messing RO, Chern Y (2001) Activation of protein kinase A and atypical protein kinase C by A(2A) adenosine receptors antagonizes apoptosis due to serum deprivation in PC12 cells. J Biol Chem 276:13838-13846.

Kaplan DR, Matsumoto K, Lucarelli E, Thiele CJ (1993) Induction of TrkB by retinoic acid mediates biologic responsiveness to BDNF and differentiation of human neuroblastoma cells. Eukaryotic Signal Transduction Group. Neuron 11:321-331.

Kobayashi S, Zimmermann H, Millhorn DE (2000) Chronic hypoxia enhances adenosine release in rat PC12 cells by altering adenosine metabolism and membrane transport. J Neurochem 74:621-632.

Laemmli UK (1970) Cleavage of structural proteins during the assembly of the head of bacteriophage T4. Nature 227:680-685.

Latini S, Pedata F (2001) Adenosine in the central nervous system: release mechanisms and extracellular concentrations. J Neurochem 79:463-484.

Luttrell LM, Daaka Y, Lefkowitz RJ (1999) Regulation of tyrosine kinase cascades by G-protein-coupled receptors. Curr Opin Cell Biol 11:177-183.

Menard C, Hein P, Paquin A, Savelson A, Yang XM, Lederfein D, Barnabe-Heider F, Mir AA, Sterneck E, Peterson AC, Johnson PF, Vinson C, Miller FD (2002) An essential role for a MEK-C/EBP pathway during growth factor-regulated cortical neurogenesis. Neuron 36:597-610.

Moreau JL, Huber, G. (1999) Central adenosine A2A receptors: an overview. Brain Research Reviews 31:65-82.

Olsson AK, Nanberg E (2001) A functional role for ERK in gene induction, but not in neurite outgrowth in differentiating neuroblastoma cells. Exp Cell Res 265:21-30.

Pahlman S, Ruusala AI, Abrahamsson L, Mattsson ME, Esscher T (1984) Retinoic acid-induced differentiation of cultured human neuroblastoma cells: a comparison with phorbolester-induced differentiation. Cell Differ 14:135-144.

Pahlman S, Hoehner JC, Nanberg E, Hedborg F, Fagerstrom S, Gestblom C, Johansson I, Larsson U, Lavenius E, Ortoft E, et al. (1995) Differentiation and survival influences of growth factors in human neuroblastoma. Eur J Cancer 31A:453-458.

Rivkees SA (1995) The ontogeny of cardiac and neural A1 adenosine receptor expression in rats. Brain Res Dev Brain Res 89:202-213.

Salim H, Ferre S, Dalal A, Peterfreund RA, Fuxe K, Vincent JD, Lledo PM (2000) Activation of adenosine A1 and A2A receptors modulates dopamine D2 receptor-induced responses in stably transfected human neuroblastoma cells. J Neurochem 74:432-439.

Schulte G, Fredholm BB (2003) Signalling from adenosine receptors to mitogen-activated protein kinases. Cell Signal 15:813-827.

Schulte G Fredholm BB (2003) Signalling from adenosine receptors to mitogen-activated protein kinases. Cellular Signalling 15:813-827.

Seidel MG, Klinger M, Freissmuth M, Holler C (1999) Activation of mitogen-activated protein kinase by the A(2A)-adenosine receptor via a rap1-dependent and via a p21(ras)-dependent pathway. J Biol Chem 274:25833-25841.

Stevens B, Porta S, Haak LL, Gallo V, Fields RD (2002) Adenosine: a neuron-glial transmitter promoting myelination in the CNS in response to action potentials. Neuron 36:855-868.

Svenningsson P, Le Moine C, Fisone G, Fredholm BB (1999) Distribution, biochemistry and function of striatal adenosine A2A receptors. Prog Neurobiol 59:355-396.

Thevananther S, Rivera A, Rivkees SA (2001) A1 adenosine receptor activation inhibits neurite process formation by Rho kinase-mediated pathways. Neuroreport 12:3057-3063.

Zeidman R, Pettersson L, Sailaja PR, Truedsson E, Fagerstrom S, Pahlman S, Larsson C (1999) Novel and classical protein kinase C isoforms have different functions in proliferation, survival and differentiation of neuroblastoma cells. Int J Cancer 81:494-501.

FIGURE LEGENDS

Figure 1. ***A_1R and A_{2A}R expression by human neuroblastoma SH-SY5Y cells.*** **(A)**. RT-PCR assays from Jurkat (Control) and SH-SY5Y cells RNAs were performed for A_1R, A_{2A}R and GADPH as indicated in Materials and Methods. **(B)**. Western blots of SH-SY5Y membranes with specific antibodies that recognize A_1R and A_{2A}R. **(C).** Immunocytochemistry of fixed SH-SY5Y cells using specific antibodies that recognize A_1R and A_{2A}R. Punctate A_1R and A_{2A}R immunoreactivity is demonstrated. *Scale bars, 10 μm.*

Figure 2. ***Neurite outgrowth induction in SH-SY5Y cells.*** SH-SY5Y cells were treated for 48 h with 10 μM of retinoic acid, 100 nM of CGS21680 or 100 nM of R-PIA and were subsequently permeabilized and processed for immunocytochemistry with an anti-MAP antibody (green images) or observed under a phase-contrast microscope. *Scale bars, 10 μm.*

Figure 3. ***A_1R and A_{2A}R agonist-induced neuritogenesis in SH-SY5Y cells*.** **(A).** Cells were treated with different concentrations of the A_1R agonist R-PIA (grey bars) or the A_{2A}R agonist CGS21680 (white bars) for 24 h and neurite outgrowth was scored as described in Materials and Methods. Results are expressed as means ± SEM of four independent experiments. One-way ANOVA showed a significant increase in differentiation processes (*post-hoc* Newman-Keuls test, $p<0.05$ in all cases). **(B).** Cells were treated with 100 nM of R-PIA (grey bars) or 100 nM of CGS21680 (white bars) for different times and analysed for neurite outgrowth. Results are expressed as means ± SEM of three independent experiments. One-way ANOVA showed a significant increase in differentiation processes (*post-hoc* Newman-Keuls test, $p<0.05$ in all cases except for 2 h of R-PIA).

Figure 4. Blockade of *A_1R and $A_{2A}R$ agonist-induced neuritogenesis by selective antagonists.* SH-SY5Y cells were treated with 100 nM of R-PIA or 100 nM of CGS21680 in presence or absence of 1 µM of either the A_1R antagonist DPCPX or the $A_{2A}R$ antagonist ZM241385. Neurite outgrowth was scored as described in Materials and Methods. Results are expressed as means ± SEM of three independent experiments. ***, $p<0.001$ compared with control; ++, $p<0.01$ compared with R-PIA; •, $p<0.05$ compared with CGS by one way ANOVA and *post-hoc* Newman-Keuls multiple comparison test.

Figure 5. *A_1R and $A_{2A}R$ agonist-induced TrkB expression and G_1 arresting in SH-SY5Y cells.* Cell were treated with 10 µM of retinoic acid, 100 nM of R-PIA or 100 nM of CGS21680 for 24 and 48 h and **(A)** lysates were analyzed by western blot or **(B)** fixed cells were processed for immunocytochemistry using an anti-TrkB antibody. Tubulin detection ensured that equal amounts of protein were loaded on the gel. **(C)** FACS analysis was performed to analyze the cell cycle distribution; a representative experiment is represented. *Scale bars, 10 µm.*

Figure 6. *A_1R and $A_{2A}R$ agonist-induced ERK1/2 phosphorylation*. ERK1/2 phosphorylation was determined as described in Materials and Methods. **(A)** Cells were treated (5 min) with increasing concentrations of R-PIA (grey bars) or CGS21680 (white bars). **(B)** Cells were treated for increasing time periods with 100 nM of R-PIA (grey bars) or 100 nM of CGS21680 (white bars). **(C)** Cells were treated (5 min) with 100 nM of R-PIA or 100nM of CGS21680 in presence or absence of 1 µM of DPCPX or ZM241385. Results are expressed as means ± SEM of three independent experiments. In A and B, **, $p<0.05$ compared with control; one-way ANOVA and *post-hoc* Newman-Keuls multiple comparison test. In C, **, $p<0.001$ compared to the control; ++, $p<0.001$ compared with R-PIA, ••, $p<0.001$ compared to CGS21680 by one-way ANOVA and *post-hoc* Newman-Keuls multiple comparison test.

Figure 7. *A_1R and $A_{2A}R$ agonist-induced p21Ras activation.* SH-SY5Y cells were incubated for different times with 100 nM of R-PIA or 100nM of CGS21680 and the activation of p21 Ras was determined (See Materials and Methods).

Figure 8. ***Effects of signal transduction inhibitors in ERK1/2 phosphorylation and neuritogenesis.*** SH-SY5Y cells were incubated for 1h with either 75 μM of the MEK inhibitor, PD98059, 5 μM of the PKC inhibitor GF109203XX, or 10 μM of the PKA inhibitor H89 and stimulated with 100 nM of R-PIA or 100 nM of CGS21680. (**A**) After 5 min cells were lysed and analysed for ERK1/2 phosphorylation. Left panel shows a representative western-blot. Right panel shows densitrometric quantitation of three independent experiments. Results are expressed as means ± SEM of three independent experiments and in the cases where an inhibitor is used, the percentage is calculated over the inhibitor alone. **, $p<0.05$ compared to the control by one-way ANOVA and *post-hoc* Newman-Keuls multiple comparison test. **(B)** After 24 h neurite outgrowth was measured as described in Materials and Methods. **, $p<0.05$ compared to R-PIA or CGS21680 by one way ANOVA and *post-hoc* Newman-Keuls multiple comparison test.

Figure 9. ***A_1R and $A_{2A}R$ agonists accelerate differentiation in primary cultures of striatal neurons***. Neuronal precursors were plated directly in medium in presence or absence of 100 nM of R-PIA or 100 nM of CGS21680. After 1 or 2 weeks, cells were fixed and permeabilized and immunocytochemistry to detect MAP immunoreactivity was performed. *Scale bars, 10 μm.*

Figure 1

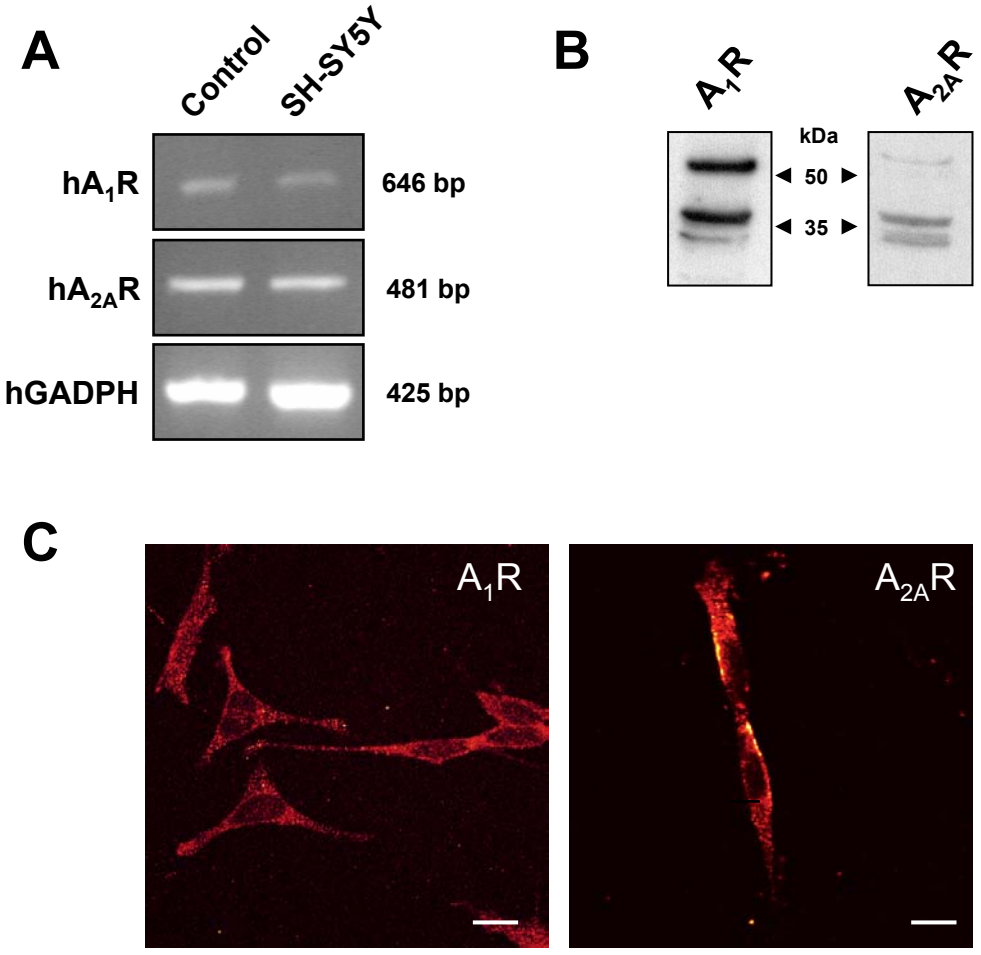
A
Control
SH-SY5Y
hA1R
646 bp
hA2AR
481 bp
hGADPH
425 bp
B
A1R
A2AR
kDa
50
35
C
A1R
A2AR

Figure 2

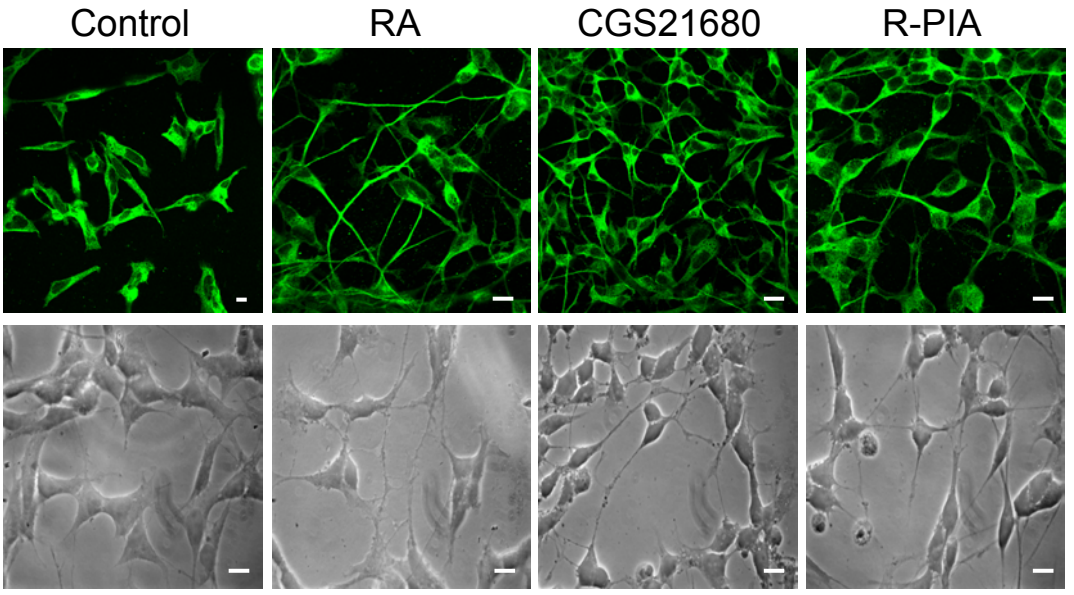

Figure 3

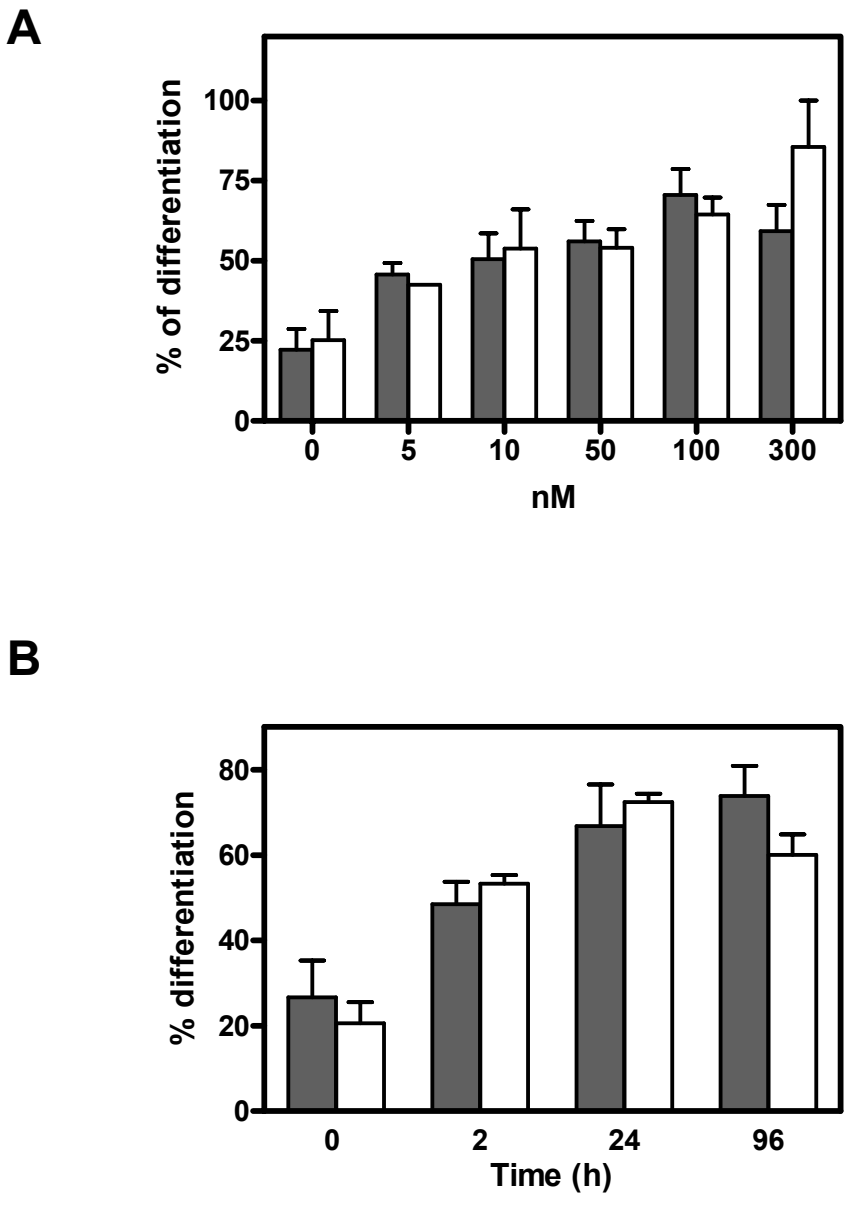
A
% of differentiation
100
75
50
25
0
0
5
10
50
100
300
nM
B
% differentiation
80
60
40
20
0
0
2
24
96
Time (h)

Figure 4

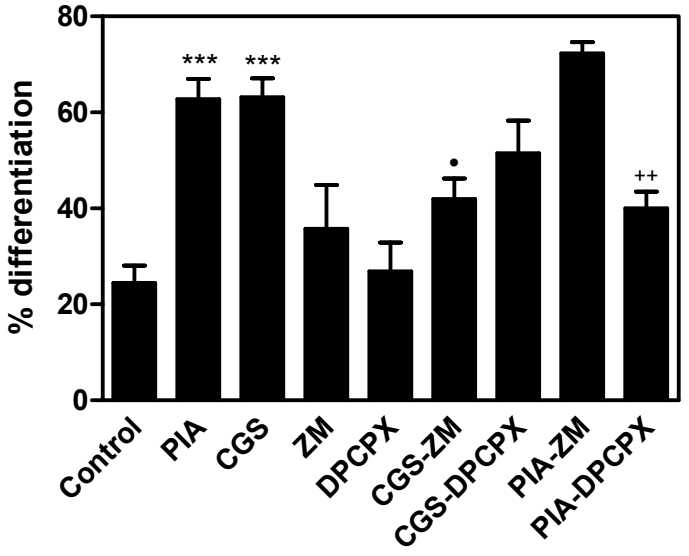
% differentiation
80
60
40
20
0
***
***
•
++
Control
PIA
CGS
ZM
DPCPX
CGS-ZM
CGS-DPCPX
PIA-ZM
PIA-DPCPX

Figure 5, Canals et al.

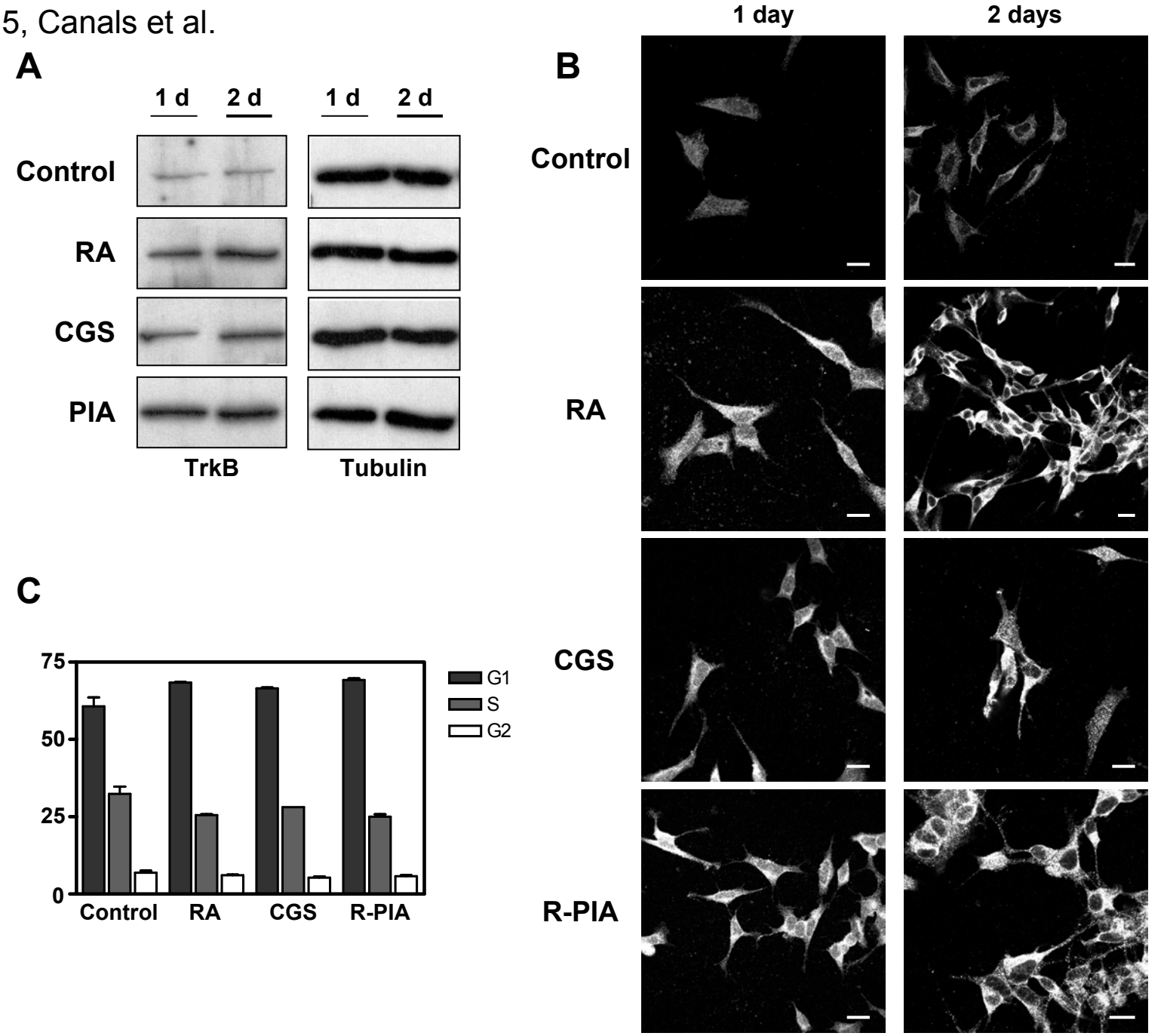

Figure 6

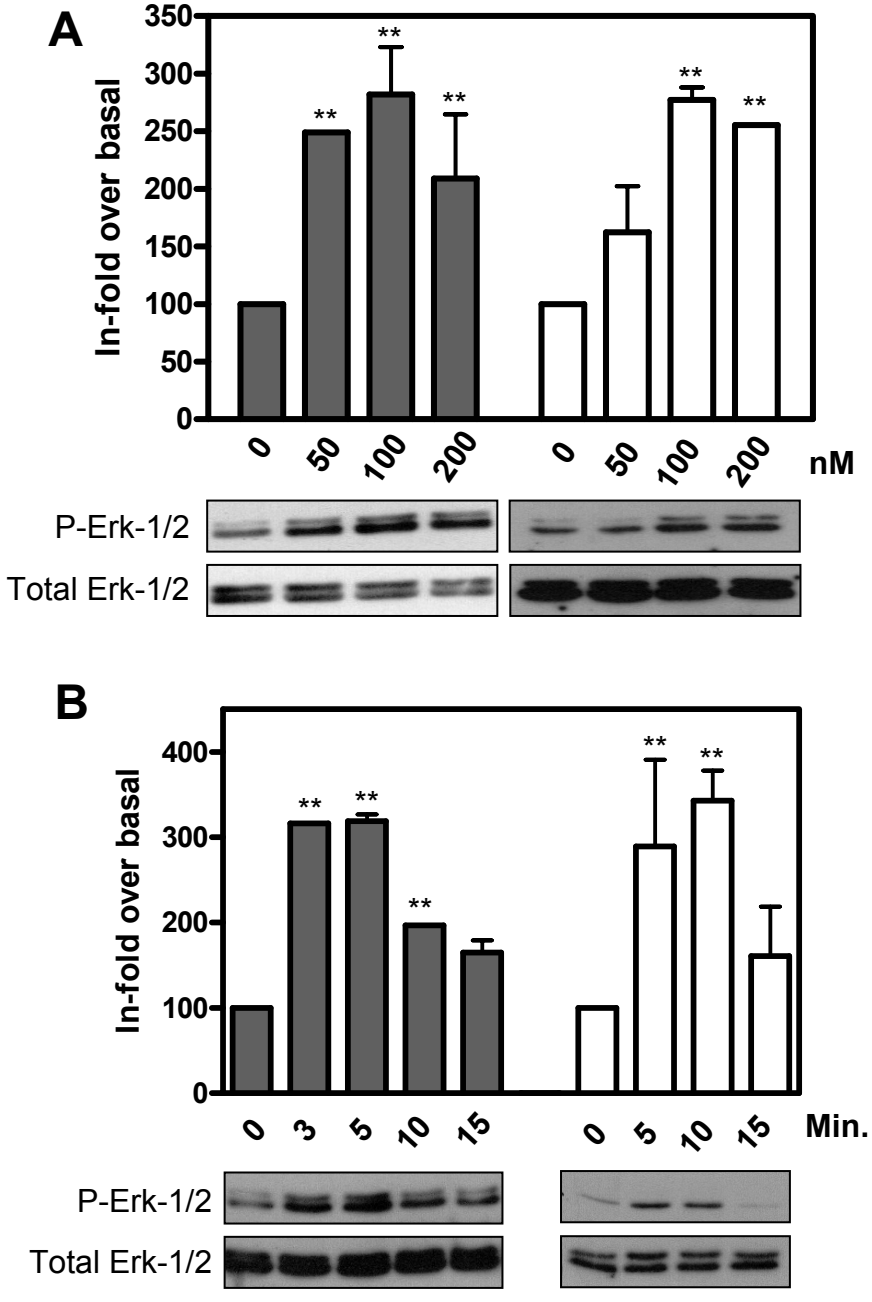
A
In-fold over basal
350
300
250
200
150
100
50
0
**
0
50
100
200
nM
P-Erk-1/2
Total Erk-1/2
B
In-fold over basal
400
300
200
100
0
0
3
5
10
15
Min.
P-Erk-1/2
Total Erk-1/2

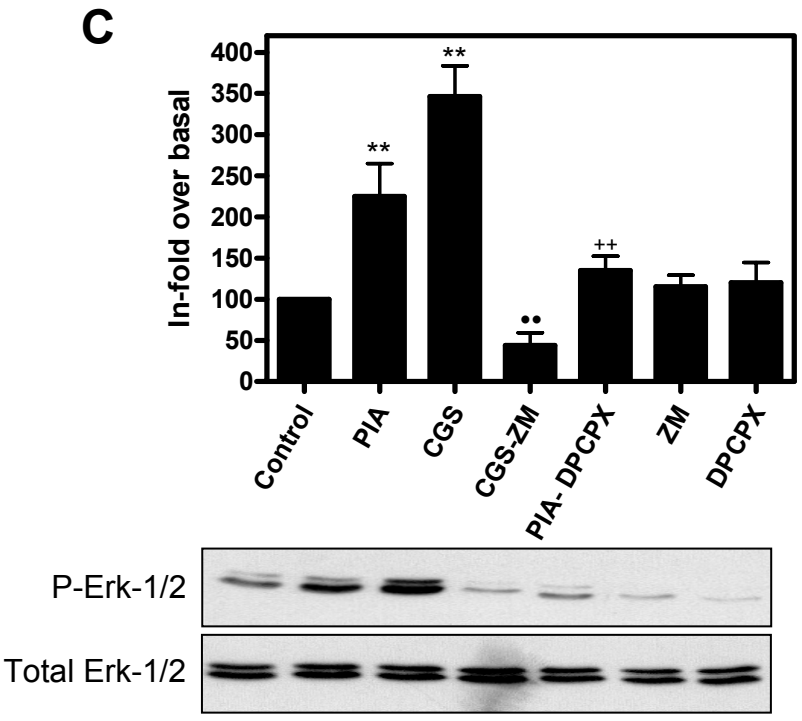
C
In-fold over basal
400
350
300
250
200
150
100
50
0
**
**
++
Control
PIA
CGS
CGS-ZM
PIA- DPCPX
ZM
DPCPX
P-Erk-1/2
Total Erk-1/2

Figure 7

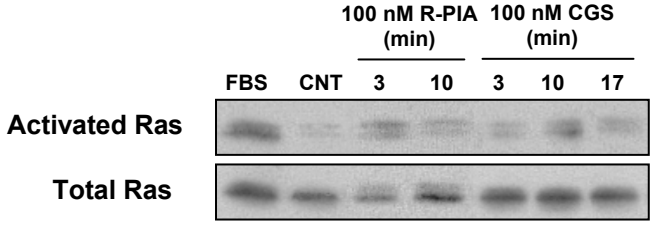
100 nM R-PIA (min)
100 nM CGS (min)
FBS
CNT
3
10
3
10
17
Activated Ras
Total Ras

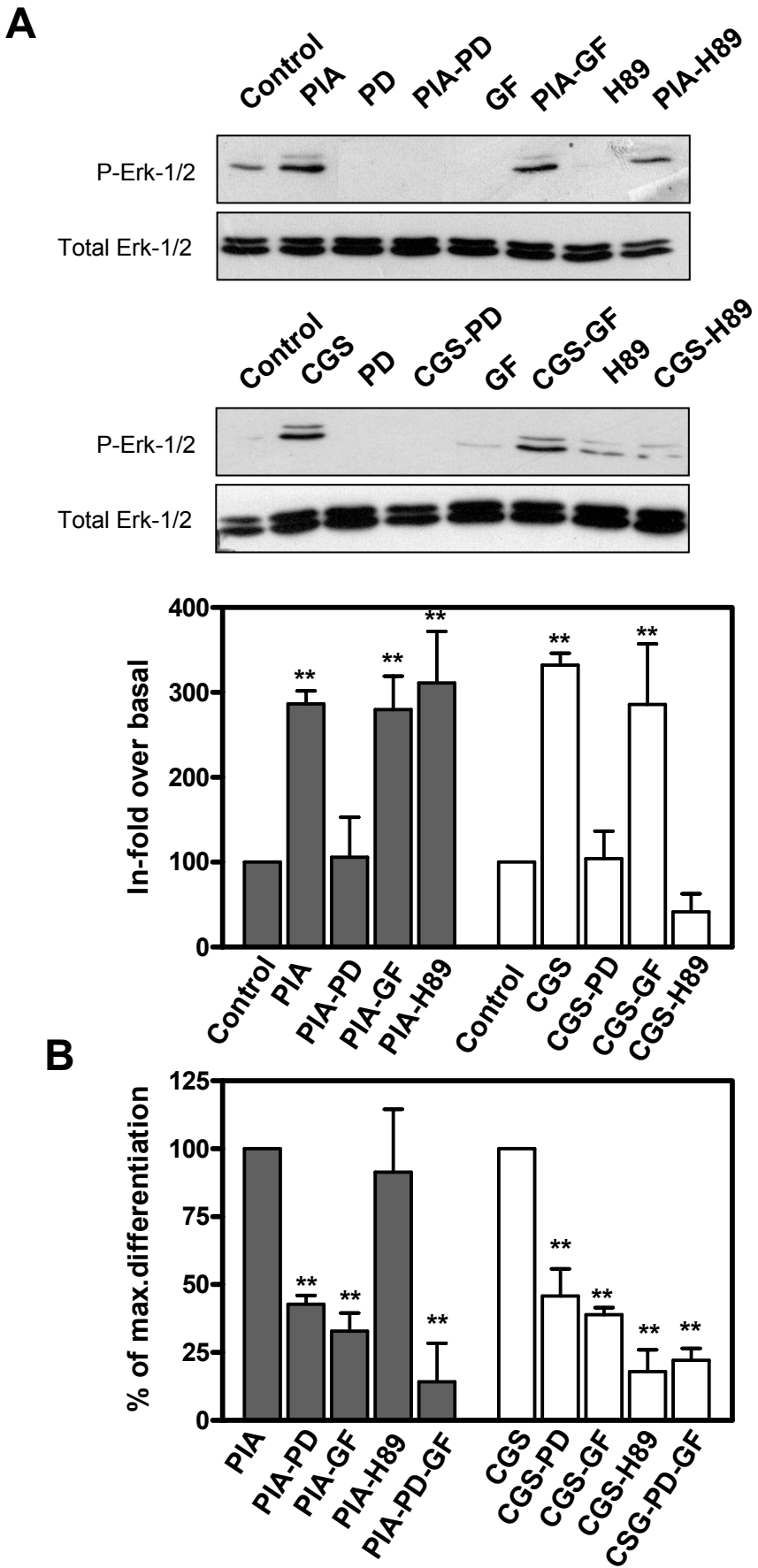
A
Control
PIA
PD
PIA-PD
GF
PIA-GF
H89
PIA-H89
P-Erk-1/2
Total Erk-1/2
Control
CGS
PD
CGS-PD
GF
CGS-GF
H89
CGS-H89
P-Erk-1/2
Total Erk-1/2
In-fold over basal
400
300
200
100
0
**
Control
PIA
PIA-PD
PIA-GF
PIA-H89
Control
CGS
CGS-PD
CGS-GF
CGS-H89
B
% of max.differentiation
125
100
75
50
25
0
**
PIA
PIA-PD
PIA-GF
PIA-H89
PIA-PD-GF
CGS
CGS-PD
CGS-GF
CGS-H89
CSG-PD-GF

Figure 9

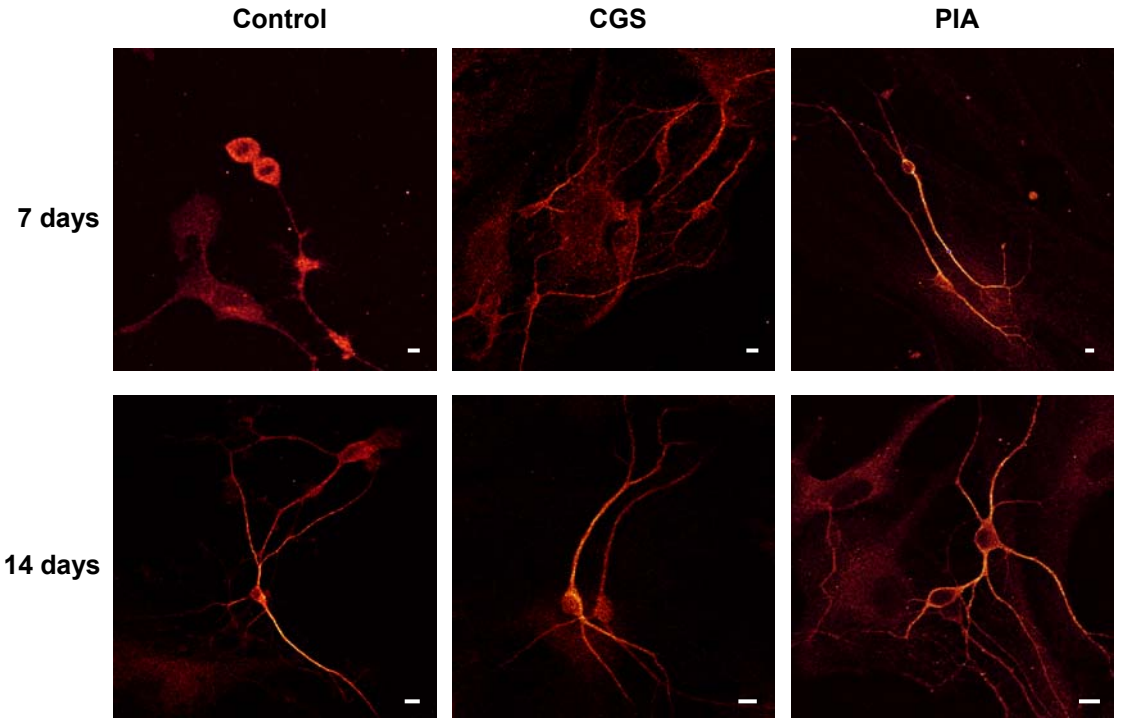

The contribution in some collaborations performed during this thesis have succeeded in the publication of two papers which are not included as "Results" but are enclosed in **ANNEX 1**. The contribution in each paper has been:

- Torvinen M, Gines S, Hillion H, Latini S, Canals M, Ciruela F, Bordoni F, Staines W, Pedata F, Agnati L, Lluis C, Franco R, Ferre S, Fuxe K., 2002, "Interactions among adenosine deaminase, adenosine A_1 receptors and dopamine D_1 receptors in stably cotransfected fibroblast cells and neurons" *Neuroscience*, 113, 709-719.
  Immunocytochemistry and confocal microscopy analysis for the study of co-localization of A_1R, D_1R and ADA in Ltk^- fibroblast cells.

- Ciruela F, Burgueño J, Casadó V, Canals M, Marcellino D, Goldberg S, Bader M, Fuxe K, Agnati L, Lluis C, Franco R, Ferré S, Woods A., 2004, "Adenosine A_{2A}-dopamine D_2 receptor-receptor heteromerization. Involvement of epitope-epitope electrostatic interactions" *Submitted manuscript*.
  Performance of BRET experiments using a mutant D_2R to characterize the possible sites of interaction between $A_{2A}R/D_2R$.